Magnetic Force Imaging Of Current in Integrated Circuits

by

Moses Teong Sen TAN

A thesis
Submitted to the Faculty of Graduate Studies
In partial fulfillment of the requirements
for the degree of

Master of Science

Department of Electrical and Computer Engineering
University of Manitoba
Winnipeg, Manitoba
Canada

THE UNIVERSITY OF MANITOBA

FACULTY OF GRADUATE STUDIES

*****

COPYRIGHT PERMISSION

Magnetic Force Imaging of Current in Integrated Circuits

BY

Moses Teong Sen Tan

A Thesis/Practicum submitted to the Faculty of Graduate Studies of The University of Manitoba in partial fulfillment of the requirement of the degree

Of

MASTER OF SCIENCE

Abstract

Integrated circuit today has becoming more advance and complicated. Narrower gate, thinner gate oxide, more metal layers, more function blocks being integrated into single dice are the trend of the integrated circuit benchmark. High efficiency test at wafer level or package level and failure analysis of the defect has becoming a critical element that directly link to the reliability, productivity and profit of the silicon industry. IDDQ testing has been proved to be able to catch about 98% of defective devices compared to scan and functional test, in contrast to perform Failure Analysis on these fails devices has become a new challenge for the industry especially in locating the failure physically on the silicon and extracting the information of the leakage current.

Liquid crystal technique has been widely used for detecting hot spot and dynamic voltage contrast. It is a simple, cost effective and non-destructive Failure Analysis technique but precisely locating the failure and leakage current information extraction is almost impossible. Emission microscope has also been used to detect photons emission from the IC, but it is a high cost equipment and with complicated setup, precisely locating physical failure takes long hours and leakage current information extraction is very difficult. With Magnetic Force Microscopy, it can become a simple and fast solution for Failure Analysis to extract leakage current information on submicron structure.

This thesis presents a technique for MFM imaging of IC current and demonstrate the ability to extract and analyze current magnitude and direction with a sensitivity of 0.08mA.

Acknowledgements

- Patiently supervised and advised by Dr. D.J. Thomson
- Concept of specific MFM implemented in this thesis conceived by Dr. D.J. Thomson.
- Understanding of all theoretical concepts assisted by Dr. D.J. Thomson, Dr Greg Bridges, Dr. Vu Ho (Nortel Networks), Dr. Richard Normandin (NRC), and Sunny Cheung (PMC Sierra).
- Figure 3.2 appears courtesy of Sunny Cheung.
- Figure 3.10, 3.13, 4.2 appears courtesy of David Shimizu.
- Micromachined cantilevers purchased by Dr. D.J. Thomson and Dr Greg Bridges.
- Mechanical probing structure in Figure 3.9 by Bill, Al Simmons and Richard Qi.
- Scanning Probe Microscope Controller (Hardware and Software) by Dr. D.J. Thomson and David Shimizu.
- Purchasing of equipments and commercial devices financially support by NSERC, CMC and Micronet.
- Cadance and HspiceS managed by Guy Jonatschuk.
- All experimental implementations by Moses Tan.
- All measurements performed by Moses Tan.
- Sample circuit designed by Moses Tan and fabricated by Nortel Networks through CMC.
- Draft editing: Dr. D.J. Thomson, Dr. Bruno Derudet (STMicroelectronics) and Moses Tan.

I like to thanks everyone who contributed to this thesis, especially Dr. D.J. Thomson and everyone who were involved in the SPM lab. Thanks to my wife and family who supported me throughout these times. Lastly, I want to thank GOD for His mighty guidance, wonderful grace and endless love.

Table of Contents

List of Figures

Chapter 1

Introduction

1.1 Introduction - Motivation

In order to keep up the semiconductor industry development swiftness ruled by Moore's law (the industry will quadrupling the number of transistors in a single chip in every three years [1.1]), the semiconductor industry today is moving with a more aggressive pace than what has been predicted by International Semiconductor Industry Association Roadmap 1997, [1.2] CMOS ICs are being design with higher transistor density and internal clock performance but lower feature size and operating voltage. The ability to develop more suitable diagnostic techniques and tools for design verification and failure analysis has become a key element to the growth of semiconductor industry.

IDDQ (VDD Current Quiescent) testing [1.4] has become more and more popular in Automated Test Equipment (ATE) at wafer and package level. It has been proved to have higher efficiency than traditional Scan and Function Test.[1.3] Normally, IDDQ test fail might be caused by transistor with high leakage current or bridging effect of interconnection line. In today's semiconductor industries, failure analysis on any defective device has become a key parameter leading to product and process qualification. Companies will save million of dollars in production if one design error is identified and corrected.

"Liquid crystal" and "Emission Microscopy" has been widely used to localized fail area, but neither of these two technique can extract precise fail location and details about the leakage current. As a result, it has become a motivation to develop and non-

invasive low cost technique that not only can locate the leakage current but also has the ability to extract attributes of the leakage current.

1.2 Introduction - Outline

This thesis presents magnetic force probing over a transmission line with different voltage levels inputs. Following this introduction, a theoretical background study of different Magnetic Force Microcopy working mode is presented in Chapter 2. In Chapter 3, the implementation of MFM is presented. Characteristics of instruments we use for this experiment is studied and analyzed. In Chapter 4, test parameters and instrument panel setup for the experiment is presented. Follow by an exhibition of MFM results form different test scenarios and the chapter closed with an analysis of the obtained results. Chapter 6 presents the simulation program we wrote using MathCAD software. Brief description of each function block in program code, analysis of the MathCAD simulated result and explanations of the found discrepancies between the MFM and the simulated results. Lastly, future considerations and conclusion are presented in Chapter 7 to finalize the thesis.

Chapter 2

Magnetic Force Microscopy

This chapter studies Magnetic Force Microscopy (MFM) in the application of IDDQ [1.4] probing for circuit failure analysis and magnetic force probing. IDDQ is depending on process technology and the width of the MOS gate. [1.5] A normal IDDQ for a CMOS circuit is in nA range, while an abnormal IDDQ by a defecting CMOS circuit will raise the current level by several orders of magnitude, usually larger then mA. [1.6] Firstly, we begin with a study of Scanning Probe Microscopy (SPM) and its siblings Atomic Force Microscopy (AFM) that inspired MFM directly. Secondly, a short introduction and the theoretical background about MFM will be studied and presented.

2.1 Scanning Probe Microscopy

SPM has been used to extracting topographical, electrical and magnetic properties of microscopic materials since the 1980's. The capability of performing measurements on an atomic scale has made this technique particularly powerful and useful. Properties of a material can be obtained by measuring the interaction between the mechanical probe and the surface of the material. Spatial resolution is defined by the spacing between the tip-surface and the radius of curvature of the probe tip and the nature of the interaction.

2.1.1 Scanning Probe Microscopy-Atomic Force Microscopy

The Atomic Force Microscopy (AFM), or Scanning Force Microscopy (SFM) which is part of the SPM family was invented in 1986 by Binnig, Quate and Gerber.[2.1] In the AFM scanning technique, a sharp probe is utilized to scan over the surface of

interest. The probe that holds a tip at the end of a cantilever deflects in response to the interaction force between the tip and surface. In order to understand more about the deflection of the cantilever, we have to define the significance of these atomic forces in term of distances between the tip and the surface. These forces are divided arbitrarily into short-range and long-range forces base on what is considered "short" and "long" for Atomic Force Microscopy instrumentation. At large distances, the electrostatic force, the magnetic force or the Van der Waals force have the dominant effect to the overall force contribution. As the probe moves closer to the surface, adhesion forces or repulsion forces which results from the overlapping of the electron clouds of the surface and tip will become more significant. [2.2]

Among these atomic forces, force that can be extracted by AFM is the negative gradient of the potential U. This force is normal to the sample surface and acting on the cantilever. It can be defined as the following equation, where z is the cantilever deflection. [2.3]

$$F = \frac{-\partial U}{\partial z}, \quad [\text{E2.1}]_{[2.3]}$$

Optical beam bounce detection technique is used to extract AFM data by measuring the cantilever deflection z. Data can then be analyzed and interpreted as a representation of certain property of the sample surface. [2.4]

The AFM can be operated in two principle modes, one is "with-feedback- control mode" and the other is "without-feedback-control mode". [2.1] In the "with feedback-control mode", user will pre-determine a certain force level limit between the probe and the sample surface for the entire surface scanning. In order to maintain this force level

limit during the scanning, a feedback system is used to control positioning piezo moving in up or down direction to adjust the separation between the probe and the sample surface. "With Feedback-control mode" is also known as "constant force microscopy", and usually it is used to yield topographical image.

In "without-feedback-control mode" referred as "constant height mode" the feedback system is not being used. The probe is set to a pre-determined height throughout the entire sample surface scanning. This mode is useful for imaging very flat surface at high resolution. [2.1]

2.1.2 Scanning Probe Microscopy - Atomic Force Microscopy – Contact Mode

Images can be obtained in two main classes of tip and sample interaction under AFM in "with feedback-control mode" or "without-feedback-control mode". These classes are "contact-mode" and "non-contact-mode". [2.1]

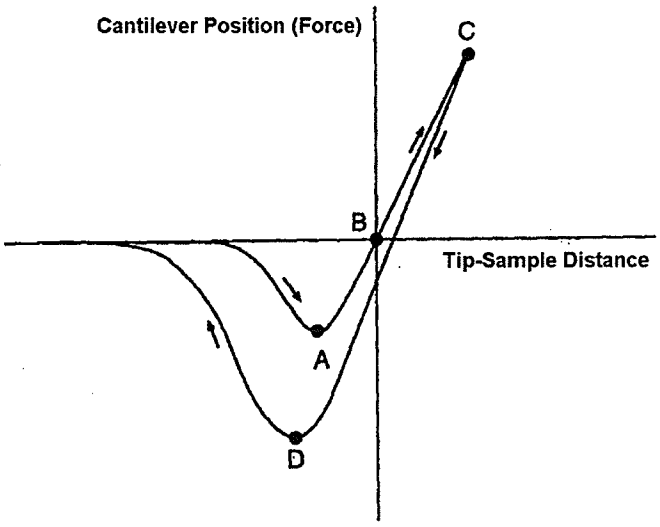

Figure [2.1] A plot of the intermolecular force versus probe sample distance.[2.5]

"Contact-mode" is when the tip and sample keep in close contact during the entire scanning process; it is the most common technique of AFM operation. In "contact-mode", image is formed by the contours of the constant force as the probe scans across the surface. So it is important for us to understand what these forces actually are as they contribute to the contours. As shown in *Figure [2.1]*, the inter-molecular force versus probe and surface distance. The curve appearing below the z-axis region represents the net attraction force between the cantilever and sample while the curve appearing above the z-axis region represents the net repulsive force.

To explain *Figure [2.1]*, we assume the sample is far away from the cantilever and the cantilever is in its rest position at the beginning. As we bring the sample closer to the cantilever, the cantilever bends toward the sample due to the attractive forces. Point A on the *Figure [2.1]* shows the maximum attractive force, which is the multiplication of the maximum forward deflection and the effective spring constant $\boldsymbol{k}$ of the cantilever. As the sample being brought forward, the sample pushes the cantilever back to its original rest position, as point B on the *Figure [2.1]*. If the cantilever is continually being brought forward, the cantilever will experience repulsive force until it reaches point C. If we reverse the sample direction by moving away from the cantilever, the cantilever will also experience force direction changes, passing through the maximum adhesive force, point D, and finally back to its rest position. In general the maximum attractive is always smaller than the maximum adhesive force due to meniscus forces hold the probe on the surface as the probe and the sample surface come to contact.[2.6] One disadvantage of using "contact-mode" is that there exist large lateral forces on the surface as the tip is "dragged" over the surface. This scanning mode is always operating in repulsive region

between the probe and the surface as shown in *Figure [2.1]*, it is the reason we also named it "repulsive-mode".

2.1.3 Scanning Probe Microscopy - Atomic Force Microscopy – Non-Contact Mode

"Non-contact-mode" or "attractive mode" operation is another method that we can employ when imaging by AFM. During "non-contact-mode" scanning, the interaction between the tip and the sample creates force gradient that will modify the resonant frequency of the cantilever. Changes in resonant frequency of cantilever can be detected by monitoring the change in amplitude, frequency and phase or forces of the vibrating cantilever. Since the shift in resonant frequency of a cantilever is corresponded to the force gradient, we can obtain the force gradient result between the tip and sample by observing the change of cantilever resonant frequency. "Non-contact-mode" AFM senses the force gradient between the tip and the sample rather than the interaction force between them, it has the advantages of enhancing the scanning resolution.[2.7] This scanning mode must take place at a certain distance above the surface because the tip is always vibrating. As a result the probe no longer operates in the repulsive regime of the inter-molecular force curve as shown in *Figure [2.1]*, and it is also named as "attractive-mode".

2.2 Magnetic Force Microscopy

Due to the rapid growth of the speed and density of integrated circuits (ICs), specific information of internal conductor voltages and currents during operation are crucial in detail analysis of integrated circuits. The ability to detect Quiescent current magnitude and its direction has become highly demanded in design verification; in analog

circuits analysis where most information conveyed by current and in failure analysis where current is the only detectable attribute.[2.8] We will study a non-invasive imaging technique for current based on "contact mode" and "non-contact mode" of AFM.

2.2.1 Magnetic Force Microscopy -Operation Principle

According to Ampere's Law, an obvious signature of current flow in a conductor is the induced "cylindrical" magnetic field about the conductor or in our case an integrated transmission line. *Figure [2.2]* displays a plot of current flow direction versus induced magnetic field. A simulation result of the magnetic field distribution of a transmission line is shown in *Figure [2.3]*.

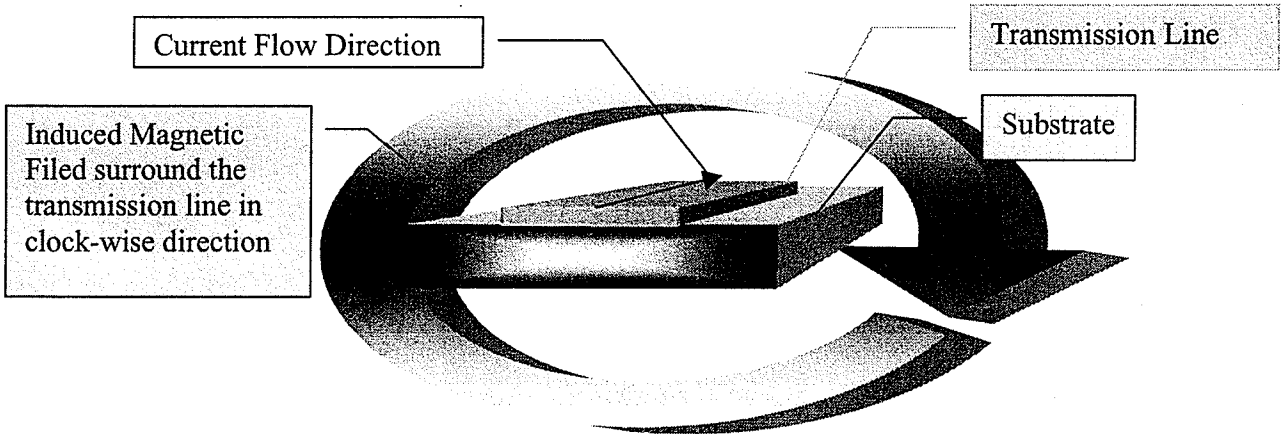

Figure [2.2] A plot of the cylindrical magnetic field about a transmission line.

Figure [2.3a] below, shows the cross section of a transmission line and the simulated magnetic field $\vec{B}$ outside the conductor. Field components in x direction are tangential components, which contribute to the least normal magnetic field. Maximum normal magnetic field is contributed by field components in z direction. *Figure [2.3b]*

shows the normal component of the magnetic field. The maximum normal magnetic field strength at a constant distance Zo from the transmission line is represented by the curve of the graph. At Yo where the middle of the cross section transmission line, the normal magnetic field vanishes. At the same location the polarity of the normal magnetic field component changes. *Figure [2.3c]* shows the top view of the normal magnetic field plot.

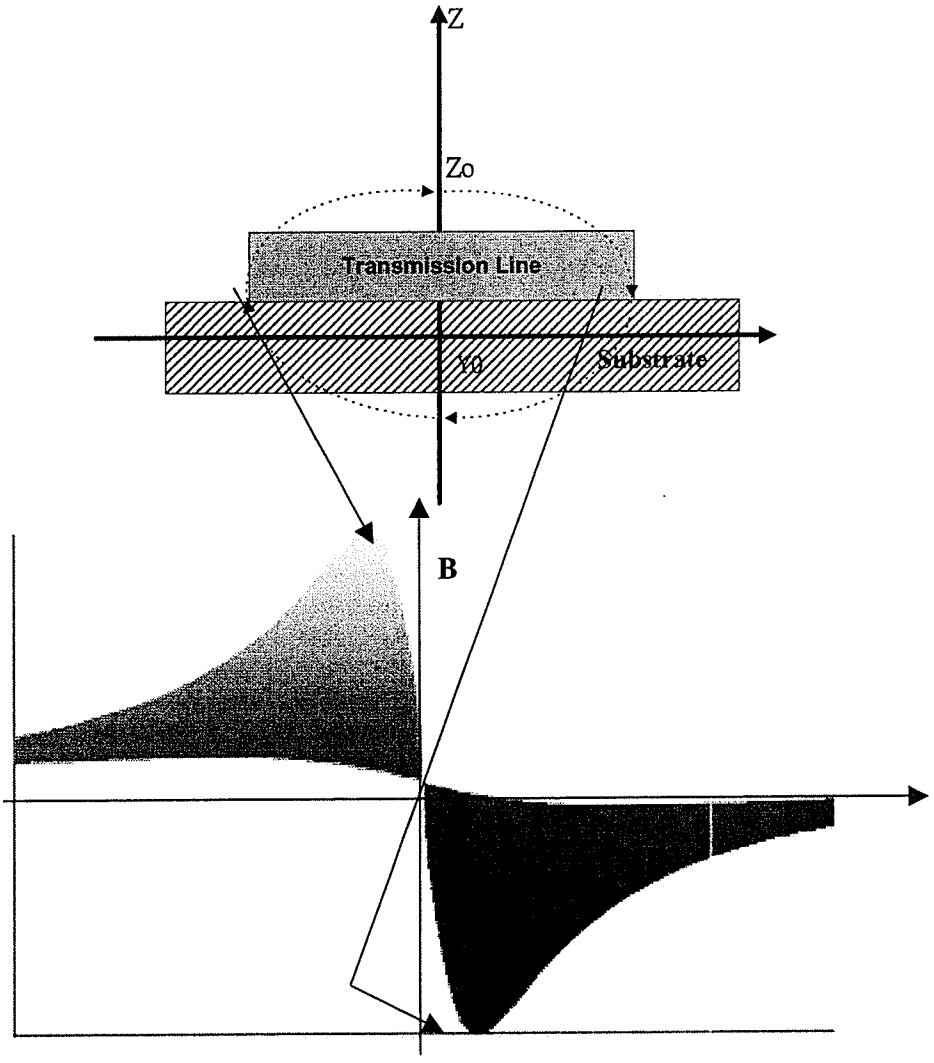

Figure [2.3] a) A plot of cross section transmission line on a substrate, the direction and location of the induced magnetic field are shown.

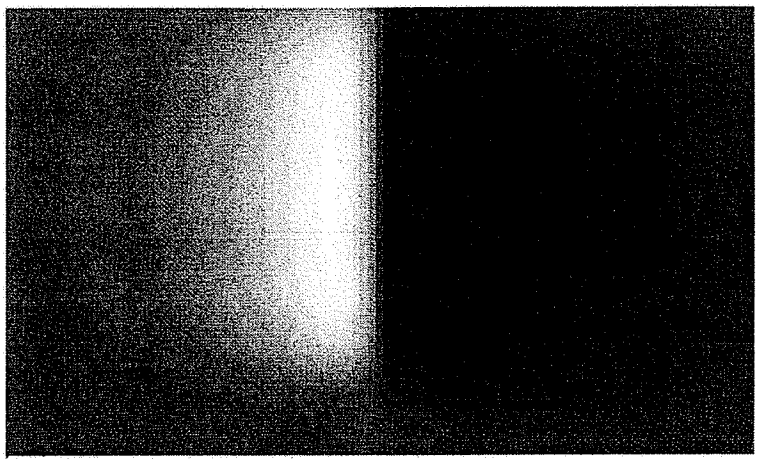

Figure [2.3] b) Shows the normal component of the simulated magnetic field

2.2.2. Magnetic Force Microscopy – Contact Mode Operation Principle

MFM is a member of the Atomic Force Microscopy family. A topographic image of the sample can be obtained by scanning with a sharp probe tip in "Contact Mode" as what is shown in *Figure [2.4]*.

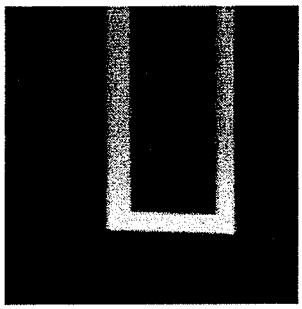

Figure [2.4] An image obtained by MFM contact mode. Probe scanned over a 6μ width NT25 metal3 line.

Tip is brought as close as possible to the sample. The repulsive force, which resulted from the short-range interaction of electron clouds of atoms between the tip and the sample, causes the cantilever to deflect in z direction.

As what has been mentioned earlier, an optical beam bounce detection technique is used to measure the z-deflection of the cantilever. During imaging the sample in x and

y direction, z-feedback control reads the z-deflection of the cantilever and adjusts the separation between the tip and sample to maintain a constant predetermined force between the two. Force interaction between the tip and sample surface can be extracted from the z-deflection of the cantilever and finally a topographic image of the sample is formed as we plot the sample height as a function of the sample x and y position, as is shown in *Figure [2.4]*

2.2.3 Magnetic Force Microscopy –Non-Contact Mode Operation Principle

In "non-contact" MFM, tip is moved 50nm-3000nm away from the surface of the sample. As MFM setup is intended to be sensitive to magnetic property of the sample surface, we will acquire the magnetic field on the sample, magnetic dipole on the tip, interaction force between the two and Relative-Interaction-Force detected by the optical beam bound system. However, it is important to note that other forces particularly electrostatic forces can also significant.

2.2.4 Magnetic Force Microscopy – Non-Contact Mode Operation Principle -Magnetic Field Induction

As voltage supply (***Vs***) is applied to the sample circuit, current (***Is***) flows through the sample circuit. According to the Biot-Savart law [2.9], at point ***P*** where the observation point, the magnetic field induction $d\vec{B}$ due to the current flow in the sample circuit at the position ***P'*** of the sample circuit is as the following equation *E2.2* and *Figure [2.5]*.

$$d\vec{\mathbf{B}} = \frac{\mu_0}{4\pi}\frac{Id\vec{l}\times\vec{r}_l}{r^2} \quad \text{[E2.2]}_{[2.10]}$$

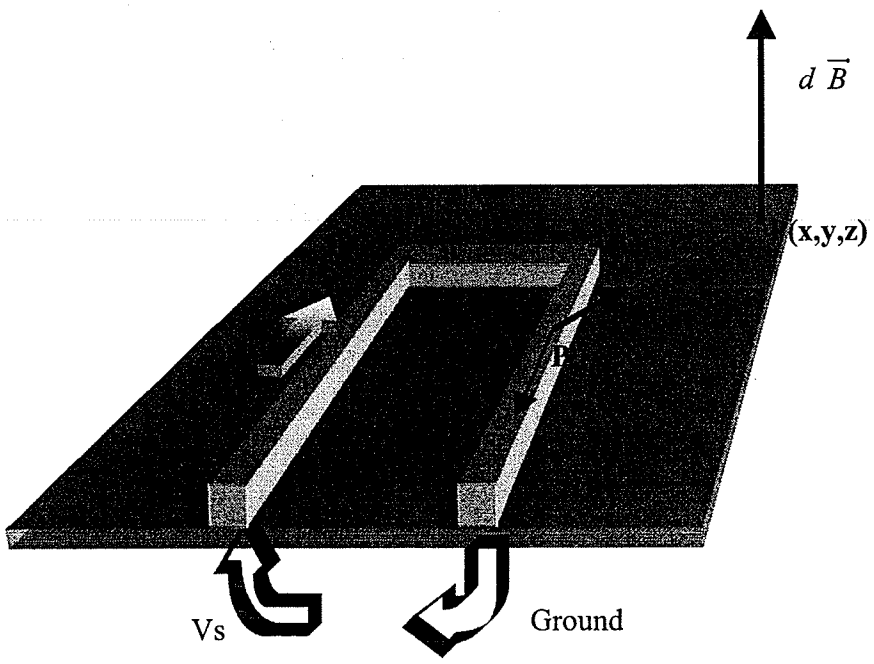

Figure [2.5] A figure of how Biot-Savart law is implemented in our application.

μ_0 is the permeability of free space, which is equal to $4\pi\times10^{-7} Wb/A.m$, r_1 is the unit vector points from the source to the observation point. $\vec{dl}$ is the vector of current element and r is the distance from source to the observation point.

The Biot-Savart law can define the magnetic field at a point on the sample due to a small segment of the transmission line, to find the total magnetic field $\vec{B}$ at a point on the sample due to the entire transmission line, we have to sum-up all the $d\vec{B}$ induced by each segment of the transmission line with equation *E2.3* which is displayed as follows. MathCAD can simulate an image of Z-magnetic field over the entire sample surface generated by the transmission line as what is shown in *Figure [2.6]*

$$\vec{B} = \frac{\mu_0 I}{4\pi}\int\frac{d\vec{l}\times\vec{r}}{r^2} \quad \text{[E2.3]}$$

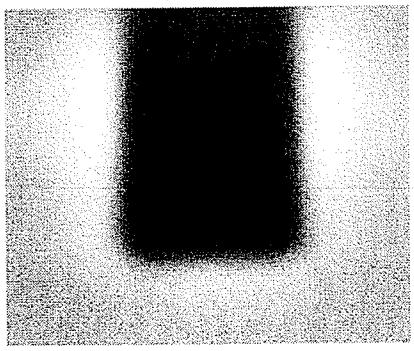

Figure [2.6] A figure displayed Biot-Savart law is simulation. Dark region represents magnetic field circulate into the page, bright region represents the magnetic field circulating out of the page.

2.2.5 Magnetic Force Microscopy –Non-Contact Mode Operation Principle -Magnetic Dipole Moment

A tip deposited with ferromagnetic material is used in this microscopy. All ferromagnetic materials contain microscopic regions called domains, which all magnetic dipole moments $\vec{m}$ within the domain are aligned. As we magnetized the ferromagnetic material on the tip by applying an external field using a magnetic bar, the domains in the ferromagnetic material tend to align with the field, giving the tip a net magnetization vector $\vec{M}$, which has the magnitude equal to the magnetic moment per unit volume of the substance. [2.11] Under the right conditions, these domains becomes aligned resulting in a net magnetic moment on the tip.

2.2.6 Magnetic Force Microscopy –Non-Contact Mode Operation Principle-Interaction Force

As we apply a current to the sample circuit on the surface, a magnetic field is induced. We than bring the tip that has been magnetized closer to the sample surface. Force occurs when the magnetic dipole of the tip interacted with the magnetic field on the sample surface. Since the magnetic dipole on the tip has been aligned and stabilized, the

main factor for determining an attractive force or repulsive force is due to the direction of the magnetic field on the sample surface. Magnetic force formula *E2.4*, can be used to explain and support the existence of this interaction force between the tip and the sample surface.

$$\vec{F} = nq\vec{\upsilon}_d \times \vec{B} \text{ [E2.4]}_{[2.12]}$$

According to the Magnetic Force formula, the magnetic force is in a direction perpendicular both to the velocity of the moving charge and to the magnetic field. This property can be used to define the interactive force that exists between the sample circuit and the magnetic tip, by taking the cross product of bound current $\vec{J}_b$ and the magnetic field $\vec{B}$ which is produced by the sample circuit. E2.5 is substituted into E2.4 to produce E2.6.

$$\nabla \times \vec{M} = \vec{J}_b \text{ [E.2.5]}_{[2.13]}$$

$$\vec{F} = \nabla(\vec{M} \cdot \vec{B}) \text{ [E2.6]}_{[2.14]}$$

2.2.7 Magnetic Force Microscopy –Non-Contact Mode Operation Principle -Relative-Interaction-Force

Due to optical beam bound system is used to detect the deflection of the cantilever, the result we obtained from the system is no longer the interaction force but the Relative-Interaction-Force. A detail study on the beam bound system concept will be discussed in Chapter3 and simulation will be presented in Chapter5.

$$\vec{F_r} = \vec{F}_{ini} - \vec{F} \text{ [E2.7]}$$

$\vec{F}_{ini}$ is the interaction force at the location on the sample surface where the tip was initially rested on. At this location we adjust the bi cell photodiode position to achieve zero voltage on the output before we start our scanning. As a result, all obtained result $\vec{F}_r$ is referenced by this initial interaction force value. *E2.7* is the equation we use to express this situation.

Chapter 3

Magnetic Force Microcopy Implementation

In this chapter, we will present and discuss the implementation of Magnetic Force Microscopy used in this work. We will start by discussing cantilever characterization, optical beam bounce deflection sensors, mechanical probing structure, tip magnetization, test circuit structure design and signal acquisition system.

3.1 Cantilever Characterization

Mechanical properties of the cantilever play a very essential role in the spatial, current sensitivity resolution of the instrument. In particular the spring constant and the frequency response of the cantilever are crucial.

3.1.1 Cantilever Characterization-Spring Constant

Spring constant of a cantilever fixed at one end is given by:

$$k = \frac{3EI}{l^3} \quad [\text{E3.1}]_{[3.1]}$$

l is the length of the cantilever, E is the modulus of the elasticity which is depending on the material composition of the cantilever. I is the moment of inertia, which is different for various cross sections of the cantilever. If we have a cantilever with a rectangular cross section of width w and thickness t, the moment of inertia is $I = \frac{wt^3}{12}$. The spring constant of this cantilever is

$$k = \frac{Ewt^3}{4l^3} \quad \text{[E3.2]}_{[3.2]}$$

In this experiment, the spring constant of the cantilever we use will remain the same as provided by the manufacture. The properties of the ferromagnetic material (γ–Fe_2O_3) we deposited are, H_c=305O_e, length of the particle is 0.6μm and the aspect ratio is 7:1. Due to the extra weight we added on the tip when we deposit γ–Fe_2O_3 on top of the cantilever the $\sqrt{\frac{k}{m}}$ ratio will be reduced. To define the effective spring constant of the cantilever is no longer as straight forward as E 3.2 because elasticity modulus is no longer unique and evenly distributed. The equation we use to define the added mass of γ–Fe_2O_3 is E 3.3 and E 3.4 is used to define effective spring constant of the added mass cantilever.

$$\omega_r = \omega_0 \left(1 - \frac{F'}{k}\right)^{\frac{1}{2}} \quad \text{[E 3.3]}_{[3.3]}$$

$$\omega_r = \left(\frac{k_{eff}}{m + m_{eff}}\right)^{\frac{1}{2}} \quad \text{[E 3.4]}_{[3.3]}$$

3.1.2 Cantilever Characterization-Frequency Response

The mechanical frequency response of the cantilever is a function, which contributes to the deflection of the cantilever. The cantilever has the tendency to vibrate at its natural resonant frequency. The cantilever will vibrate at its maximum amplitude if the frequency of the applied force is equal to the cantilever natural resonant frequency.

The fundamental resonant frequency of a vibrating cantilever with a rectangular cross section, ω_r, is given by;

$$\omega_r \approx \sqrt{\frac{k}{0.24\rho wtl + m_{eff}}} \quad [E\ 3.5]_{[3.1]}$$

ω_r can also be expressed as $\omega_r = 2\pi f_r$, k is the spring constant, and ρ is the mass

density of the material composition of the cantilever. When an external force with unit amplitude is applied on the cantilever, the vibration of the cantilever as a function of frequency response is

$$|G(\omega)| = \frac{(\frac{Q}{k})(\frac{\omega_r}{\omega})}{\sqrt{1 + Q^2(\frac{\omega_r}{\omega} - \frac{\omega}{\omega_r})^2}}, \omega > 0;,$$

$$|G(\omega)| = \frac{1}{k}, \omega = 0 \quad [E\ 3.6]_{[3.1]}$$

Q is the quality factor which is a measure of how fast energy is dissipated by the system. It is defined as $\frac{\omega_r}{\Delta\omega}$, with $\Delta\omega$ being the $3dB$ bandwidth from the resonance [3.27]. The deflection of the cantilever due to the force F_z can be defined as follows:

$$\Delta z(\omega) = F_z(\omega)\frac{(\frac{Q}{k})(\frac{\omega_r}{\omega})}{\sqrt{1+Q^2(\frac{\omega_r}{\omega}-\frac{\omega}{\omega_r})^2}},\ \omega>0;$$

$$\Delta z(\omega)\big|_{\omega=0} = \frac{F_z}{k} \text{ [E 3.7]}$$

If the driving frequency is equal to the resonance frequency $\omega=\omega_r$, the cantilever deflection can be defined as:

$$\Delta z\ |_{\omega_r} = \frac{Q}{k} F_z\ |_{\omega_r} \text{ [E 3.8]}$$

The magnitude of the vibration at the resonance frequency ω_r, is enhanced by Q from the DC vibration magnitude.

3.1.3 Cantilever Characterization-Micromachined Cantilever

An ideal cantilever for probing should have a high resonance frequency and quality factor, low in mass and spring constant. A cantilever with high resonance frequency is less susceptible to low frequency noise; it also has a better spatial resolution and less parasitic loading if a smaller cantilever is used. The sensitivity of the measurement will increase, if the spring constant of the cantilever we used is lower, due to less forces are needed to induce deflection of the cantilever. [3.4]

The micromachined cantilever we used in this experiment is a V-shaped silicon nitride (Si_3N_4) cantilever as shown in *Figure [3.1]*.

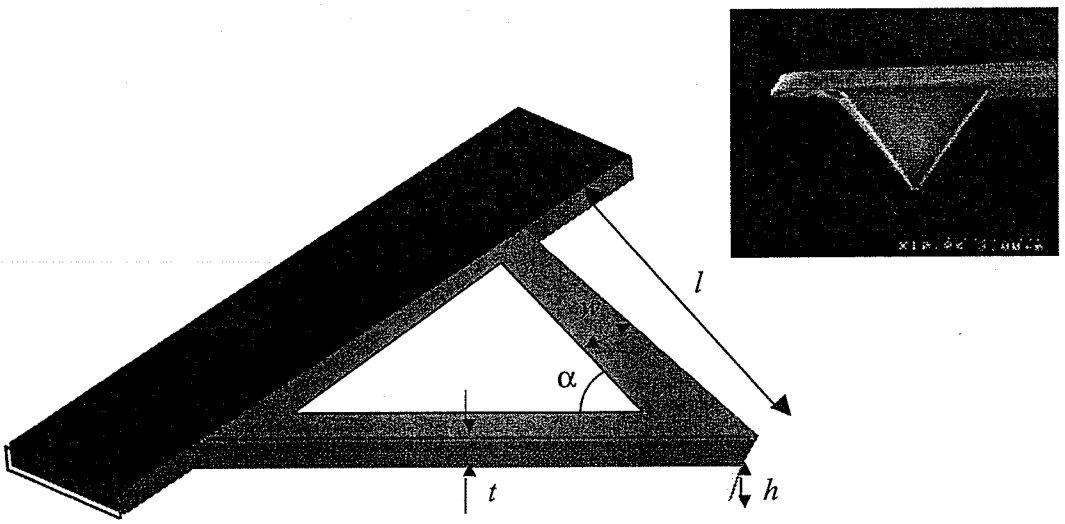

Figure [3.1] A diagram of the micromachined Si_3N_4 cantilever. [3.5]

The length (l) of the cantilever is 200μm, the height (h) of the tip is about 3-5μm, the width (w) of the cantilever is 36μm, and the thickness of the cantilever (t) is 1μm. The radius curvature of the tip is about 300nm, which is used to define the sharpness of the tip. A thin gold film is coated on the cantilever for the sake of better optical reflection. [3.5]

Figure [3.2] is the frequency response of the Si_3N_4 cantilever. The experimental curve was found by measuring the thermally induced frequency spectrum of cantilever vibration. It is the intrinsic cantilever vibration induced by thermal noise. The Si_3N_4 cantilever has a resonant frequency of 12.275kHz. The spring constant of the cantilever is 0.064N/m with tolerant of +/-20% according to specifications from the manufacture. *E 3.6* is used to determine the value of quality factor by substituting the most appropriate value of Q to match the experimental frequency response. The Si_3N_4 cantilever has a Q=32. [3.6] This Q factor determination work was done by a former graduate student in our department.

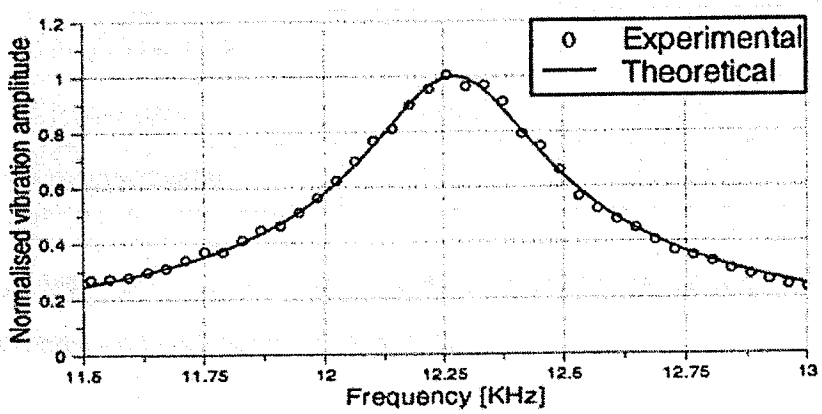

Figure [3.2] Normalized mechanical frequency response of the Si_3N_4 cantilever for this experiment. Resonant frequency=12.275kHz, k=0.064N/m +/-20%, Q=32 [3.6]

3.1.4 Cantilever Characterization-Spatial Resolution

Spatial resolution defines the region from which the instrument gathers information. This is an important parameter given that small size of present day integrated circuit. Spatial resolution of MFM depends on the separation between the tip to sample and the properties of the magnetized tip as well as the properties of the stray field distribution.

There are some limitations that prevent us to use tip to sample separations that are very small. For alternative current detection methods which we use in this experiment, the tip to sample separation cannot be smaller than the oscillation amplitude of the cantilever. If the tip to sample separation is chosen too small, the derivative of the force between the tip to sample will become too large and exceed the cantilever spring constant and create undesired instabilities. As a result, we chose the tip to sample separation to be around 1000nm at the expense of a reduction in sensitivity. [3.7]

Since in MFM, we are imaging the interaction force between the tip and sample and we assume current is always flowing at the middle of transmission line, current sensitivity has played a vital role in defining the limitation of our MFM system.

3.1.5 Cantilever Characterization-Tip Magnetization

As we have mentioned before, the micromachined cantilever we use in this thesis is a V-shaped silicon nitride (Si_3N_4) cantilever. In order to perform MFM, we need to magnetize the tip. We manually deposit some γ–Fe_2O_3 powder which is a single domain particle on the backside of the tip. We then magnetized the tip with a permanent magnet. The magnetization of the magnet (magnetic dipole per unit volume within the magnetic material) is estimated to be 300k A/m. We then baked it at 125 degree for two hours until the adhesive dry as shown in *Figure [3.4]*. We assumed all γ–Fe_2O_3 particles have aligned in single direction and fixed permanently by the epoxy.

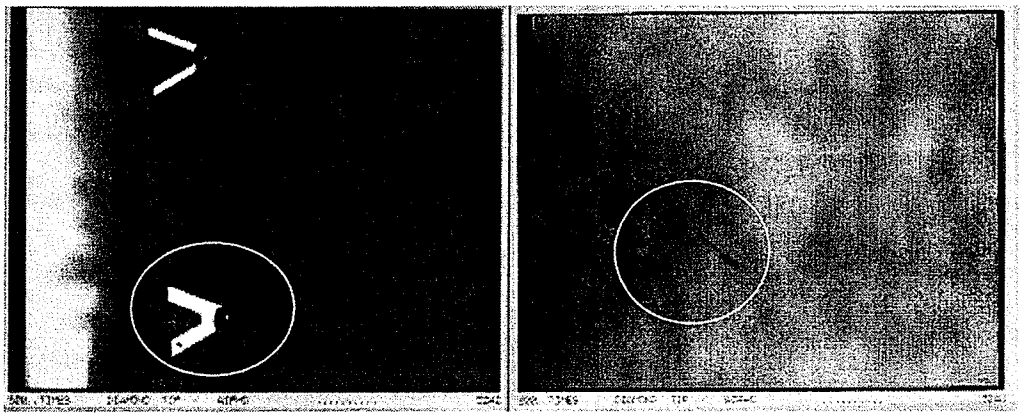

Figure [3.4] Picture taken form microscope on the tip that has been deposited with γ–Fe_2O_3. Probes are facing down.

In order to determine the value of the magnetic moment on the tip we like to define the mass of the γ–Fe_2O_3, which we deposited on the tip. As mentioned in the previous

section 3.1.3, we know the resonant frequency of the Si_3N_4 cantilever without any γ–Fe_2O_3 deposition is 12.275kHz and the spring constant of the cantilever is 0.064N/m according to specifications from the manufacture. After having γ–Fe_2O_3 deposition on the tip, we found that the resonant frequency of the Si_3N_4 cantilever has shifted to 7.4kHz. The mass on the tip can then be calculated by *E 3.3* and *E 3.9*. The typical range for ∂z is from 1nm to 10nm, which is the deflection range of the cantilever. [3.9] Using *E 4.6* from Chapter4, we find that the maximum deflection range for $4mA_{pp}$ test-scenario dose not exceeded 1nm. g in *E 3.9* is the gravity force, 9.807 kg/s^2 .

$$\omega = \omega_0 \left(1 - \frac{F'}{k}\right)^{\frac{1}{2}} \quad \text{[E 3.3]}$$

$$F' = \frac{m_{eff} \cdot g}{\partial z} \quad \text{[E 3.9]}$$

m_{eff} is calculated as 4.155E-12 kg. According to this reference book[3.10], the magnetic moment per atom (P_A) of γ–Fe_2O_3 is $5\mu_B$, which is obtained from neutron diffraction measurements in the ordered state. [3.10] Since μ_B=9.27e-24 Am^2, the magnetic moment per atom of γ–Fe_2O_3 is 46.35e-24 Am^2.

The molecular weight of γ–Fe_2O_3 is 231.54g.[3.11] We can obtained the number of γ–Fe_2O_3 atom which has been deposited on the tip by dividing the molecular weight by Δm and multiplying by the Avogadro constant. The number of γ–Fe_2O_3 atoms we obtained from this calculation is 10.808+E9. Finally, as we multiply the magnetic moment per atom of γ–Fe_2O_3 with the number of atoms, we estimated the maximum magnetic moment of the tip, which is 5e-13 Am^2.

3.2 AC Stimulation

In this work, we utilize an AC detection method. We supply an AC signal at cantilever resonant frequency to the sample, not to the cantilever. The polarity of the magnetic field induced by the AC current alters at the resonant frequency of the cantilever. Due to the fact that the signal polarity oscillates at the resonant frequency, the induced attraction and the deflection force between the tip and sample is also alters at this frequency. The cantilever is then oscillated at the resonant frequency. The current sensitivity of the system is increased about 250 times compared to DC stimulation. [3.28] The amplitude of the cantilever vibration, A, of a simple harmonic oscillator with external force applied can be expressed as:

$$A\alpha\frac{1}{(\omega_0^2-\omega_1^2)} \quad \text{[E 3.10]}_{[3.12]}$$

ω_0 is the resonant frequency of the cantilever. ω_1 is the frequency that drove the cantilever. When ω_1 approaches ω_0 the amplitude of the vibration, A, increases dramatically. With a lock in amplifier in the system, we can amplify the signal detected from the beam bounce detection system according to the reference signal phase. The final output from the lock-in amplifier is the Relative-Interaction-Force between the tip and sample surface.

3.3 Optical Beam Deflection Sensor

An optical beam bounce detection system [3.13] is employed in this experiment. *Figure [3.5]* portrays the method. The laser beam from a laser source is directed on the

top of the gold-coated cantilever. A bi-cell photodiode is used to capture the reflection of the laser beam from the cantilever.

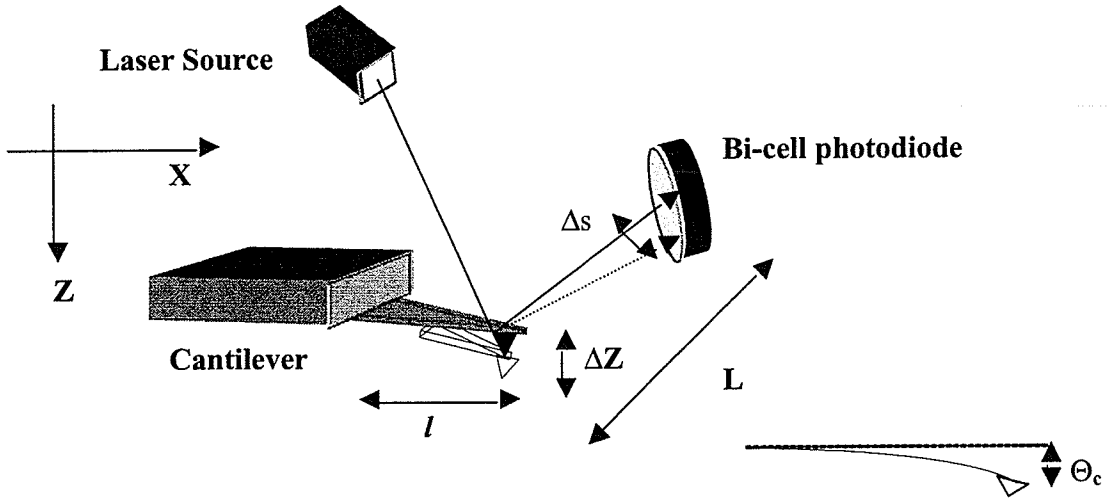

Figure [3.5] Illustrating how the cantilever reflection is detected by the laser beam bounce system.

When a vertical force ***F*** is applied to the cantilever, the deflection of the cantilever is as the following equation. [3.14]

$$z(x) = \frac{F}{6EI}(3lx^2 - x^3) \text{ [E 3.11]}$$

l is the length of the cantilever, ***E*** is the modulus of elasticity, and ***I*** is the moment of inertia of the cantilever. Due to the very small deflection magnitude of the cantilever, the angle of the deflection Θ_c at the end of the cantilever where x=***l***, can be approximated as follows:

$$\Theta_c \approx \left.\frac{dz}{dx}\right|_{x=l} = \frac{Fl^2}{2EI} \text{ [E 3.12]}$$

By using equation *E 3.1* and substituting $F = k\Delta z$, we obtain:

$$\Theta_c \approx \frac{3}{2}\frac{\Delta z}{l} \text{ [E 3.13]}$$

Δs in *Figure [3.5]* represents the displacement of the reflected laser beam on the bi-cell photodiode which causes by Δz (the deflection of the cantilever). By using similar triangles, we can find that $\Theta_c \approx \frac{\Delta s}{L}$ [E 3.14] [3.15], where the distance between the bi-cell photodiode and the cantilever is L. Therefore the result is:

$$\Delta s \approx \frac{3L\Delta z}{2l} \text{ [E3.15]}_{[3.15]}$$

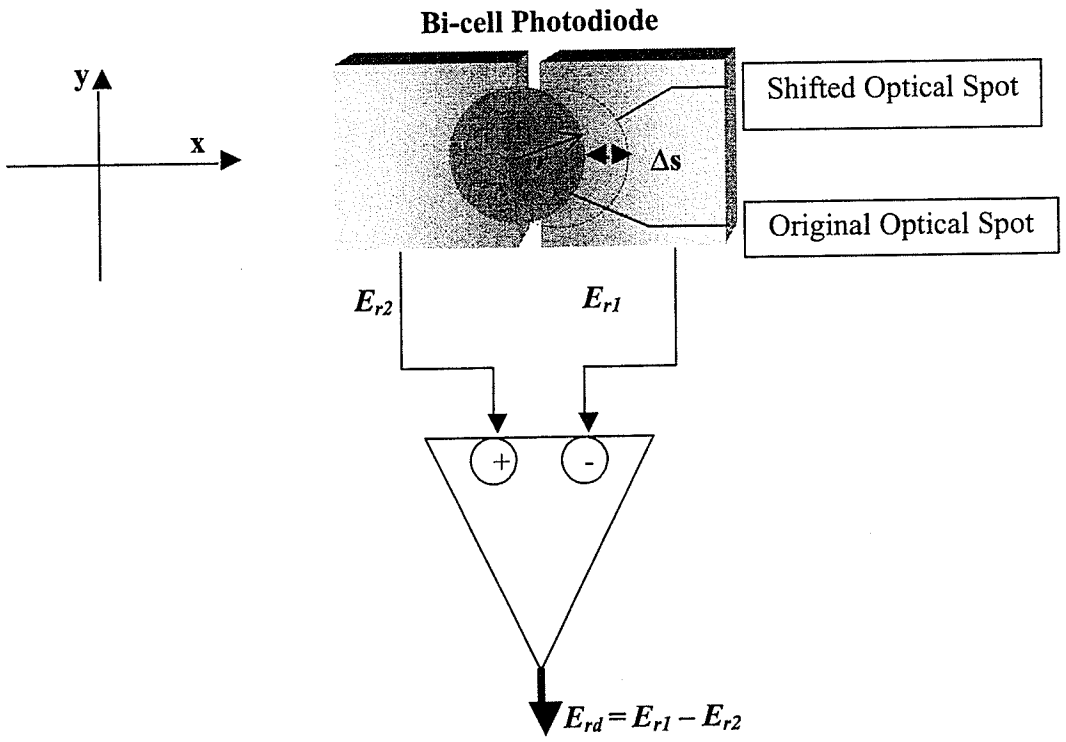

Figure [3.6] Illustrating the shift of ΔS due to cantilever reflection. Output from differential amplifier is the difference between the optical signals received by the bi cell photodiode.

The bi-cell photodiode position is adjusted to where both photodiodes receive equal optical power from the reflected laser beam and hence E_{rd}=0. Whenever the cantilever defects by Δz, the reflection laser beam will shift by Δs, and it will cause either one of the photodiode receiving more power than the other. From *Figure [3.6]*, we can see that the voltage output from the differential amplifier E_{rd} is the difference between E_{r1} and E_{r2}. Every single Δz shift of the laser beam will no only increase the photocurrent on one of the cell but would also cause a photocurrent decrease on the other cell at the same time. As a result, each single cantilever deflection would bring double effect to E_{rd}.

Unlike others A.C. detection methods, the force gradient is measured through the detection of changes in the amplitude of oscillation of the cantilever at a given frequency. In our experiment, each E_{rd} is directly taken down as the interaction force between the tip and the sample in term of voltage because E_{rd} from the bi cell photodiode is directly linked to amplitude of the tip deflection which is also directly linked to the interaction force. One thing we have to take care of is the reference point. Since we assume the interaction force at the initial tip location is made to be zero by adjusting the reflected laser beam to the center of the bi cell photodiode, this initial interaction force become a reference to all obtained results. *Figure [3.7a]* is an example showing how the shape of the curve is shifted when Relative-Interaction-Force is taken into account on interaction force.

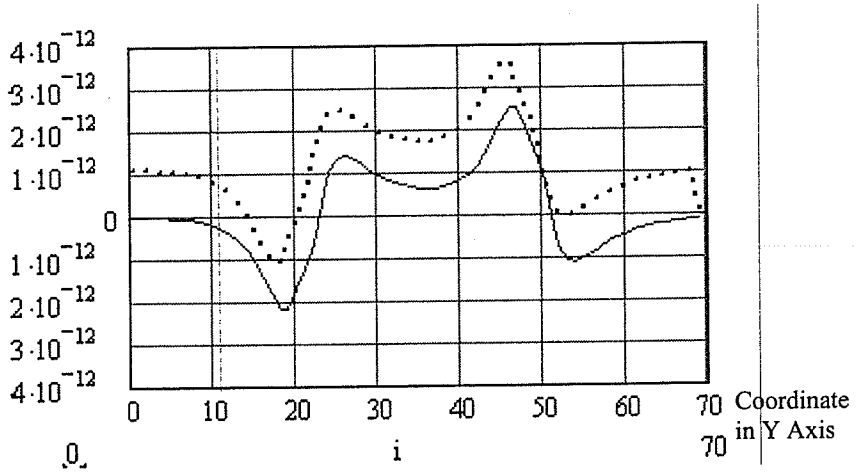

Figure [3.7a] Red line plot is the cross section view of interaction force taken from the center of the sample. Blue line plot is the cross section view of Relative-Interaction-Force of Red line, which i =14 of Red line is taken as reference.

Figure [3.7b] is an example showing the sensitivity of the Force Gradient method and how the sensitivity of this method has dominated the overall result.

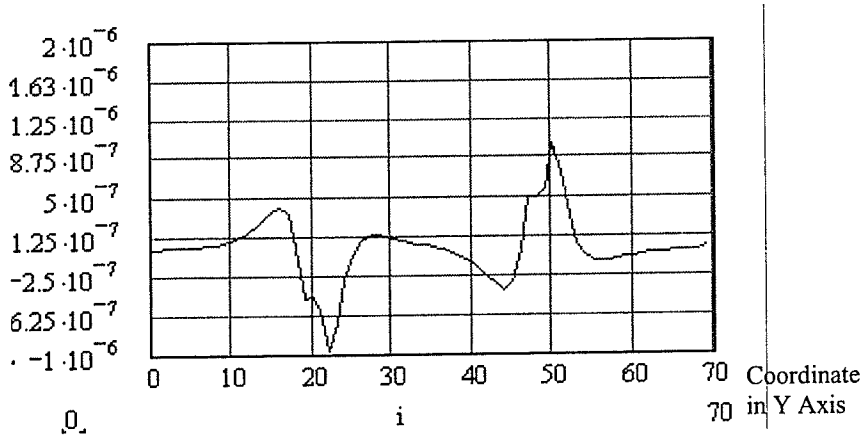

Figure [3.7b] Show the plot of force gradient ($\frac{\partial F_z}{\partial y}$) of the interaction force (red line plot on Figure [3.7a]). The amplitude of the signal is about 1000 times stronger. Y is the scanning direction.

A Laser diode is used as the optical source in this experiment. The laser beam is assumed to be monochromatic and possess a Gaussian power distribution. The optical power per unit area, or the irradiance distribution of the Gaussian laser beam is:

$$E_r = E_0 e^{\frac{-2r^2}{r_0^2}} = E_0 e^{\frac{-2}{r_0^2}(x^2+y^2)} \quad \text{[E 3.16]}_{[3.16]}$$

E_0 is the irradiance at the center of the laser beam and r_0 is the radius of the laser beam where the irradiance falls to $\frac{1}{e^2}$ from E_0. The total accumulated photocurrent is equal to the total number (N) of photons penetrating the photodiode multiplied by the unit charge q. We assume all optical power received by the photodiode is completely converted into electrical power. As the cantilever deflects, the reflected laser beam will shift away from its original spot, by neglecting the spacing between the two cells, the gained current by one cell will be similar to the lost current by the other cell. The total photocurrent produced by the bi-cell photodiode will always remain the same. The difference in photocurrent between the two halves of the bi-cell, I_d, can be calculated by integrating the normalized Gaussian laser beam over the gained area of the cell due to the shift Δs.

$$I_d = 2Nq \int_0^{\Delta s} \int_{-Y}^{Y} \frac{e^{\frac{-2}{r_0^2}(x^2+y^2)}}{(\frac{\pi}{2})r_0^2} dxdy \quad \text{[E 3.17]}_{[3.15]}$$

Y is the size in y dimension of the gain area. Due to $Y >> r_o$, we can simplify equation *E 3.17* as follows:

$$I_d \approx \frac{4Nq}{r_o^2 \pi} \int_0^{\Delta s} e^{(\frac{-2}{r_0^2})x^2} dx \int_{-\infty}^{\infty} e^{(-\frac{2}{r_0^2})y^2} dy \text{ [E 3.18]}_{[3.17]}$$

According to mathematical table provided by [3.18] ;

$$\int_{-\infty}^{\infty} e^{(-\frac{2}{r_0^2})y^2} dy = \sqrt{\frac{\pi}{2}} r_o \text{ [E 3.19]}$$

As a result;

$$I_d \approx \frac{2\sqrt{2}Nq}{r_o\sqrt{\pi}} \int_0^{\Delta s} e^{(\frac{-2}{r_0^2})x^2} dx \text{ [E 3.20]}$$

Using change in variable by letting $t = \sqrt{2}\frac{x}{r_o}$, equation [E 3.20] can be as follows;

$$I_d \approx \frac{2\sqrt{2}Nq}{r_o\sqrt{\pi}} \int_0^{\sqrt{2}\frac{\Delta s}{r_o}} e^{-t^2} dt \text{ [E 3.21]}$$

By referring to the mathematical table [3.18], the equation can be solved as follows:

$$I_d \approx \frac{\sqrt{2}Nqerf}{r_o}\left(\frac{\sqrt{2}\Delta s}{r_o}\right) \cong \frac{2Nq\Delta s}{r_o^2\sqrt{\pi}} \text{ [E 3.22]}$$

Using *E 3.15*, the photocurrent I_d can be expressed as a function of the cantilever deflection Δz;

$$I_d \approx \frac{2Nq\Delta s}{r_o^2\sqrt{\pi}} \approx \frac{3LNq}{lr_o^2\sqrt{\pi}}\Delta z \text{ [E 3.23]}$$

From the equation *E 3.23*, the relative changes in the difference output signal of the detection system can be interpreted as the corresponding change in the cantilever deflection.

The performance of the optical beam deflection sensor we use in this experiment is mostly limited by the shot noise, which is created by the random photons arrival at the detector. Shot noise can be defined as *E 3.24* by W. Schottky in 1918.

$$i_{SN} = \sqrt{(2q(I_1 + I_2)B} \text{ [E3.24]}_{[3.19]}$$

where B is the noise bandwidth, I_1, I_2 are the current from the bi-cell photodiode. We can minimize the impact by compromising the geometry of the detection system, which is r_o. However, our optical beam bounce system is insensitive to 1/f noise because it is a differential type of measurement. The output signal is derived from the difference between the photocurrent from the two halves of the bi cell photodiode. [3.15] The sensitivity of the optical beam-bounce system was hypothetical to be

$$\frac{7.9x10^{-6}nm}{\sqrt{Hz}} \text{ in } [3.20].$$

In the next section we will show that shot noise is typically not the dominant source of noise in MFM measurements.

3.3.1 Optical Beam Deflection Sensor-Current Sensitivity

Current sensitivity is defined as the minimum root-mean-square current that can be detected by the instrument. Any signal detected by the deflection sensor that is not induced by the magnetic force between the tip and the sample is considered as noise. Among the sources of noise, typically thermal noise is the most dominant effect and is fundamental source of noise.

Thermal noise results from the cantilever being in thermal equilibrium with its surrounding and hence having some thermal energy. This energy caused the cantilever to vibrate in a random manner. The RMS deflection of the cantilever due to thermal noise can be expressed as a function of frequency as follows. [3.22]

$$\left[\Delta Z_{th}^2\right]^{\frac{1}{2}} = \sqrt{\frac{4Qk_BT_mB}{k\omega_r}} \quad \text{[E 3.25]}$$

k_B is the Boltzman constant, T_m is the temperature of the cantilever and B is the bandwidth of the measuring system.

Since our Si_3N_4 cantilever effective spring constant is no longer k=0.064 N/m +/- 20%, *E 3.4* is used to find the effective spring constants k_{eff} and the mass of the cantilever without deposition, m=10.76e-12kg.

$$\omega = \left(\frac{k_{eff}}{m+m_{eff}}\right)^{\frac{1}{2}} \omega_0 = \left(\frac{k}{m}\right)^{\frac{1}{2}} \quad \text{[E 3.4]}$$

With m_{eff}=4.155e-12kg, Q=32, resonant frequency of the cantilever deposited with magnetic powder is around 7.4kHz, k_{eff}=0.032 N/m +/-20%. At room temperature, the maximum deflection due to thermal noise is $0.03\frac{nm}{\sqrt{Hz}}$. This finding proves to us that thermal noise has dominant effect to the overall noise as compared with the short noise which was defined as $\frac{7.9x10^{-6}nm}{\sqrt{Hz}}$. As a result, Signal to Noise Ratio (SNR) and current sensitivity of the instrument will be estimated based on thermal noise. Since the cantilever is always oscillating at its resonant frequency, ω_r, the SNR of the instrument can be defined as:

$$SNR = \frac{(\Delta Z_F)}{(\Delta Z_{th})} \text{[E 3.27]}$$

(ΔZ_F) is the cantilever RMS deflection by the magnetic force, it can be derived from *[E 3.8]*, *[E2.21]* and *[E2.3]*.

$$\Delta z\,|_{\omega_r} = \frac{Q}{k} F\,|_{\omega_r}, \text{[E 3.8]}$$

$$F = \nabla(\vec{M}\cdot\vec{B}) \text{ ,[E2.21]}$$

$$B = \frac{\mu_0 I}{4\pi}\int \frac{d\vec{l}\times\vec{r}}{r^2} \text{ [E 2.3]}$$

$$(\Delta Z_F) = \left[\frac{Q}{k}\left(\vec{M}_z\left[\frac{\partial\vec{B}_z}{\partial z}+\frac{\partial\vec{B}_y}{\partial z}+\frac{\partial\vec{B}_x}{\partial z}\right]+\vec{M}_y\left[\frac{\partial\vec{B}_z}{\partial y}+\frac{\partial\vec{B}_y}{\partial y}+\frac{\partial\vec{B}_x}{\partial y}\right]+\vec{M}_x\left[\frac{\partial\vec{B}_z}{\partial x}+\frac{\partial\vec{B}_y}{\partial x}+\frac{\partial\vec{B}_x}{\partial x}\right]\right)\right] \text{[E3.28]}$$

The current sensitivity can be determined when we equate the RMS deflection of the cantilever due to thermal noise to the RMS deflection due to the magnetic force:

$$(\Delta Z_F) = (\Delta Z_{th}) \text{[E 3.29]}$$

Since the magnetic field for each point on the sample is influenced by each segment of the transmission line as stated in Biot-Savart Law, it is not easy to calculate I_{th} for (ΔZ_F)=0.03nm. We have used MathCAD to simulate the magnetic forces. The result showed of I_{th}=17.3μA, for a transmission line with 6μm in width and 1000nm in tip and surface spacing. In the next chapter, experimental result and MathCAD simulated result are used to calculate the SNR for different input current levels and geometries.

3.4 Mechanical Probing Structures

We integrate the cantilever and optical beam bounce detection system into a mechanical structure as shown in *Figure [3.9]* and *Figure [3.10]*. This probing structure is designed with high rigidity in order to minimize the noise due to environmental mechanical vibration.

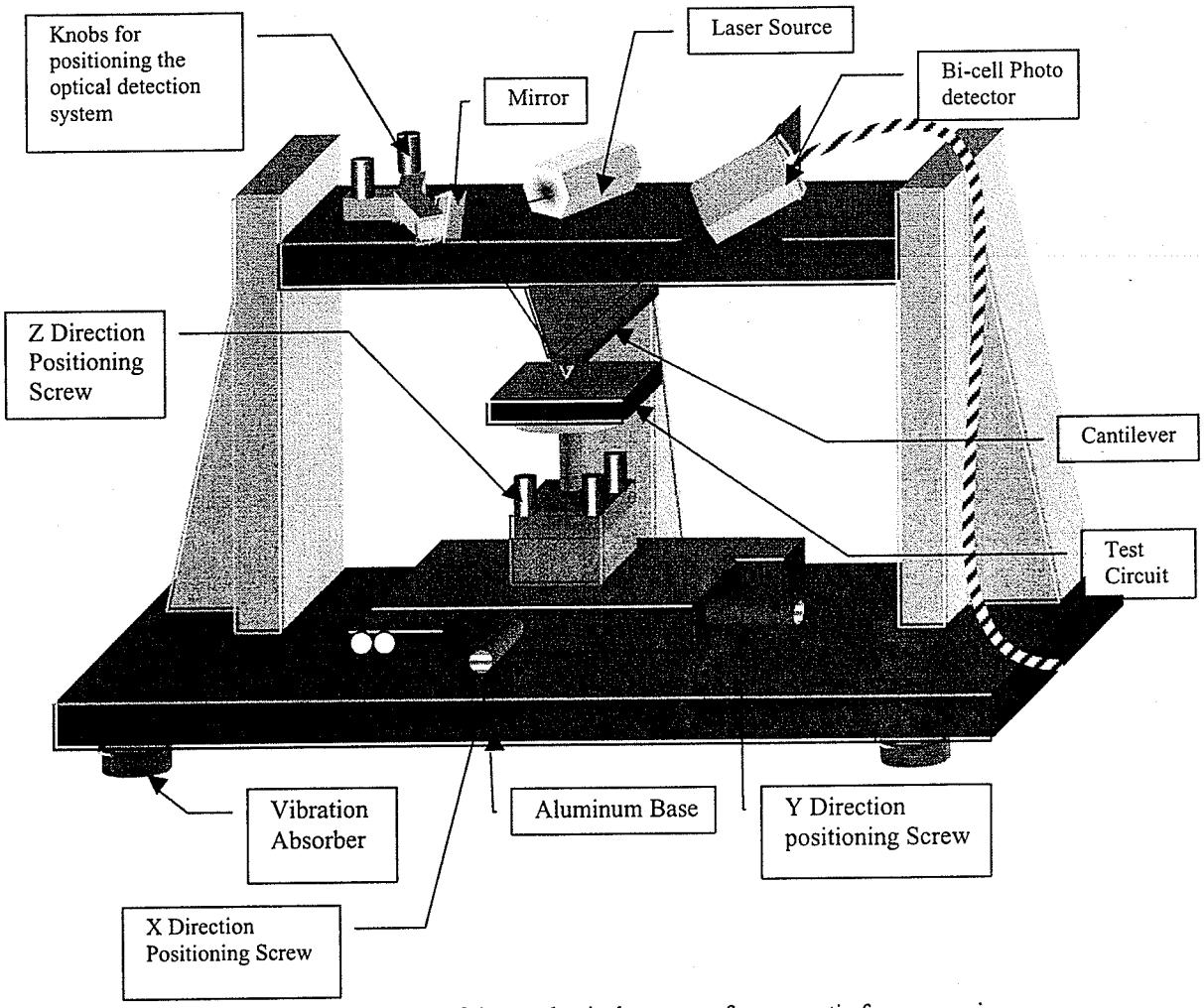

Figure [3.9] A drawing of the mechanical structure for magnetic force scanning.

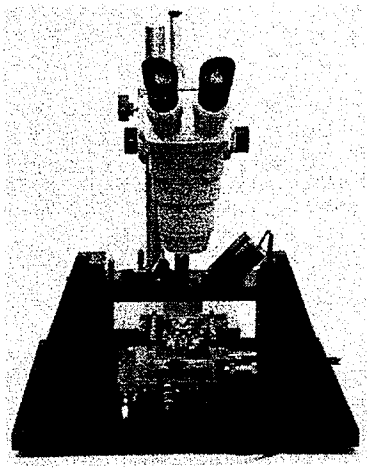

Figure [3.10] A picture of the mechanical structure for MFM including microscope and sample circuit. This picture is taken by a former graduate student.

The stage is supported by an anodized aluminum structure. The structure holds a cantilever, a 3-D piezoelectric positioner, an optical beam bounce detection system and a test circuit. We put four vibration absorbers at each corner at the bottom of the base for better vibration isolation. We can either manually adjust the circuit piezoelectric positioner using micrometer-pitched screws or by piezoelectric controller. On the upper stage, we have a laser source, a manual positioning system to focus and align the laser beam so that it will aim on the top of cantilever and deflect to the bi-cell photodiode.

3.5 Test Circuit Structure

A 900μm x 760μm test circuit structure is designed for this experiment at transistor level using NT25 technology as shown in *Figure [3.11]*.

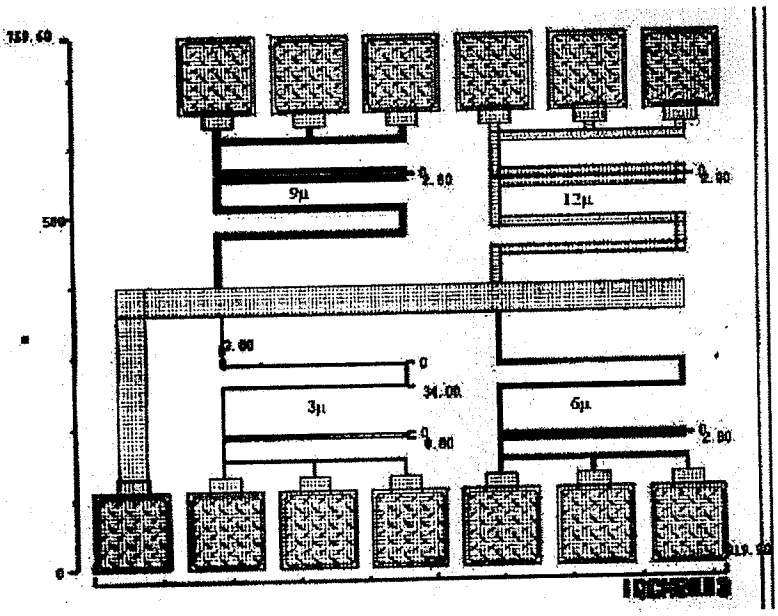

Figure [3.11] Layout of the sample circuit, which is designed in NT25 technology using metal3 interconnection line.

All transmission lines are metal 3, which is the top metal interconnection transmission line for NT25 technology. The design rule for NT25 allows 2.8 μm as the minimum spacing between two metal-3 transmission lines, 3 μm as the minimum line width for each metal-3 transmission line. 34 μm is the typical distance between VDD and VSS of CMOS transistor in year 1998. [3.23] The passivation thickness of the circuit is 1.7 μm, which is the combination of 1.175μm oxide and 0.55 μm Si_3N_4. A cross section SEM image is presented in Chapter4 for detail information.

The test circuit structure contains four different line width specifications which are 3 μm, 6 μm, 9 μm and 12 μm, but for the construction pattern, we have one rectangular turn of the transmission line separated in 2.8μm which is the minimum spacing specification, and the other rectangular turn of the transmission line separated in 34μm which is the typical transistor spacing.

3.6 Signal Acquisition System

In this section, equipments and setup for the signal acquisition system we use for this Magnetic Force Microscopy test will be introduced. They are Digital Scanning Probe Microscopy(SPM) controller[3.24], Piezo Positioner, Lock-in Amplifier.

3.6.1 Signal Acquisition System -Digital SPM Controller

The digital SPM controller is for use with all of the microscopes in the University of Manitoba SPM laboratory. The primary function of this controller in this experiment is to control the relative positions of the circuit sample and acts as a compensator in a feedback control system that can perform MFM contact mode and MFM non-contact

mode. The heart of the controller is a software proportional-integral compensator, it runs on DSP56001, a Motorola Digital Signal processor. The software senses the cantilever deflection signal through six analog to digital converters (ADC) and with a digitally programmable low pass filter at the input of one of the ADC, and returns signals to the microscope through a set of digital to analog converters (DAC). The interface between the DSP and the other devices is implemented on a field programmable gate array (FPGA), *Figure [3.12]* shows the schematic diagram of the digital SPM controller hardware. A graphical user interface is used to control the scan location and size, the scan frequency, the STM bias voltage and compensator parameters. The input signals are digitized by ADC and are being translated into a 256 pixels by 256 pixels with 65,536 grayscale image which can be stored on the PC in *tiff* format. [3.24] *Figure [3.13]* shows the inside view of the SPM digital controller hardware which is used in SPM laboratory at The University of Manitoba. The picture is taken from a formal graduate student.

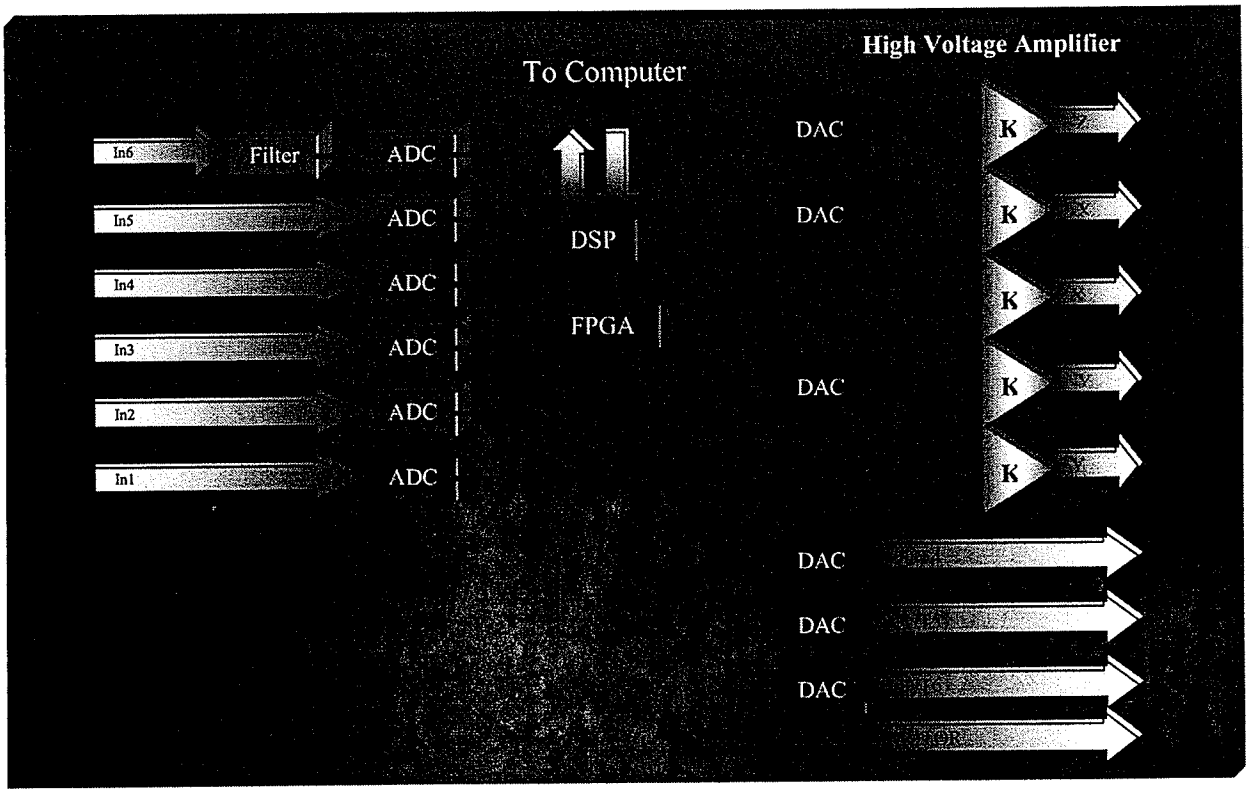

Figure [3.12] Block diagram of the digital SPM controller. [3.24]

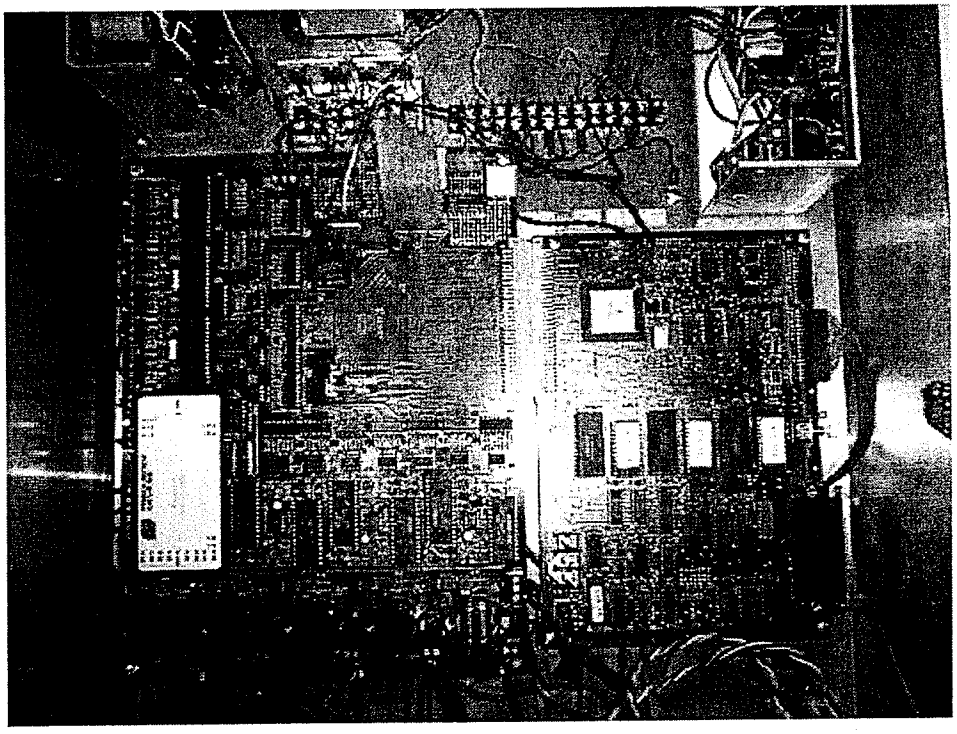

Figure [3.13] Inside view of the SPM digital controller hardware

3.6.2 Signal Acquisition System-Piezo Positioner Controller

The Melles Griot 17 PCZ Piezo Positioner controller, which is used with the ultra-precision-range of active feedback actuators incorporated in nanopositioners. The position readout range is from 0 to 20μm with 1nm resolution.[3.25] The Piezo Positioner is remote controled by our Digital SPM controller. X, Y and Z position signals from digital SPM controller are connected to Piezo Positioner Controller signal inputs. *Figure [3.14]* shows the exterior look of the controller.

Figure [3.14] The Melles Griot 17 PCZ Piezo Positioner controller

3.6.3 Signal Acquisition System-Lock-In Amplifier

SR510 Lock-in amplifier from Stanford Research Systems is used in this experiment. [3.26] The signal is amplified by a low noise differential amplifier at the input and selectively filtered and amplified by a high-gain AC amplifier and delivered to the signal monitor output terminal. *Figure [3.15]* shows the exterior look of the lock-in amplifier.

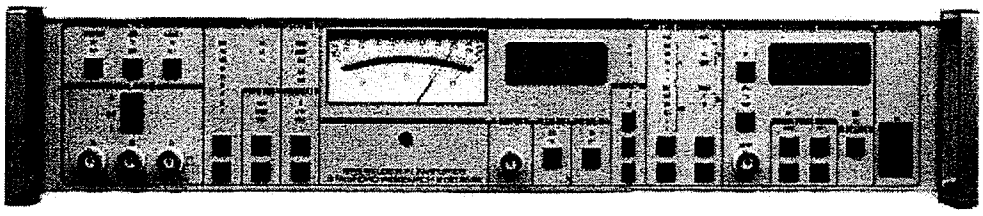

Figure [3.15] SR510 Lock-in amplifier from Stanford Research Systems. [3.26]

To generate the lock-in output, the signal is multiplied by a reference sine wave, which is phase-locked to the reference input. The output of the multiplier contains frequency components near DC, $(f_{signal} - f_{reference})$ and $2f\ (f_{signal} + f_{reference})$. [3.33] The signal then goes through the two stages of low pass filtering and provides the lock-in time constants. First, the filters remove the second harmonic components, which are introduced by the multipliers. Secondly, the filters reduce the noise by narrowing the detection bandwidth. The output of the filter is finally amplified by a chopper stabilized DC amplifier, before being delivered to the lock-in output terminal. The schematic of the lock-in amplifier is shown in *Figure [3.16]*.

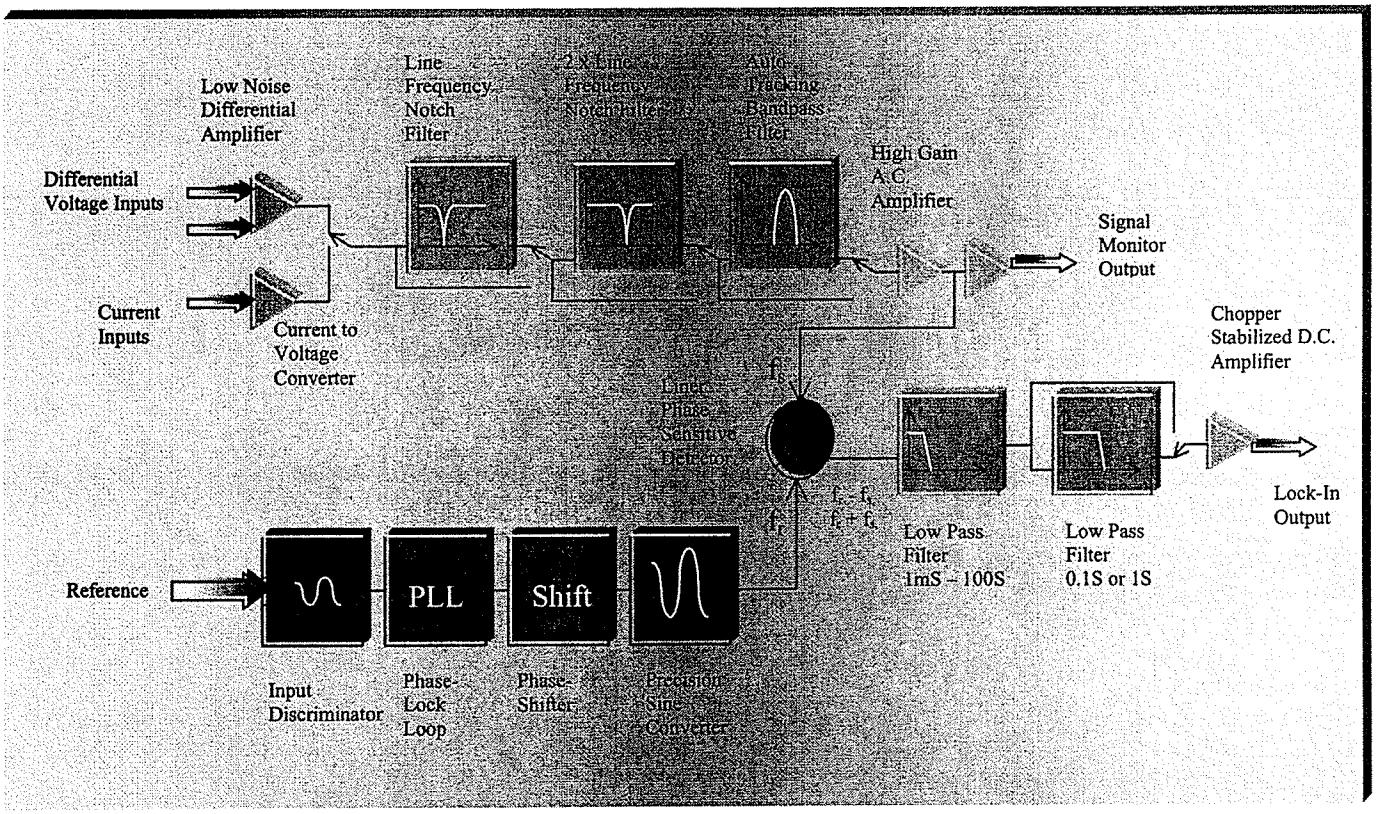

Figure [3.16] A block diagram of SR510 Lock-in amplifier from Stanford Research Systems [3.26]

Chapter 4

Magnetic Force Microscopy Measurement

This chapter exhibits and analyzes measurements conducted by MFM. Performance of MFM will be evaluated through the measurements result obtained over the designed sample circuit with five different input signal voltages.

4.1 Test Parameters & Setup

This paragraph presents all test parameters that are chosen for each instrument in this experiment setup. *Figure [4.1]* on the next page virtually presents the connectivity between each instrument in this experiment setup.

4.1.1 Test Parameters & Setup-Digital SPM Control

University of Manitoba's SPM digital control system interacts with user through a very user-friendly graphical user interface. [4.1] With this interface user can operate the system in different test conditions by just modifying their test parameters. *Figure [4.2]* presents the graphical user interface with the test parameters we use for this test. Detail of how to setup the SPM digital controller is presented at Appendix 2.

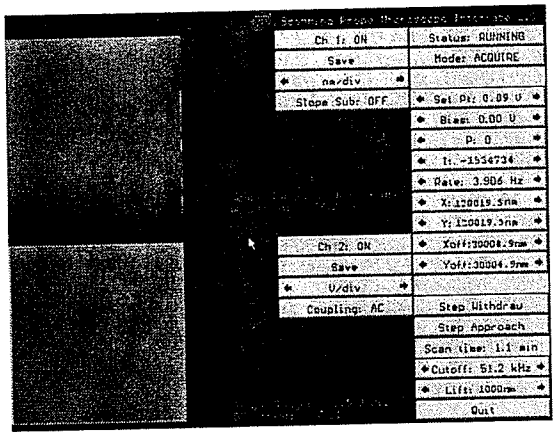

Figure [4.2] User interface layout in acquired mode. [4.1]

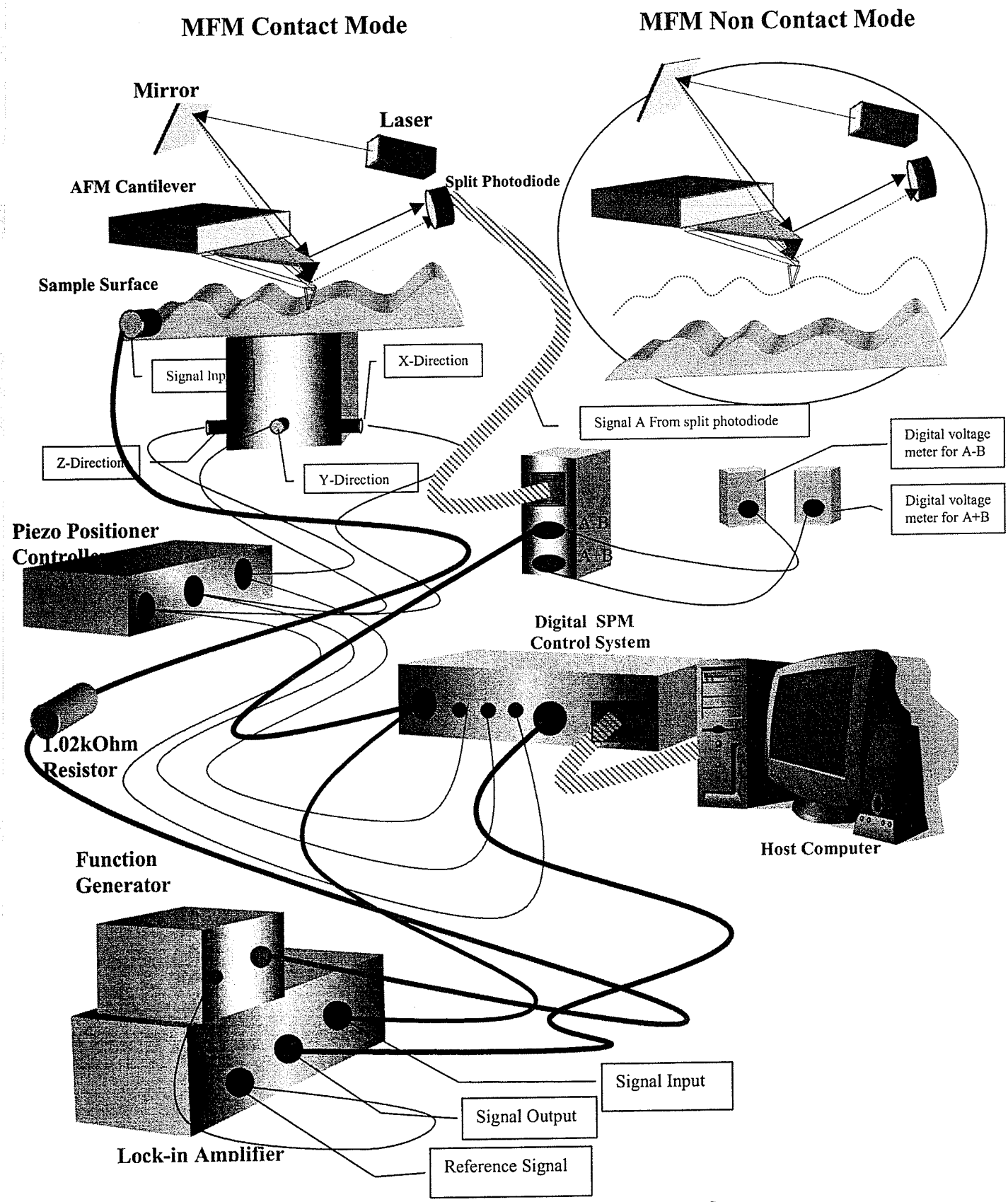

Figure [4.1] Display the Experiment Instruments Setup

4.1.2 Test Parameters & Setup-Tip & Laser Beam

We ground the cantilever to prevent any others parasitic effect between the tip and the surface. Tip is then brought as close to the sample surface as possible. We adjusted the laser lens and the angle of the mirror, to have the laser beam focused on the top of the tip. The distance between the tip and the bi-cell photodiode is also adjusted to have most of the reflected laser beam captured; we verified this by measuring the voltage sum from the bi-cell photodiode. A digital meter is used to locate the center of the reflected laser beam by measuring the difference in voltage from the bi-cell photodiode. The higher the sum voltage represent the more reflected laser beam is captured. This brings higher signal resolution and better signal to noise ratio. On the other hand, the lower the differential voltage represent the more evenly distributed the laser beam between both sides of the bi-cell photodiode. With maximum sum voltage and minimum differential voltage, we located the bi-cell photodiode at the center of the reflected laser beam.

The differential signal from the photodiode was fed to a spectrum analyzer, where we find a thermal peak on the scope at the resonant frequency, which is 7.4kHz. The sample is then moved up to the tip very slowly and manually. Three steps are used to monitor the progress of elevating the sample to the tip. First, a microscope allowed us to monitor the movement of the sample visually. We begin by focusing the microscope on the tip, and left the sample out of focus. As the sample being moved toward the tip, the view of the sample under the microscope will come into focus. When we obtain almost the same forces for the tip and the surface, we switch to observe the shadow of the tip on the sample surface. The area of the shadow will gradually decrease as the sample move

closer to the tip. As the tip come very close to touch the surface, we switch to monitor the resonant frequency peak in the spectrum analyzer. When the thermal resonant frequency peak disappears from the spectrum analyzer, we know that the tip has touched the surface. Before we started the scanning, we move the sample back-up to the position right before the tip touch the surface of the sample because as mentioned in the previous paragraph, the function of the feature Set Point in Digital SPM Controller is to maintain a certain force level between the surface and the tip during the scan. Since the Set Point is set to 0.09V and we do not wish to push the tip too hard on the surface to prevent scraping the surface and damaging the tip.

4.1.3 Test Parameters & Setup- Function Generator & Lock-In-Amplifier

A function generator was used to generate a sinusoidal current at the resonant frequency of the cantilever, which is 7.4kHz. Five different peak-to-peak current levels: 4V, 2V, 1V, 0.5V and 0.25V peak-to-peak voltages are sent to the sample circuit in series with a 1.02kohm resistor produced peak-to-peak currents of 4mA, 2mA, 1mA, 0.5mA and 0.25mA.

Due to the AC stimulation signal being chosen as test signal to test circuit, the lock-in amplifier was used to lock the phase between the AC input signal from the function generator and the output signal from the bi-cell photodiode so that the AC stimulation signal will not affect the DC result we wished to obtain. The time constant of the Lock-In Amplifier is set to 10ms. We choose the time constant such that most details will not be averaged out but as much noise as possible is eliminated. To obtain the right reference phase degree, we begin with adjusting the reference phase degree by degree

until we reach a point where we almost cancel out the output signal. At this particular phase, the reference signal is shifted 90 degree out of phase from the input signal. In order to have the reference signal in phase with the input signal, a shift of 90 degree in phase is added to the reference signal.

4.2 Magnetic Force Microscopy on the Sample Circuit

This section exhibits the measurements results conduct by MFM. Topographic images of the sample circuit and magnetic force distribution images from five different input voltage levels are presented.

4.2.1 Magnetic Force Microscopy on the Sample Circuit - Topographic Images and Analysis

The following topographic image *Figure [4.3]* of the sample circuit is the scanning result from MFM contact mode. MathCAD is used to plot the image in 3-Dimemsion. Result images are being plot in 2D grayscale and 3D 32-bits color. The cross section profile plot is taken on the image and the result from the cross section profile plot is studied and analyzed.

The topographic analysis concluded two points. Firstly, the result image is within the spatial resolution of the system. From the measurement done on the image, the average of transmission line width M1 and M3 is around 8μm and the spacing of the transmission line M3 is 35μm. The measurement results are relatively close to the NT25 design rules, which is 6μm for line width and 34μm for line spacing. Secondly, the result also shows that the sample circuit is not stretched out flat horizontally. From *Figure 4.3* point of view, upper right corner of the sample is tilted higher. This can be proved by the

diagonal, horizontal and vertical cross section profile plot of the images, which are shown in *Figure 4.4*. Due to our existing setup, it is very difficult to achieve a perfectly horizontal flat test sample manually. A study is made to find the tilted angle on the next section 4.3.2. The result of the study has proven that the effect of the tilted angle is not significant.

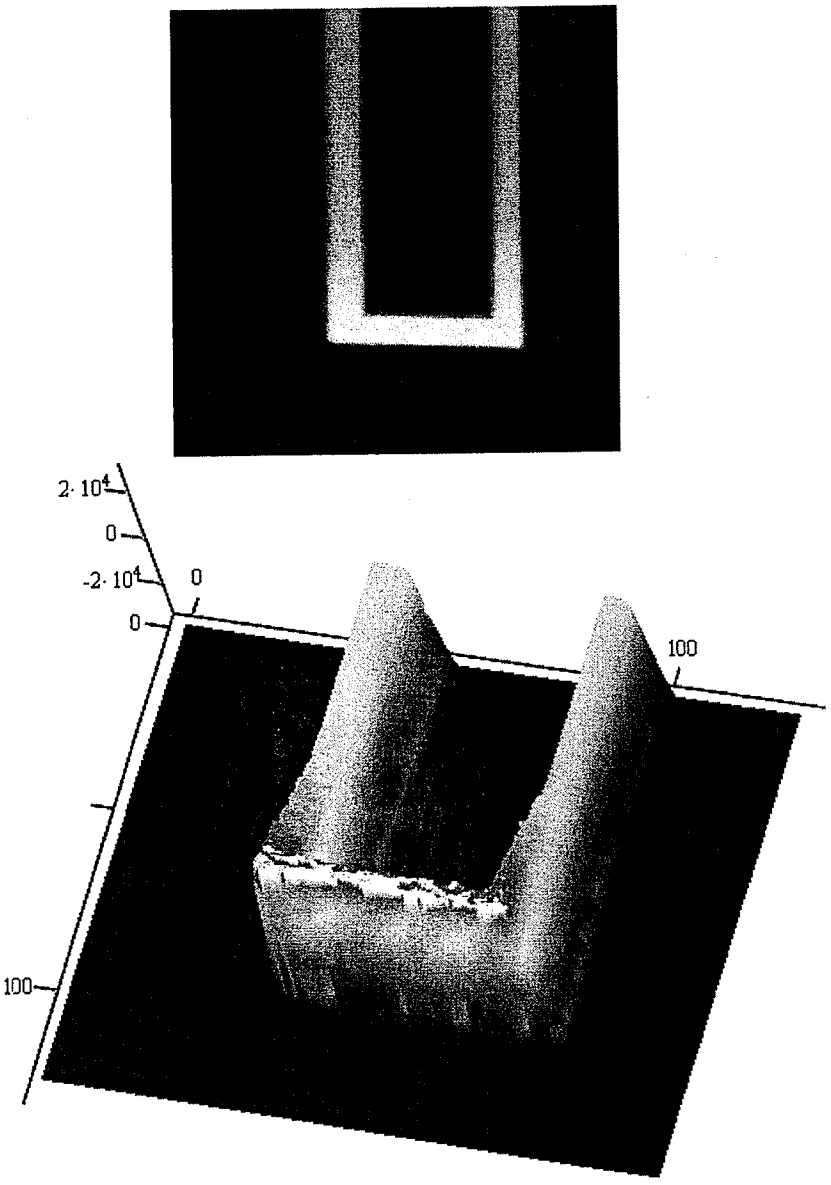

Figure [4.3] Topographic image of the sample circuit by MFM contact mode. A color change on the base of the 3D plot, proved the sample is tilted.

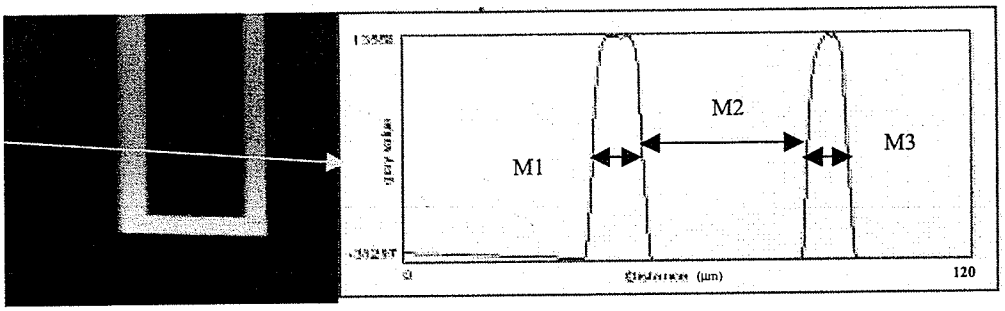

Figure [4.4a] A diagonal cross section profile plot of the TLine. Yellow line shows the location where it is taken.

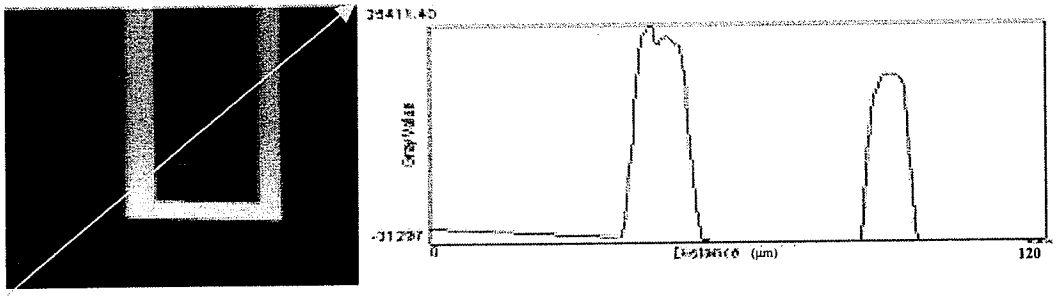

Figure [4.4b] A diagonal cross section profile plot of the surface. Yellow line shows the location where it is taken.

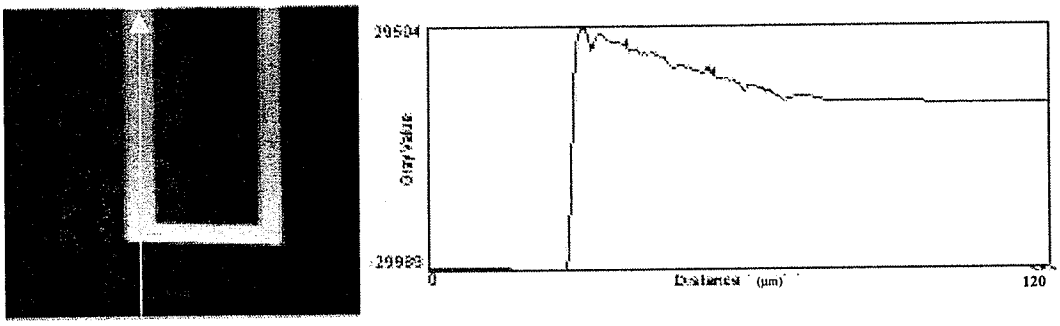

Figure [4.4c] A vertical cross section profile plot of the TLine.. Yellow line shows the location where it is taken.

4.2.2 Magnetic Force Microscopy on the Sample Circuit- Magnetic Force Distribution
($4mA_{pp}$, $2mA_{pp}$, $1mA_{pp}$, $0.5mA_{pp}$, $0.25mA_{pp}$)

The test input current level for these scenarios were 4mA peak-to-peak, 2mA peak-to-peak, 1mA peak-to-peak, 0.5mA peak-to-peak and 0.25mA peak-to-peak sinusoidal current. *Figure [4.5], Figure [4.6], Figure [4.7], Figure [4.8] and Figure [4.9]* display the magnetic force distribution images acquired by MFM Non-contact mode by each different input voltage level. From the quick visual comparison of these MFM images, we can concluded that the magnetic force strength is weaker as the test input voltage level or input current is lower. These results from the observation are consistent with our theoretical discussion in Chapter2.

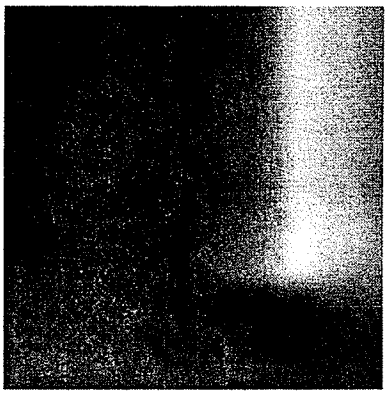

Figure [4.5] Result image form $4mA_{pp}$ MFM non-contact mode.

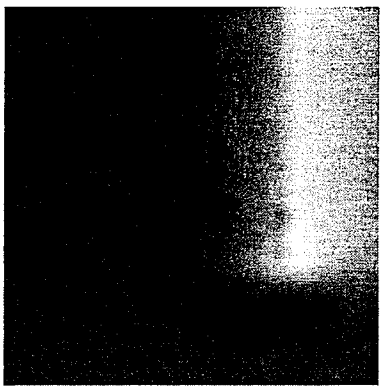

Figure [4.6] Result image form $2mA_{pp}$ MFM non-contact mode.

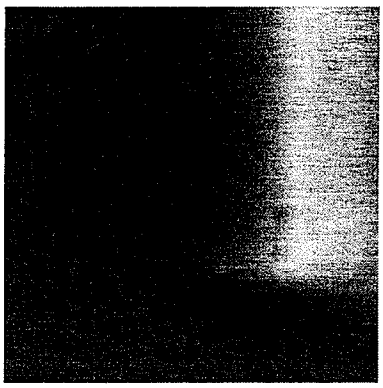

Figure [4.7] Result image form $1mA_{pp}$ MFM non-contact mode.

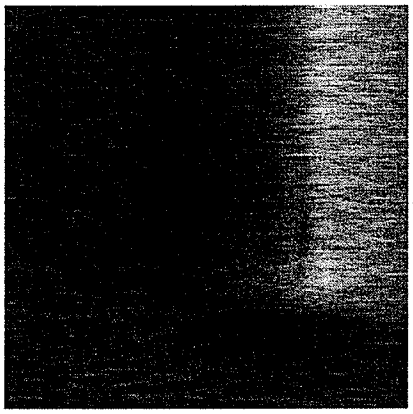

Figure [4.8] Result image form 0.5mA$_{pp}$ MFM non-contact mode.

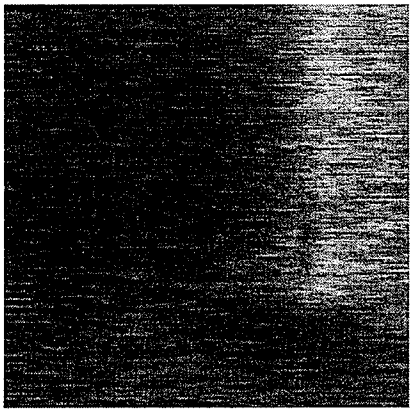

Figure [4.9] Result image form 0.25mA$_{pp}$ MFM non-contact mode.

4.3 Magnetic Force Microscopy Result Analysis

All measurements are performed on the 6μm width, 2μm thickness and 34μm spacing transmission pattern, and the tip is scanning in Y-axis direction as what is shown in *Figure [4.10]* below.

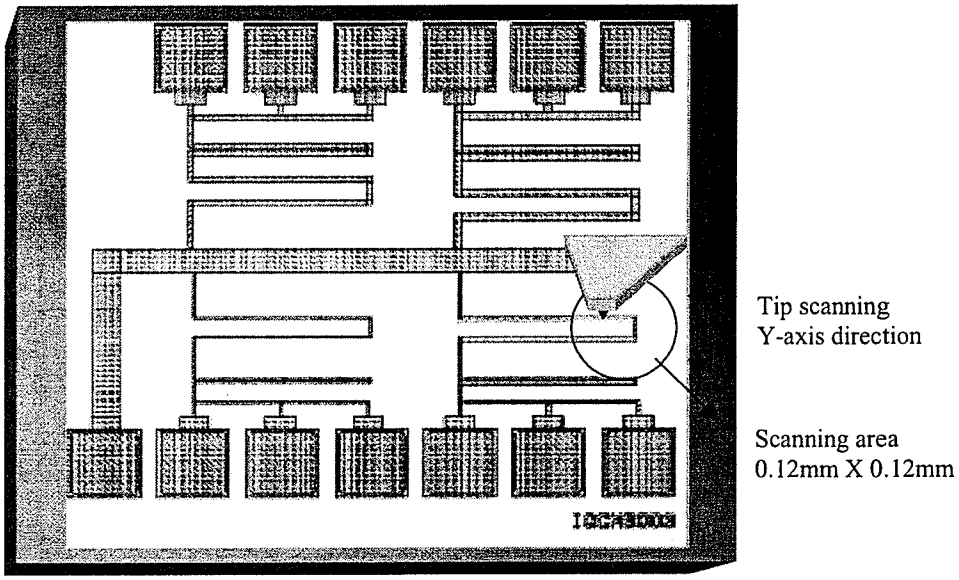

Figure [4.10] Display of the location on the sample surface where MFM took place.

4.3.1 Magnetic Force Microscopy Result Analysis– Scanning Height of Non-contact mode

When the tip is scanning on the surface in Contact Mode, the scanning height is assumed to be zero. But when MFM is operated in Non-Contact Mode, scanning height is considered as an important parameter.

As what is mentioned on the next section, 4.3.2, the passivation thickness of NT25 is 1.7μm. In section 4.1.1, we set the height in the *Lift Mode* at 1000nm. Since we deposited the γ–Fe_2O_3 powder on the backside of the tip, the total scanning height must include the height of the tip, which is defined as 3-5μm and also the thickness of the cantilever, which is 1μm by the cantilever manufacturing specification. [4.2] Since we are not sure about the actual tip height that we used, 4μm is chosen as the tip height in the range of 3-5μm. As a result, the total scanning height for MFM is around 7.7μm. *Figure [4.11]* below shows how scanning height is defined in our experiment.

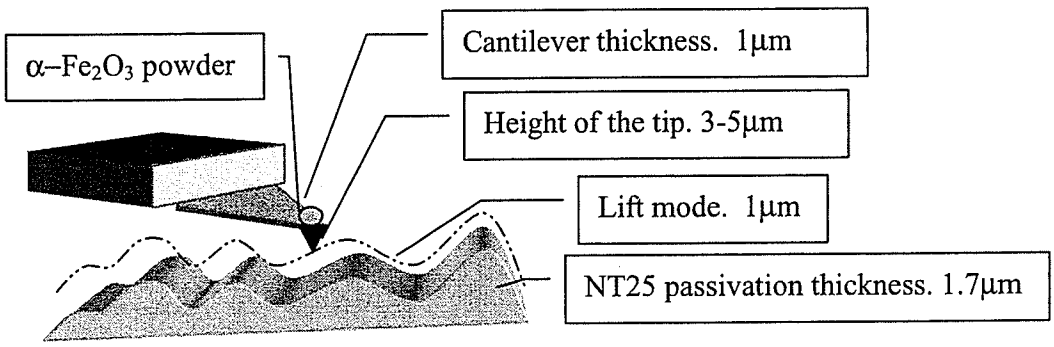

Figure [4.11] Display of how the scanning height is defined.

4.3.2 Magnetic Force Microscopy Result Analysis - Sample Tilted Angle Definition

In order to find the sample tilted angle in X and Y direction, the grayscale value on y-axis and pixels on x-axis needs to be defined in micrometer. The definition begins with finding the correlation between the grayscale value thickness and the real metal-3 transmission thickness. From *Figure [4.4b]* in section 4.2.1, the thickness of the transmission line is 59493-grayscale values; the real thickness of NT25 metal-3 transmission line is defined as 2.125μm in the NT25 process specification [4.3], which is supported by the following transmission line cross-section SEM image *Figure [4.12]*. With these two pieces of information, we can convert the y-axis grayscale value into micrometer. For y-axis, 1 grayscale unit represents 35.72pm. For x-axis, since our X scanning length is set to 120μm and 256 pixels is used to display each line on the image, 1 pixel represents 468.75nm.

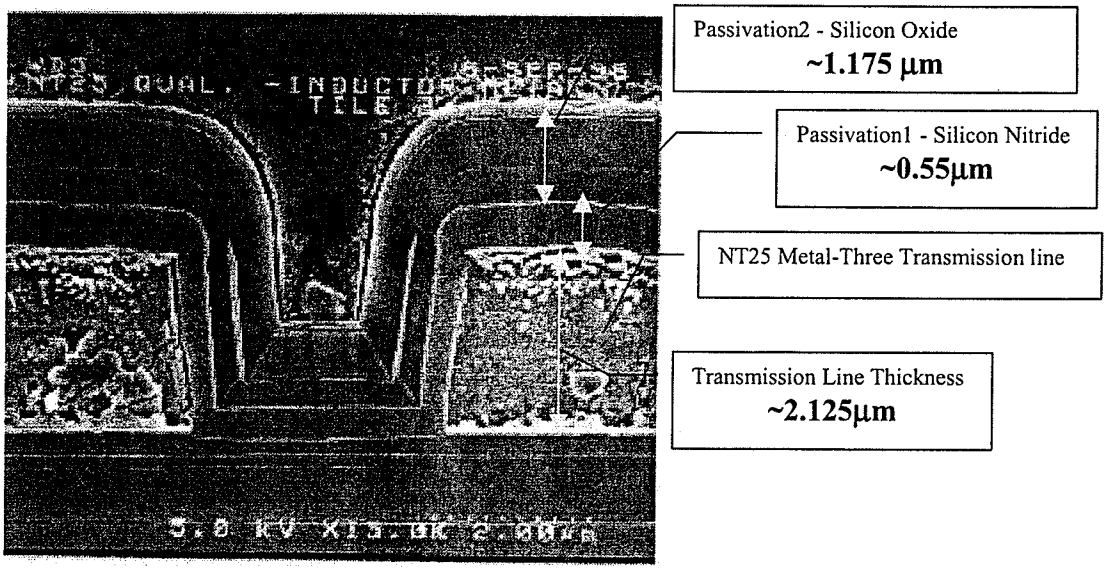

Figure [4.12] Display of NT25 metal3 and passivation thickness. [4.3]

As a conclusion, the tilted angle of the sample in Y direction as shown in *Figure [4.4c]* in section 4.1.1 is 0.08°. The tilted angle of the sample in X direction as shown in *Figure [4.4d]* in section 4.1.1 is 0.057°. The tilted angle is considered as not significant.

4.3.3 Magnetic Force Microscopy Result Analysis – Magnetic Force Definition

In the ideal case, the cantilever is parallel with the sample circuit and the tip is always perpendicular to the surface of the sample circuit and the force acting on the cantilever is the direct result of the interaction between the Z component of the magnetic field from the sample circuit and the Z component of the magnetic dipole moment from the magnetic tip. The following equation *E 2.21* was defined in Chapter2.

$$\vec{F} = \nabla(\vec{M} \cdot \vec{B}) \text{ [E 2.21]}$$

However, the test system we used is slightly different from the assumption we have made above. Due to the probe station structure, the cantilever is actually tilted about 15^0 between Y-axis and Z-axis. As a result, the cantilever reflection force is no longer solely contributed by the interaction between Z components of magnetic field and Z components of the magnetic moment but it also involved the interaction of both Y components. These additional Y components to the equation are derived as follows:

$$\begin{aligned} \vec{F} &= \nabla\left(\vec{M} \cdot \vec{B}\right) \\ &= \nabla\left(M_z B_z + M_y B_y\right) \\ &= \nabla\left(M \cdot \cos(15°) B_z + M \cdot \sin(15°) B_y\right) \end{aligned} \quad \text{[E 4.1]}$$

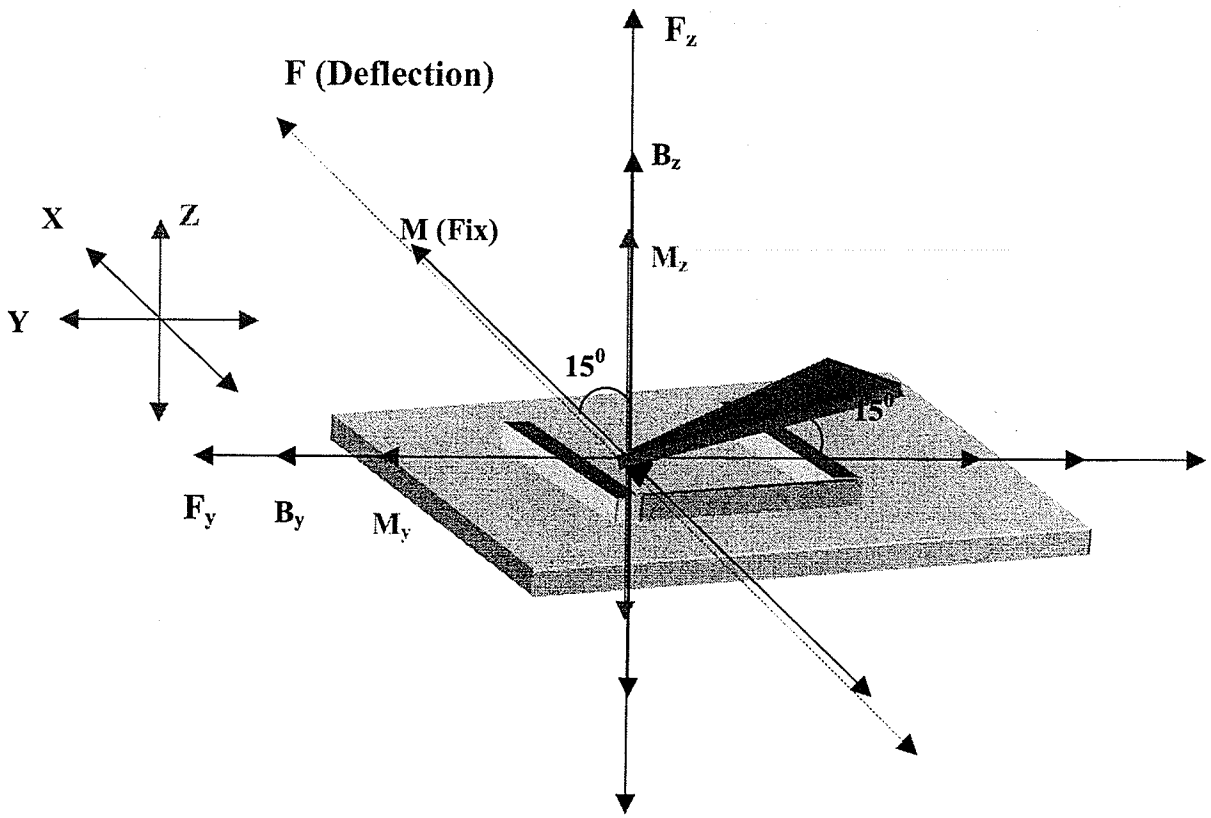

Figure [4.13] Display of the definition of F in F_y , F_z and the tip 15^0 tilted angle.

From Chapter 3 we know that the magnetic moments in the γ–Fe_2O_3 are fixed because the epoxy fixed the particles in one direction. So we have to consider 15 degree tilted angle when we define M_z and M_y.

From *Figure [4.13]*, F_z and F_y being defined below:

$$F_z = M\cos(15^0)\frac{\partial B_z}{\partial z} + M\sin(15^0)\frac{\partial B_y}{\partial z} = M\left[\cos(15^0)\frac{\partial B_z}{\partial z} + \sin(15^0)\frac{\partial B_y}{\partial z}\right] \quad \text{[E 4.3]}$$

$$F_y = M\cos(15^0)\frac{\partial B_z}{\partial y} + M\sin(15^0)\frac{\partial B_y}{\partial y} = M\left[\cos(15^0)\frac{\partial B_z}{\partial y} + \sin(15^0)\frac{\partial B_y}{\partial y}\right] \quad \text{[E 4.4]}$$

The total magnetic interaction force (F), is the combination F_y and F_z. But since our cantilever is tilted in 15 degree, we only consider the forces that act on the cantilever. The total interaction force is as *E4.5*.

$$\vec{F} = M\left[\cos(15^0)\frac{\partial B_z}{\partial z} + \sin(15^0)\frac{\partial B_y}{\partial z}\right]\cos(15^0) + M\left[\cos(15^0)\frac{\partial B_z}{\partial y} + \sin(15^0)\frac{\partial B_y}{\partial y}\right]\sin(15^0) \quad \text{[E 4.5]}$$

Before the Magnetic Force Microscopy result can be analyzed, the correlation between the output voltage from the Lock-In Amplifier and the interaction magnetic force that deflects the cantilever must be defined first. We start with defining ΔZ of the system in term of voltage. While *Set Point* is changed from 0V to 0.1V, the difference of DC offset voltage display on the *Top oscilloscope i*s 7V. The maximum Z travel of this system is 7μm, and the maximum applied voltage for maximum Z travel is 200V. $\frac{V}{Z}$ is calculated as follow:

$$\frac{V}{Z} = \frac{\Delta V_{(Set\_Point)}}{\frac{\Delta V_{(DC\_Offset)}}{V_{(Max)}} \cdot Z_{(\max)}}$$

$$= \frac{0.1V}{\frac{7V}{200V} \cdot 7000nm} \approx 0.4\frac{mV}{nm} \quad \text{[E 4.6]}$$

Secondly, we need to define the voltage output from the Lock-In Amplifier in term of tip Z motion. The sensitivity of the Lock-In Amplifier is set to 5mV and 10V is

the full-scale signal amplification. As a result, the Lock-In Amplifier amplifies the AC input signal 2000 time and multiplies it with the reference signal and produces an output signal with frequency components near DC. Therefore 1V output from the Lock-In Amplifier represents $0.354mV_{rms}$ from the scanning system. From *E 4.6*, 1V output from the Lock-In Amplifier represents $0.884nm_{rms}$ of tip Z-travel.

Thirdly, we need to define the voltage output from the Lock-In Amplifier in term of deflection force on the tip. The effective spring constant, k_{eff}, was defined as 0.032 N/m +/-20% in *Chapter3,* Q as 32 and Δz as $0.884nm_{rms}$. The reason Q of the cantilever is taken into consideration is because in our experiment, the cantilever is oscillating at its resonant frequency all the time. With all elements in *E 4.7* are defined, we find 1V output from the Lock-In Amplifier represent 0.88 pN_{rms} cantilever force. If we take the range of spring constant variation into consideration, the range of force variation is from 1.06 pN_{rms} to 0.70 pN_{rms}

$$F = \frac{k_{eff}}{Q}\Delta z \quad \text{[E 4.7]}$$

On the other hand, ΔZ can also be defined theoretically by the following formula, which was mentioned in Chapter3 section 3.2.

$$I_d \approx \frac{3LNq}{lr_o^2\sqrt{\pi}}\Delta z \quad \text{[E 3.23]}$$

But due to the difficulty of obtaining all the required parameters in the formula, for instance, r_0, which is the radius of the laser beam, we finally decided to define ΔZ experimentally.

4.3.4 Magnetic Force Microscopy Result Analysis

–Magnetic Interaction Force Image Analysis ($4mA_{pp}$)

In this section we present the analysis work done on $4mA_{pp}$ test scenario result. We will begin with analyzing the distribution of the magnetic interaction force, and then we define the maximum deflection in term of force and distance. Finally, we examine the SNR for this test scenario.

The test input voltage for this scenario is 4mA peak-to-peak sinusoidal current. With 1.02k Ohm as resistance current input is 1.386 mA_{rms}. *Figure [4.14]* is the magnetic force distribution image acquired from MFM Non-contact mode. In *Figure [4.15]*, an outline of the transmission line is superimposed onto the magnetic force distribution image. A horizontal profile of the image with transmission line outline superimposed is shown in *Figure [4.16]*.

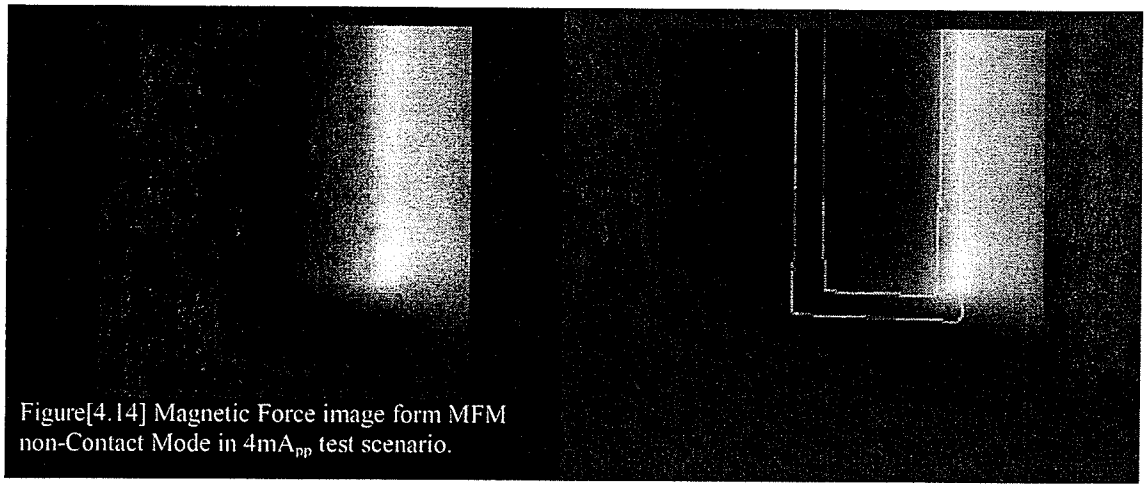

Figure[4.14] Magnetic Force image form MFM non-Contact Mode in $4mA_{pp}$ test scenario.

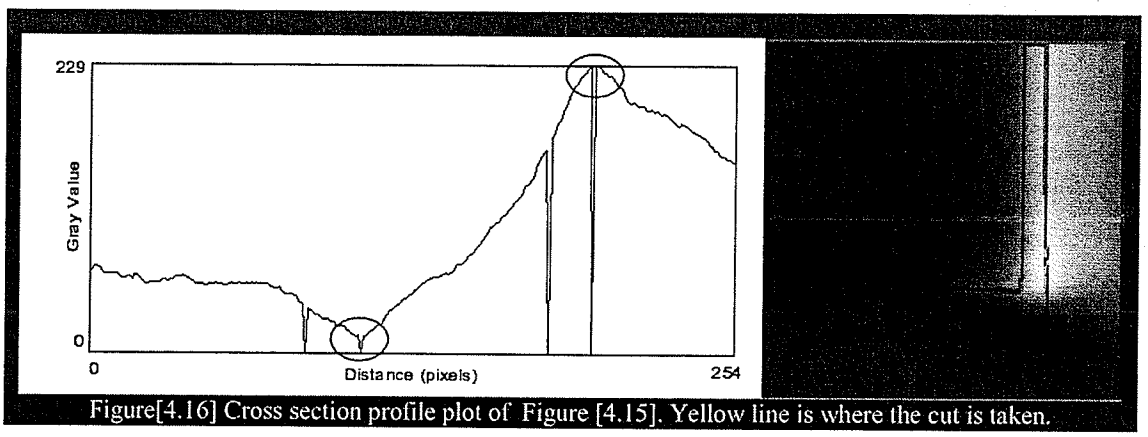

Figure[4.16] Cross section profile plot of Figure [4.15]. Yellow line is where the cut is taken.

4.3.5 Magnetic Force Microscopy Result Analysis

-Magnetic Interaction Force Image Analysis ($4mA_{pp}$)

-Force Distribution

To verify the magnetic interaction force distribution, we begin with analyzing the location where the maximum interaction force occurs by comparing the theoretical simulation result and the experimental result, and then compare the shape of the curve. Lastly, some discussion of the discrepancies is present.

From the images above *Figure [4.16],* we notice that the maximum magnetic interaction forces are located at the edge of the transmission line, where the red circles are located. To verify this occurrence, we have to examine the distribution of the magnetic field both in Z-direction and Y-direction, since these magnetic fields are the main contributors to the magnetic interaction force occurring between the tip and the surface.

From the Biot-Savart's Law and Ampere's Law theoretical point of view, strong magnetic field, which is the direct result of current flowing through a transmission line, is always located at both edges of the transmission line for magnetic field in Z direction. At the center of the transmission line where the change of the Z magnetic field polarity takes place, the Z magnetic field is always equal to zero, while at the center of the two

transmission line where the change of the Y magnetic field polarity takes place, the Y magnetic field is zero.[4.3] MathCAD is used to simulate a cross section view of the transmission line and both Z and Y direction magnetic field and magnetic interaction force. They are shown below in *Figure [4.17], Figure [4.18].*

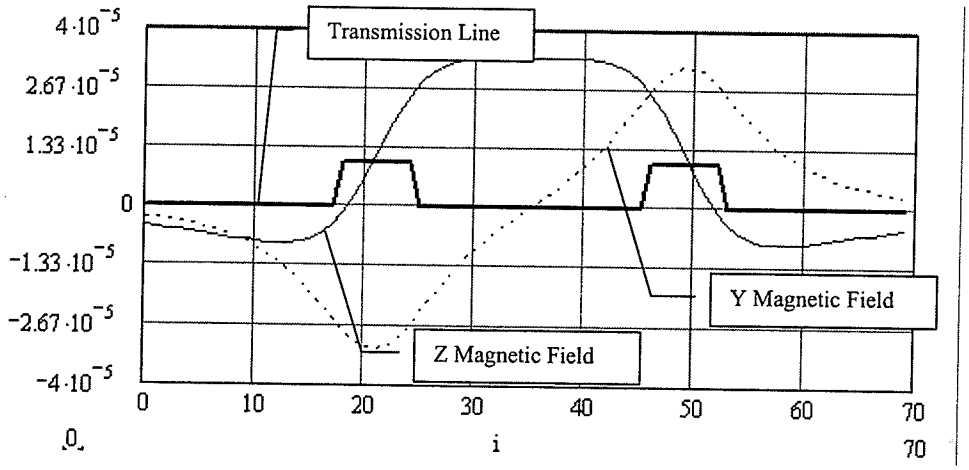

Figure [4.17] MathCAD simulation on the Y, Z magnetic fields. TLine (black-solid), Z magnetic field (red-solid), Y magnetic field (blue-dash). Unit for Y-axis is Tesla for X-axis is in μm

The black line in the middle is the cross section view of the transmission line. The red line is the magnetic field in Z direction. It crosses the zero magnetic field line at the center of the transmission line while reaches its maximum and minimum magnetic field at both edges of the line. The blue dotted line is the magnetic field in Y direction. It reaches its maximum and minimum magnetic field at the center of the transmission line and crosses the zero magnetic field line at the middle of both transmission lines.

As what is shown in *E 4.5,* the magnetic interaction force occurs when the magnetic field from the surface interacts with the magnetic moment of the tip. The gradient function transforms the dot-product of the magnetic field and the magnetic moment into a vector which point to the direction which has greatest rate of change.

Figure [4.18] is the plot of the interaction force in Z and Y directions and the sum of the two forces. Basically, the MFM result image shown in *Figure [4.16]* matches the MathCAD simulation result, which is the green dotted curve in *Figure [4.18]*, showing strong magnetic interaction force present at the edges of the transmission lines.

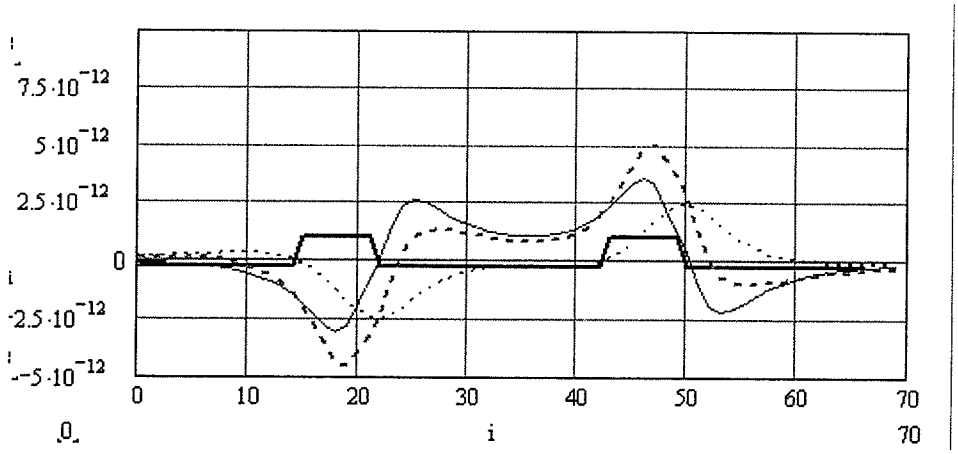

Figure [4.18] MathCAD simulation on the magnetic interaction force location. TLine (black-solid), Z magnetic force (red-solid), Y magnetic force (blue-dash) and sum of the two (green-dash) Unit for Y-axis is N for X-axis is in μm

By comparison between the green dotted line in *Figure [4.18] and [4.16]*, we can conclude that the shape of the two curves are very similar while these are also some minor discrepancies between them which can be explained as follow: The MFM image in *Figure [4.16],* is a plot of the force interaction resulted from a 3-dimensional magnetic forces interaction. It is more complicated than what we can represent in *Figure [4.18]*, using MathCAD, because the magnetic interaction force in X direction is ignored and assumed to be insignificant for simplicity. On the other hand, there are others parasitic effects, which we do not include in our analysis that might also contribute to this final result.

4.3.6 Magnetic Force Microscopy Result Analysis

-Magnetic Interaction Force Image Analysis ($4mA_{pp}$)
-Quantify Deflection Force and Distance, SNR

During the MFM scanning, not only the result image which is recorded in *.exp* file format, *.inf* file also recorded some basic parameters of the scanning. In the $4mA_{pp}$ test scenario *.inf* file, the largest voltage output from the Lock-In Amplifier is recorded as 0.8465V. The maximum deflection of the cantilever in term of gray value is recorded as 7748 and the minimum is –2338. From the cantilever deflection force definition in the previous section 4.3.3, we can conclude that the largest cantilever positive deflection force in the $4mA_{pp}$ test scenario is about $0.74pN_{rms}$ and the largest negative deflection is $-0.22pN_{rms}$ at Q=32, k_{eff}=0.032N/m.

The SNR for this test scenario, where $I=1.386mA_{rms}$, can be defined as follows:

$$SNR = \frac{(\Delta Z_F)}{(\Delta Z_{th})}$$

$$SNR = \frac{0.74}{0.03} = 25$$

Since there is +/-20% variation on the spring constant value, the following table shows the range of the deflection force according to the range of the variation.

Effective Spring Constant (N/m)	Peak-to-peak Deflection Force (pN)
0.038	1.16
0.032	0.96
0.026	0.79

Figure [4.19] Display the range of peak-to-peak deflection force corresponding to the spring constant variation.

The following *Figure [4.19]* is the MFM result plotted in 3-dimensional plot graph by MathCAD to enabling a better visualization for the viewer.

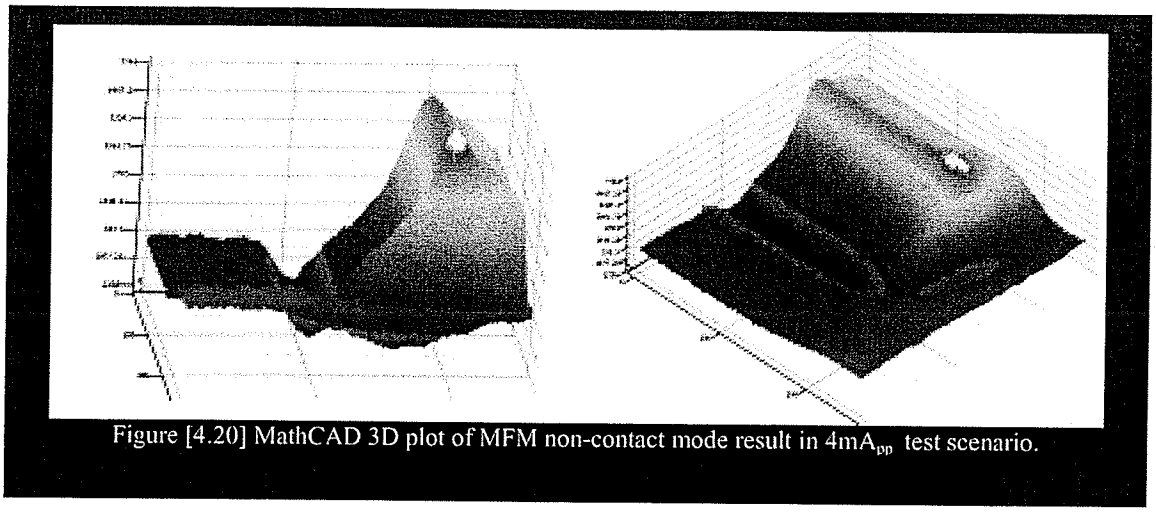

Figure [4.20] MathCAD 3D plot of MFM non-contact mode result in $4mA_{pp}$ test scenario.

4.3.7 Magnetic Force Microscopy Result Analysis – Magnetic Interaction Force Image Analysis ($2mA_{pp}$, $1mA_{pp}$, $0.5mA_{pp}$, $0.25mA_{pp}$)

This section presents the MFM results of 2V peak-to-peak, 1V peak-to-peak, 0.5V peak-to-peak, 0.25V peak-to-peak test scenario. For each test scenario, we present a figure with the outline of the transmission line superimposed onto the magnetic force distribution image, a figure with horizontal profile of the transmission line and a 3 dimensional plot.

We perform the same analysis work on these MFM images and find that the distributions of the magnetic forces are consistent for all test scenarios. *Figure [4.20]* presents a table summary of the analysis result on the different test scenarios.

Voltage Input (V_{pp})	Current (mA_{rms})	Max V (in .inf) (V)	Gray Value (in .inf)		Max Deflection Force (pN_{rms}) @ k_{eff}=0.032N/m.		Max Deflection Distance (nm_{rms})		SNR ΔZ_{th}=0.03nm	No. Figure
			Max	Min	Positive	Negative	Positive	Negative		
4	1.386	0.846	7748	-2338	0.74	-0.22	0.748	-0.225	25.0	4.14
2	0.693	0.430	4056	-1072	0.37	-0.10	0.380	-0.100	12.6	4.22
1	0.346	0.237	2359	-464	0.20	-0.04	0.210	-0.041	7.0	4.25
0.5	0.173	0.154	1636	-201	0.13	-0.01	0.136	-0.017	4.5	4.28
0.25	0.086	0.118	1000	-401	0.10	-0.04	0.104	-0.042	3.5	4.31
Estimate										
0.1	0.02	~	~	~	~	~	0.03	~	1	~

Figure [4.21a] A summary of the result form the MFM Non-Contact Mode image analysis work.

Since spring constant of the cantilever also played a very vital role in defining deflection, the following table shows a summary of peak-to-peak deflection force corresponding to the variation of the spring constant.

Voltage Input (V_{pp})	Current (mA_{rms})	Peak-to-peak Deflection Force (pN_{rms}) @ k_{eff}=0.026N/m.	Peak-to-peak Deflection Force (pN_{rms}) @ k_{eff}=0.032N/m.	Peak-to-peak Deflection Force (pN_{rms}) @ k_{eff}=0.038N/m.
4	1.386	0.79	0.96	1.16
2	0.693	0.46	0.47	0.57
1	0.346	0.20	0.24	0.30
0.5	0.173	0.12	0.14	0.18
0.25	0.086	0.11	0.14	0.17

Figure [4.21b] Display the range of peak-to-peak deflection force corresponding to the spring constant variation.

Unfortunately we did not perform any MFM at input voltage level lower than $0.25V_{pp}$. In order to estimate the current sensitivity, where SNR=1, we add a trend line to the SNR Vs Input Current curve in *Figure [4.21]*, and extend the line until it crosses SNR=1. The correspondence input current at SNR=1 is around $20\mu A_{rms}$. This current value is closed to what we calculate in *E3.29*, which is $17.3\mu A_{rms}$.

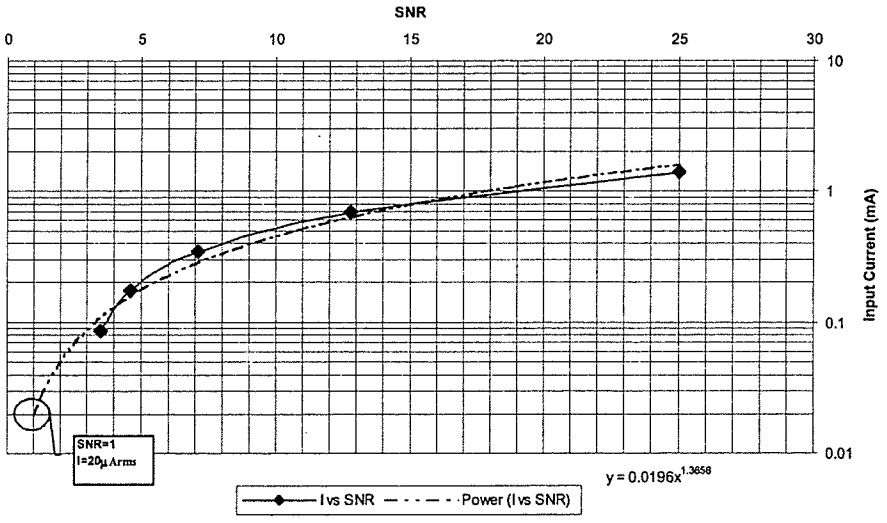

Figure [4.22] A plot of SNR vs Input Current. Trend line is added to estimate SNR=1.

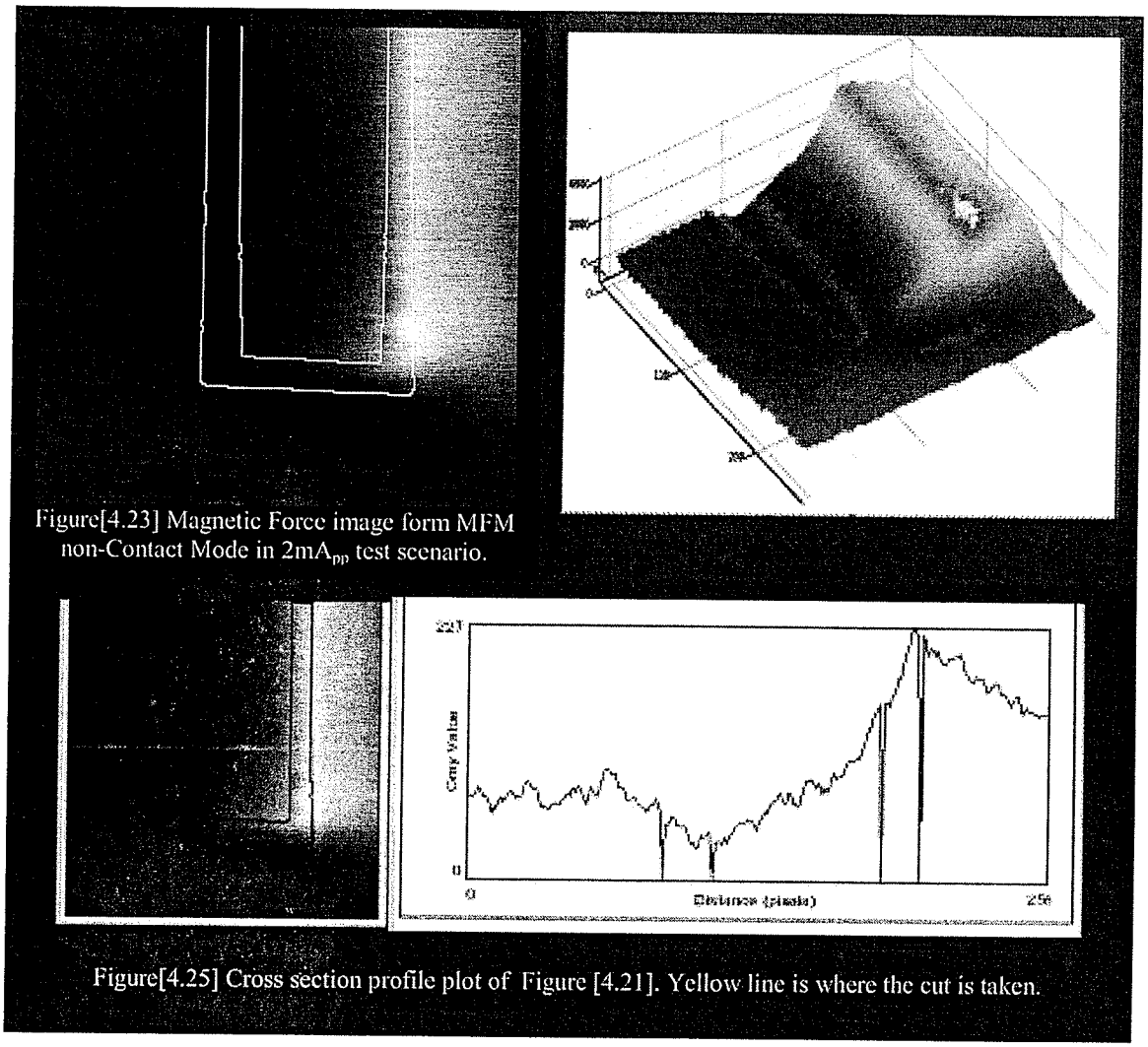

Figure[4.23] Magnetic Force image form MFM non-Contact Mode in $2mA_{pp}$ test scenario.

Figure[4.25] Cross section profile plot of Figure [4.21]. Yellow line is where the cut is taken.

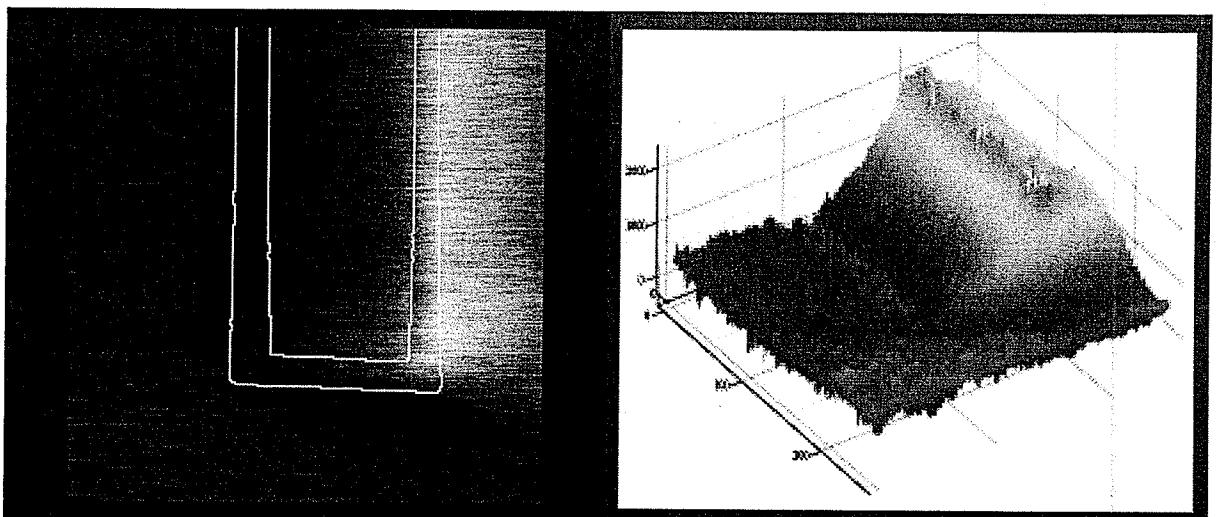

Figure[4.26] Magnetic Force image form MFM non-Contact Mode in $1mA_{pp}$ test scenario.

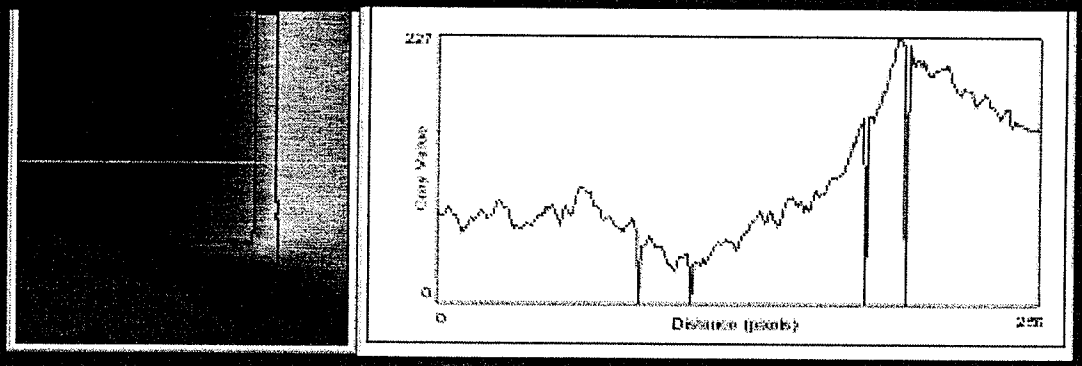

Figure[4.28] Cross section profile plot of Figure [4.24]. Yellow line is where the cut is taken.

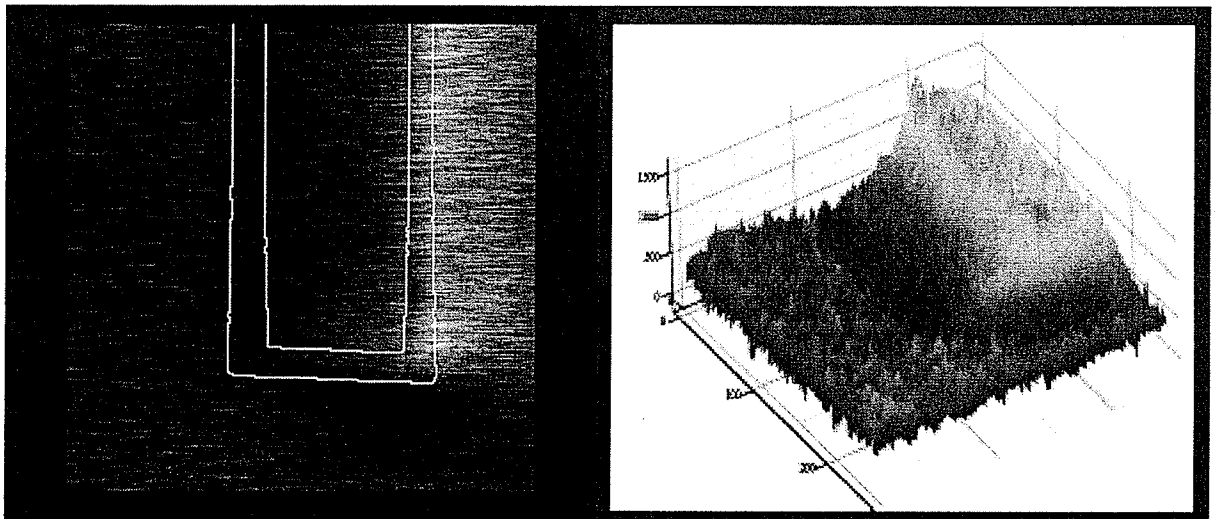

Figure [4.29] Magnetic Force image form MFM non-Contact Mode in 0.5mA$_{pp}$ test scenario.

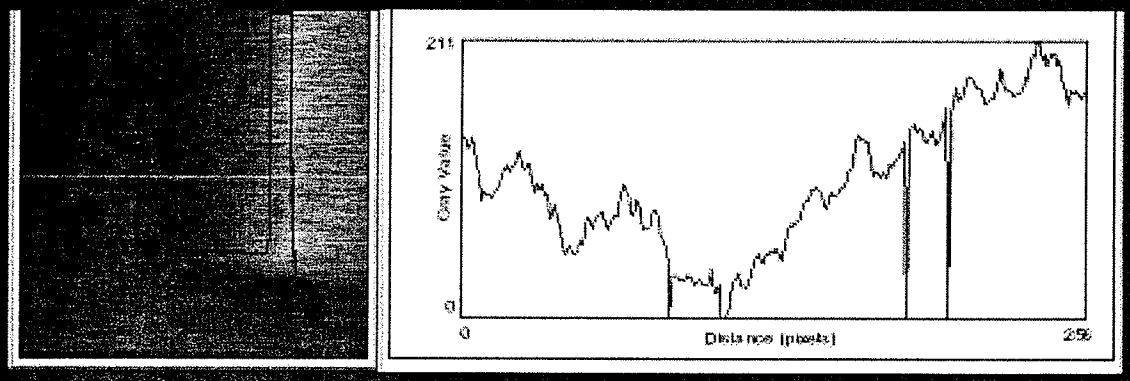

Figure[4.31] Cross section profile plot of Figure [4.27]. Yellow line is where the cut is taken.

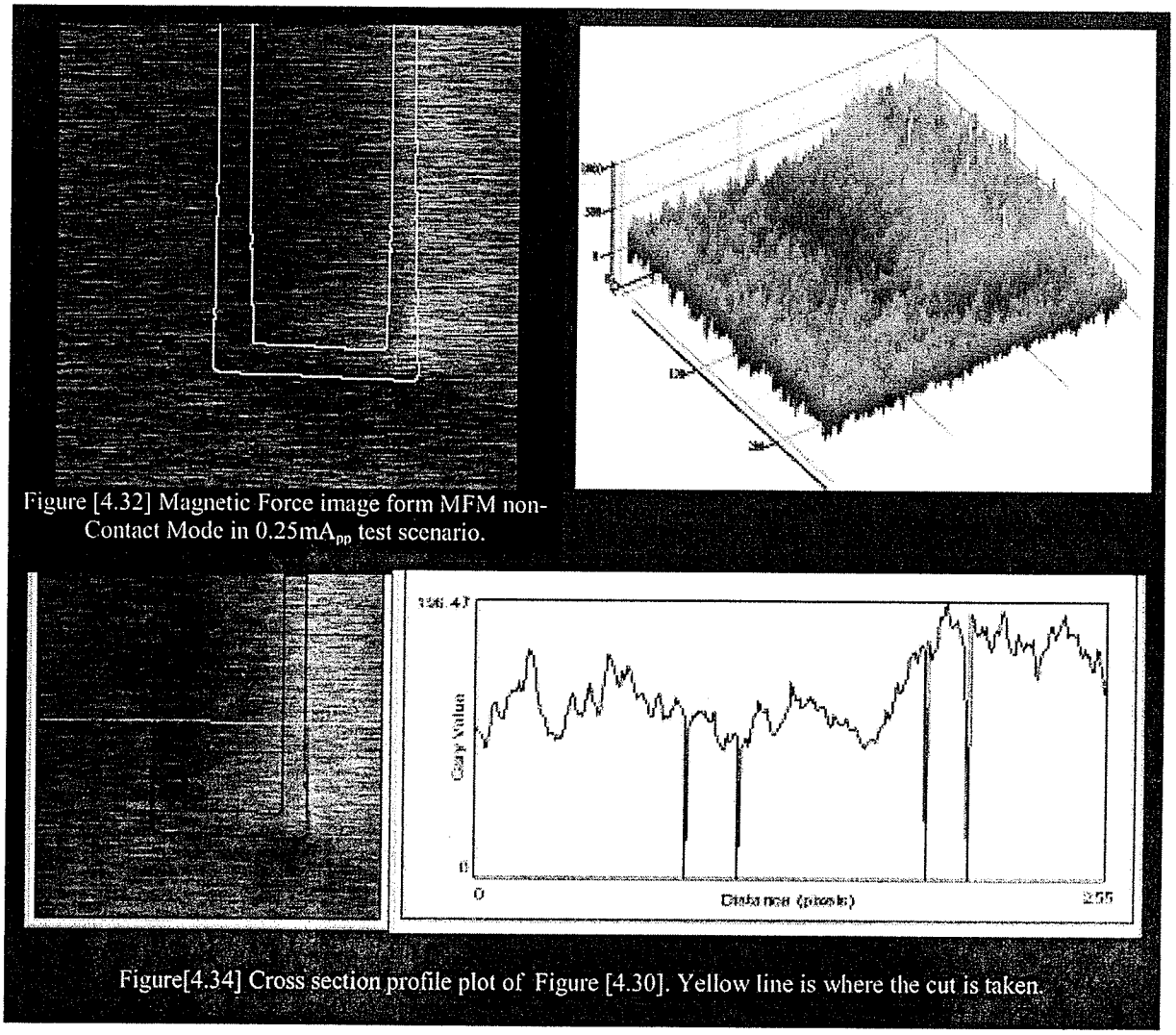

Figure [4.32] Magnetic Force image form MFM non-Contact Mode in 0.25mA$_{pp}$ test scenario.

Figure[4.34] Cross section profile plot of Figure [4.30]. Yellow line is where the cut is taken.

Chapter 5

Software Simulation by MathCAD

MathCAD is selected as the CAD tool to simulate the magnetic field and the distribution of the magnetic interaction force as close to the MFM as possible. We start with modeling the transmission line on a sample circuit area, simulate the induced magnetic field as a result of current flow through the line, simulate the magnetization of the tilted tip and the magnetic deflection force on the cantilever as the result of interaction between the two magnetic fields.

Finally, a comparison between the MFM result and the MathCAD simulated result is performed. Differences from the comparison are analyzed and explanations as well as suggestions are presented. A complete soft code is presented at the Appendix of this thesis.

5.1 MathCAD Modeling

In order to use this mathematic software, we have to construct a data structure with 1μm x 1μm square as single unit to model the transmission line, sample area and all dimensions that we take into consideration. We also have to use some mathematic formulas to model the inducted magnetic field distribution, the magnetic moment of the tip, the gradient operation and the Relative-Interaction-Force.

5.1.1 MathCAD Modeling -Sample Area and Transmission Line

Due to the limited resources on the PC and the lengthy simulation time, we decide to simulate the sample circuit as a transmission line (TLine) lying on a 70μm x 70μm

square surface with 1μm x 1μm as its unit square. X-axis began at 0 unit and ended at 70 unit, Y-axis began at –35 unit and ended at 35 unit. The coordinate for each unit square of the sample area is defined by command *C 5.1,* inside the *Define Coordinate for Area* subroutine.

$$Area := CorA(nBx, nBy, nBz, IniX, IniY, IniZ, unit) \quad [C\ 5.1]$$

The tilted angle of the sample is taken into account; in X direction *TiltX* is 0.06 degree while in Y direction *TiltY* is 0.08237 degree. The result is shown in *Figure [5.1]* and *Figure [5.3]*. The row number of the array represents the total number of segments on the sample area, while column 0, 1 and 2 represent X, Y and Z coordinates of the segment.

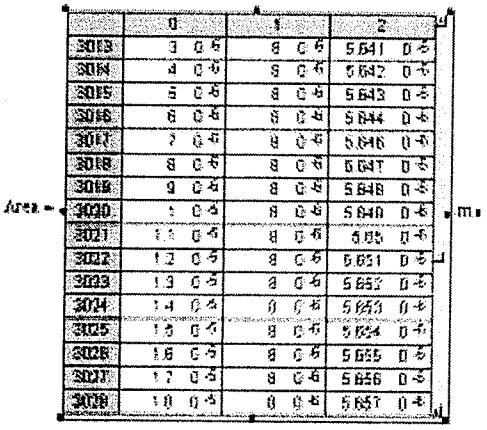

Figure [5.1] Display of the coordinates of the sample of the area in x, y and z.

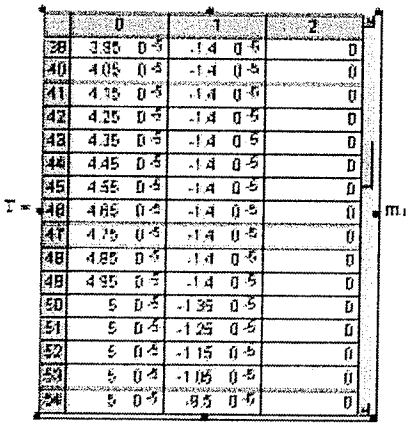

Figure [5.2] Display of the coordinates TLine in x, y and z

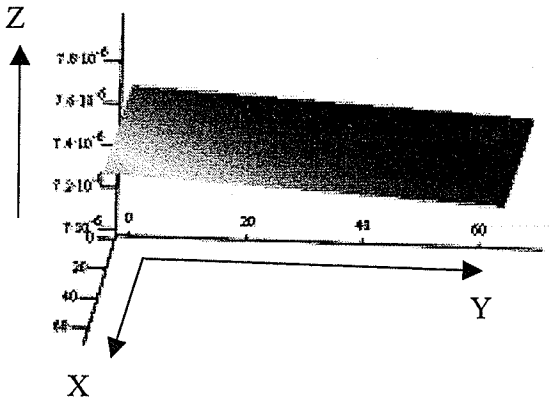

Figure [5.3] Display of the sample surface tilted in the lower right direction

We placed the TLine at the middle of the sample circuit, it was divided into three segments. Their coordinates are displayed in *Figure [5.4]*. The length of the vertical lines is not mandatory while the separation between the two vertical lines must be 28μm. The coordinates of the transmission line are also defined by the following command *C 5.2* inside *Define Coordinate for TLine* subroutine:

```
T1 := CorTL(T1Xini,T1Xend,T1Yini,T1Yend,T1Zini,T1Zend,T1steps,unit)
T2 := CorTL(T2Xini,T2Xend,T2Yini,T2Yend,T2Zini,T2Zend,T2steps,unit)
T3 := CorTL(T3Xini,T3Xend,T3Yini,T3Yend,T3Zini,T3Zend,T3steps,unit)
T := stack(T1,T2,T3)
```

[C 5.2]

Figure [5.2] shows the array of the transmission line with 128 segments in row and X, Y and Z coordinates in corresponding column.

Unit=1μm	Coordinates at the beginning		Coordinates at the end	
	X(unit)	Y(unit)	X(unit)	Y(unit)
Transmission Line Segment 1	0	-14	50	-14
Transmission Line Segment 2	50	-14	50	+14
Transmission Line Segment 3	50	+14	0	+14

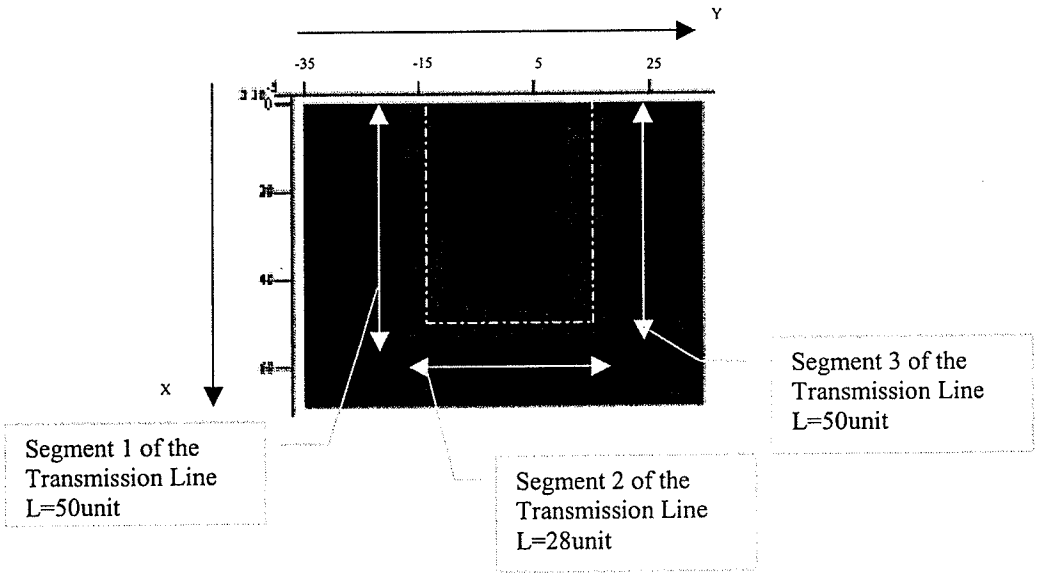

Figure [5.4] Display of the coordinates of the three transmission line segments.

Then the unit vector, $\hat{v} = \frac{\vec{v}}{|v|}$, of the transmission line is defined in the current flow direction by this command *C 5.3,* inside the *Defining Unit Vector of TLine* subroutine.

$$TUV := Unit\_V\_TL(T, SumSegTL)_{[C\ 5.3]}$$

Figure [5.5] is the unit vector array displayed in table format. The row of the table represent the segment of the transmission line that started from 0 to 128; columns 0, 1, 2 of the table represent the coordinates x, y and z.

According to Biot-Savart Law, the magnetic field at a given point on the sample area is the sum of the magnetic field contribution from all transmission line segments to the point. Since we have already defined the coordinates for each segment of the transmission

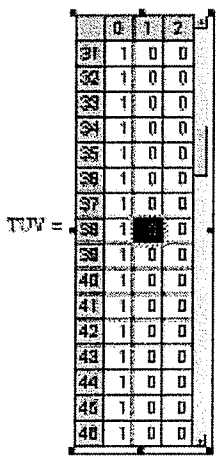

Figure [5.5]
TUV displays the unit vector of the TLine.

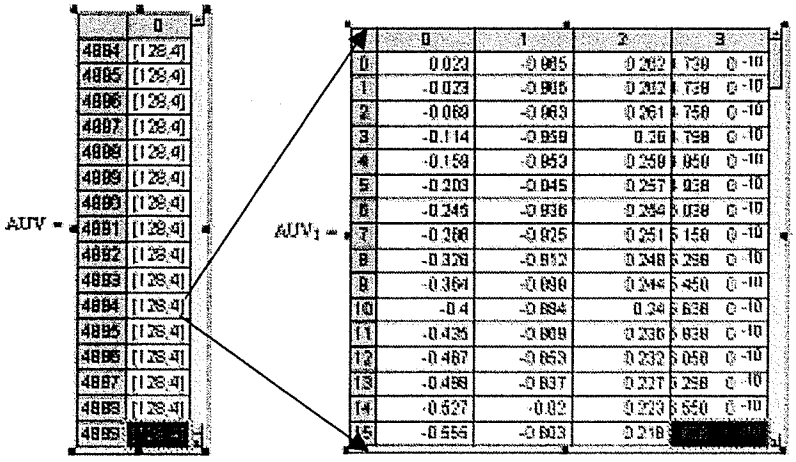

Figure [5.6]
AUV displays the unit vector from each TLine segment to each sample area segment

line and sample area, the unit vector from each line segment to all segments of the sample area and the corresponding distance can be obtained by this command *C5.4*. 7.7μm as the sample height is taken into account when distance between sample and tip is calculated.

$$AUV := Unit\_V\_TL\_Fp(T, Area)_{[C\ 5.4]}.$$

Figure [5.6] shows the nested array in table format. The row number, 0 to 4899, represents the total number of sample segments in the sample area. Each row consists of another array with row number from 0 to 127, which is the number of transmission line segments; column 0, 1 and 2 contain X, Y and Z components of the unit vector from each

segment of the line to a segment of the sample area. Column 3 consists of the square of the distance from each segment of the line to a segment of the sample.

5.1.2 MathCAD Modeling -Magnetic Field

According to Biot-Savart Law, the magnetic field on a given point on the sample area is as follow:

$$d\mathbf{B} = \frac{\mu_0}{4\pi}\frac{Id\vec{l}\times\vec{r}_l}{r^2} \quad \text{[E2.2]}$$

where $\mu_0$is the permeability of free space, which is equal to $4\pi\times10^{-7}\,\mathbf{Wb/A.m}$. I is the current that apply to the transmission line. r_l is the unit vector points from a segment of TLine to a segment of the sample area. ***dl*** is the unit segment of the line in direction of the current flow and ***r*** is the distance from the line segment to the sample area segment.

We start with calculating the cross product of r_l and ***dl***. The following is the equation for vector cross product *E 5.1*, subroutine $CPofUV_{[C\ 5.5]}$ is used to calculate the result. Subscript of any array, $A_{x,y}$, means row "x" and column "y" of array "A".

$$\vec{rl}\times\vec{dl} = \vec{i}(rl_y dl_z - rl_z dl_y) - \vec{j}(rl_x dl_z - rl_z dl_x) + \vec{k}(rl_x dl_y - rl_y dl_x) \quad \text{[E 5.1]}$$

```
CPofUV := | for i ∈ 0..SumSegA - 1
          |   for j ∈ 0..SumSegTL - 1
          |     CP_{j,0} ← TUV_{j,1}·(AUV_i)_{j,2} - TUV_{j,2}·(AUV_i)_{j,1}
          |     CP_{j,1} ← [TUV_{j,0}·(AUV_i)_{j,2} - TUV_{j,2}·(AUV_i)_{j,0}]·(-1)
          |     CP_{j,2} ← TUV_{j,0}·(AUV_i)_{j,1} - TUV_{j,1}·(AUV_i)_{j,0}
          |     Table_i ← CP
          | Table
```

[C 5.5]

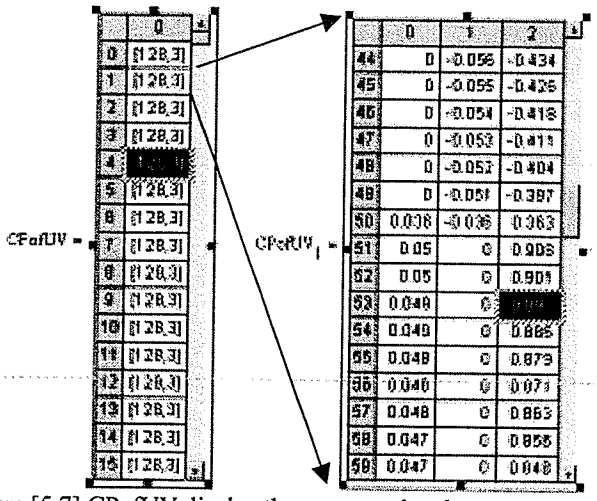

Figure [5.7] CPofUV display the cross product between r_1 and dl.

Subroutine *CPofUV*$_{[C\ 5.5]}$ created a nested array with 4900 rows represent each segment of the sample area, as shown in *Figure [5.7]*. In each row, there is another array with 128 rows representing each segment of the TLine. Column 0, 1 and 2 represent i, j and k directions from the cross-product of TLine unit vector and TLine to sample unit vector.

The following subroutine is used to calculate the magnetic field induced by the TLine over the sample area. $B_{i,0}$ $B_{i,1}$ and $B_{i,2}$ is for magnetic field in X, Y and Z direction.

$$
\begin{aligned}
&\text{BField} := \Big|\ \text{for } i \in 0..\text{SumSegA}-1 \\
&\quad \Big|\ B_{i,0} \leftarrow \sum_{j=0}^{\text{SumSegTL}-1} \frac{\mu o \cdot I}{4\cdot\pi\cdot\left(\text{AUV}_i\right)_{j,3}\cdot m^2}\cdot\left(\text{CPofUV}_i\right)_{j,0}\cdot\mu\cdot m \\
&\quad\ \ B_{i,1} \leftarrow \sum_{j=0}^{\text{SumSegTL}-1} \frac{\mu o \cdot I}{4\cdot\pi\cdot\left(\text{AUV}_i\right)_{j,3}\cdot m^2}\cdot\left(\text{CPofUV}_i\right)_{j,1}\cdot\mu\cdot m \\
&\quad\ \ B_{i,2} \leftarrow \sum_{j=0}^{\text{SumSegTL}-1} \frac{\mu o \cdot I}{4\cdot\pi\cdot\left(\text{AUV}_i\right)_{j,3}\cdot m^2}\cdot\left(\text{CPofUV}_i\right)_{j,2}\cdot\mu\cdot m \\
&\ B
\end{aligned}
\qquad [C\ 5.6]
$$

$\left(\text{CPofUV}_i\right)_{j,0}\cdot\mu\cdot m$ is the X component of the cross-product located at specific row and column. $\left(\text{AUV}_i\right)_{j,3}\cdot m^2$ is the square of the distance between a segment on the TLine and a given point on the sample area. $\sum_{j=0}^{\text{SumSegTL}-1}$ adds up all the magnetic field contribute to a segment of the sample area and assigns the result to a designated address in *Bfield* array. After *C 5.6* has finished its execution, the magnetic field for X,Y and Z direction is then divided into BFieldX, BfieldY and BfieldZ.

Figure 5.8, Figure 5.9 and Figure 5.10 below are the plot of X, Y and Z magnetic fields induced by TLine with a $4V_{pp}$ sine wave as an input voltage.

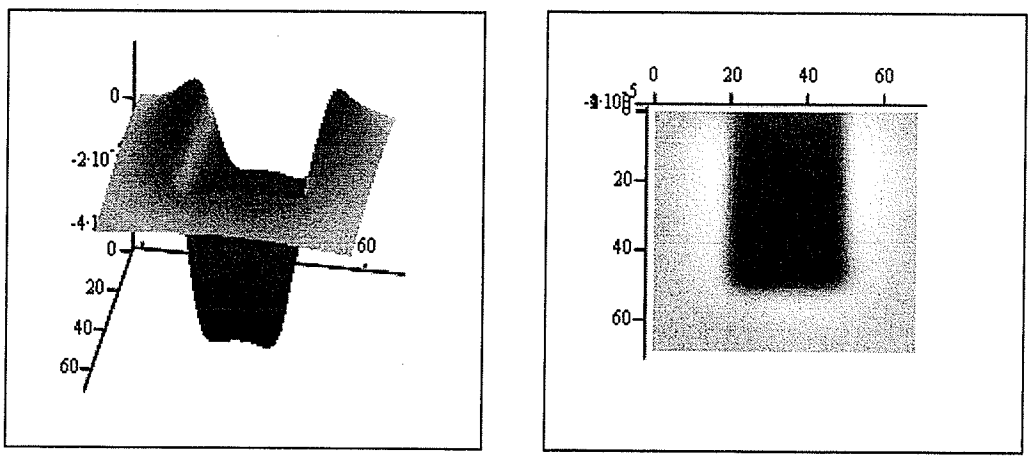

Figure [5.8] Displays of the Z-magnetic field. Maximum magnetic strength in Z direction is around 1.626e-5 T. The minimum magnetic strength in Z direction is around –4.505e-5 T.

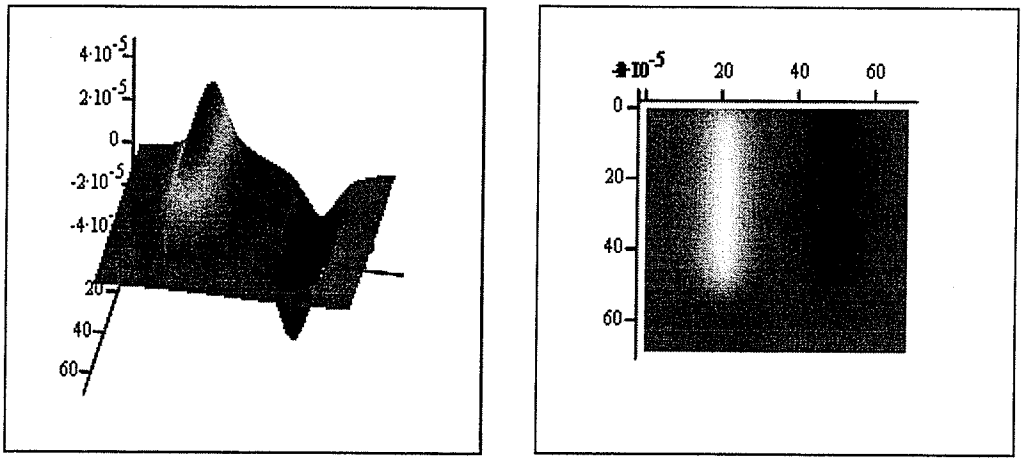

Figure [5.9] Displays of the Y-magnetic field. The maximum magnetic strength in Z direction is around 4.617e-5 T. The minimum magnetic strength in Z direction is around –4.655e-5 T.

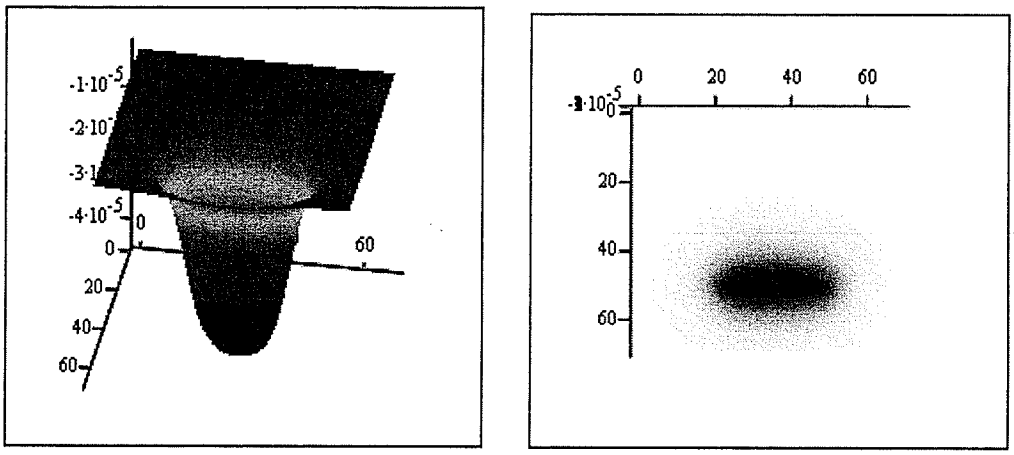

Figure [5.10] Displays of the X-magnetic field. The maximum magnetic strength in Z direction is around -9.773e-8 T. The minimum magnetic strength in Z direction is around –4.514e-5 T.

5.1.3 MathCAD Modeling -Magnetic Moment of the Tip

As what has been discussed in Chapter3, the magnetic field sensitive tip we used in the experiment is obtained by deposition of some γ–Fe_2O_3 powder on the backside of the tip and magnetizes the tip with a permanent magnet. For simplicity, we assumed all magnetic moment of the tip is aligned in Z-direction with 5e-13 Am^2 magnetic strength after the magnetization. Since the tip is tilted 15° in Y and Z axis, we define the Z-magnetic moment as 5e-13 Am^2 * cos(15°) in subroutine $(MomentZ)_{[C\ 5.7]}$, Y-magnetic moment as 5e-13 Am^2 * sin(15°) in subroutine $(MomentY)_{[C\ 5.8]}$. There is almost no X-magnetic moment, since the tilted angle between X and Z axis is 0.06 degree.

5.1.4 MathCAD Modeling-Gradient

The magnetic force resulted from the interaction between the magnetic moment on the tip and magnetic field induced by the TLine is defined as the gradient of the scalar-product of the two magnetic sources as shown in the following equation.

$$\begin{aligned}\vec{F} &= \nabla\left(\vec{M}\cdot\vec{B}\right)\\ &= \nabla\left(\vec{M}_z\vec{B}_z + \vec{M}_y\vec{B}_y\right)\\ &= \nabla\left(\vec{M}\cdot\cos(15°)\vec{B}_z + \vec{M}\cdot\sin(15°)\vec{B}_y\right)\end{aligned} \quad [\text{E } 4.1]$$

We then decompose the force into two components, F_z and F_y. Each component can be defined as follows:

$$\vec{F} = \vec{F}_z\cos(15^0) + \vec{F}_y\sin(15^0); \quad [\text{E } 4.2]$$

$$\vec{F}_z = \vec{M}\cos(15^0)\frac{\partial\vec{B}_z}{\partial z} + \vec{M}\sin(15^0)\frac{\partial\vec{B}_y}{\partial z} = \vec{M}\left[\cos(15^0)\frac{\partial\vec{B}_z}{\partial z} + \sin(15^0)\frac{\partial\vec{B}_y}{\partial z}\right] \quad [\text{E}4.3]$$

$$\vec{F}_y = \vec{M}\cos(15^0)\frac{\partial\vec{B}_z}{\partial y} + \vec{M}\sin(15^0)\frac{\partial\vec{B}_y}{\partial y} = \vec{M}\left[\cos(15^0)\frac{\partial\vec{B}_z}{\partial y} + \sin(15^0)\frac{\partial\vec{B}_y}{\partial y}\right] \quad [\text{E}4.4]$$

In order to perform gradient function on a scalar in MathCAD, we must first define how we want to perform ∂.

$$\nabla\vec{B} = \left(\frac{\partial\vec{B}_x}{\partial x}i + \frac{\partial\vec{B}_y}{\partial y}j + \frac{\partial\vec{B}_z}{\partial z}k\right) \quad [\text{E } 5.2]$$

The purpose of the gradient function is to find the direction of the greatest rate of change of a scalar out of a field, as *E5.2*. To obtain ∂ of the simulated data in the Discrete-Approach, we have to find the different between the two data points in the same direction that we are interested in and divide it by the unit direction. The result is then the slope with direction of the two data points. Unfortunately, due to too small the sampling size of the simulation data, we are not able to obtained a smooth result by using this approach.

On the other hand, to obtain ∂ of the simulated data in Continues-Approach, we choose a series of data points along the direction that we want to perform ∂ on, used curve-fitting function to obtain an equation out of the series data. Then we perform derivative function on the equation with respect to the desire direction. From the derivative result we can find the ∂ of each data point and a smoother image. The following figures show the result of the two approached. *Figure [5.12]* shows the result yielded by the Discrete-Approach and *Figure [5.11]* shows the result yielded by the Continues-Approach. Due to Discrete-Approach is more sensitive to the slope of the curve; it yielded high peak value, which is almost double to the peck value on the Continues-Approach and steeper slope.

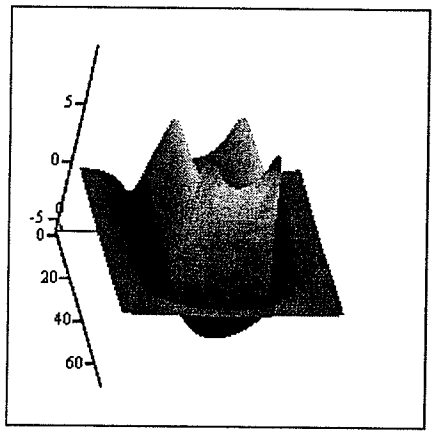

Figure [5.11] Displays of the $\frac{\partial F_z}{\partial z}$ in Continues-Approach.

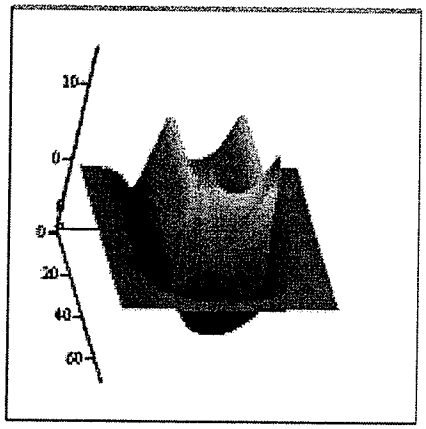

Figure [5.12] Displays of the $\frac{\partial F_z}{\partial z}$ in Discrete- Approach.

5.1.5 MathCAD Modeling -Gradient-∂y

In our application, we chose 5 simulated data points for each curve-fitting operation. The degree of polynomial equation for curve-fitting is set to 4. For BFieldY / ∂y, we divide the BFieldY into an array with 980 columns and 5 rows by the following

command *C 5.7*, where nD is the number of data for each derivative that is defined at the beginning of the program as 5. *Figure [5.13]* shows the new array. We can also perform the same function to X-magnetic field, *Dyx*, and to Z-magnetic field, *Dyz*.

$$\begin{aligned}
&Dyy := \left|\begin{array}{l} n \leftarrow -1 \\ \text{for } i \in 0..nBx-1 \\ \quad \text{for } j \in 0..nBy-1 \\ \quad\quad \left|\begin{array}{l} n \leftarrow n+1 \text{ if } mod(j,nD)=0 \\ D_{mod(j,nD),n} \leftarrow BFieldY_{i,j} \end{array}\right. \\ D \end{array}\right. \\
&\qquad\qquad\qquad\qquad\qquad\qquad\qquad\qquad\qquad\qquad\qquad\qquad\qquad\qquad\qquad\qquad [C\ 5.9]
\end{aligned}$$

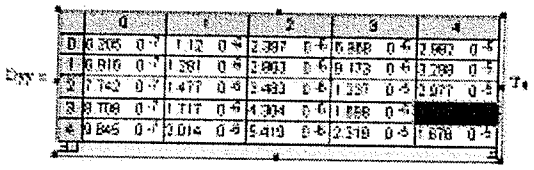

Figure [5.13] Displays of the rearrange data from BFieldY.

We then extract column by column from the array *Dyy* by this command line.

$$x \leftarrow submatrix\left(\frac{df}{tesla}, 0, nD-1, i, i\right) \qquad [C\ 5.10],$$

For each column we extract, we perform polynomial regression on these data by this command line *C 5.9*,

$$z \leftarrow regress(y, x, Poly) \qquad [C\ 5.11].$$

We then perform the polynomial fitting function and Y-derivative with 1μm as its step size on the curve with function *C 5.10*.

$$dCF_{k,i} \leftarrow \frac{d}{dn} interp(z, x, y, n) \qquad [C\ 5.12],$$

Then we assign the result to the *dCFy* array which has the same data format as *Dyy*. The following displays the whole *dCFy* subroutine.

$$
\begin{aligned}
&\text{dCFy}(df, yn) := \left|\begin{array}{l}
\text{for } m \in 0..nD-1 \\
\quad y_m \leftarrow m \\
\text{for } i \in 0..nDAxisY-1 \\
\quad \left|\begin{array}{l}
x \leftarrow \text{submatrix}\left(\frac{df}{tesla}, 0, nD-1, i, i\right) \\
z \leftarrow \text{regress}(y, x, Poly) \\
k \leftarrow 0 \\
\text{for } n \in 0, yn..nD-1 \\
\quad \left|\begin{array}{l}
dCF_{k,i} \leftarrow \frac{d}{dn}\text{interp}(z, x, y, n) \\
k \leftarrow k+1
\end{array}\right.
\end{array}\right. \\
\frac{dCF}{\mu}
\end{array}\right. \qquad \text{[C 5.13]}
\end{aligned}
$$

Finally, we reconstruct the data back into a 70 x 70 array. The following shows the subroutine.

$$
\begin{aligned}
&\text{Rgroupy}(df) := \left|\begin{array}{l}
A \leftarrow 0 \\
B \leftarrow 0 \\
\text{for } i \in 0, \frac{nBy}{nD}..nDAxisY - \frac{nBy}{nD} \\
\quad \left|\begin{array}{l}
\text{for } j \in 0..\frac{nBy}{nD}-1 \\
\quad \left|\begin{array}{l}
\text{if } j = 0 \\
\quad \left|\begin{array}{l}
A \leftarrow 0 \\
A \leftarrow \text{submatrix}(df, 0, nD-1, j+i, j+i)
\end{array}\right. \\
A \leftarrow \text{stack}(A, \text{submatrix}(df, 0, nD-1, j+i, j+i)) \quad \text{otherwise}
\end{array}\right. \\
B \leftarrow A \quad \text{if } i = 0 \\
B \leftarrow \text{augment}(B, A) \quad \text{otherwise}
\end{array}\right. \\
B \cdot \frac{kg}{m\,s^2 A}
\end{array}\right. \qquad \text{[C 5.14]}
\end{aligned}
$$

Figure [5.14] displays the original Y-magnetic field, *Figure [5.15]* displays the Y- derivative of Y-magnetic field.

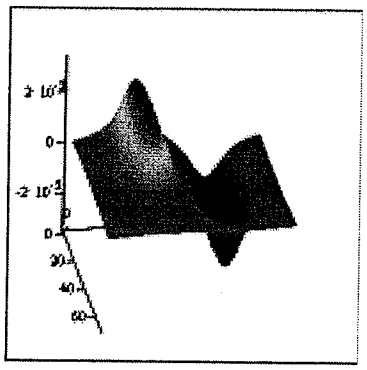

Figure [5.14] Displays of the Y-magnetic field.

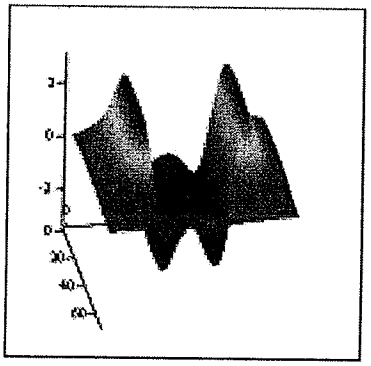

Figure [5.15] Displays of the Y-derivative of Figure [5.14]

Subroutines have also been written for X-magnetic field. But due to the insignificant values of X-magnetic moment, we disable the subroutines in MathCAD in order to save time and memory resources.

5.1.6 MathCAD Modeling -Gradient-∂z

On our MFM setup, the tip is set 1μm away from the sample surface before performing non-contact scanning. But from what we have discussed in section 4.3.1 the actual scanning height is 7.7 μm.

For BFieldZ / ∂z, we decide to take a different approach than BFieldY / ∂y. First, we simulate the test with similar test conditions but in different tip to sample distance, 1.7 μm, 3.7 μm, 5.7 μm, 7.7 μm and 9.7 μm. Results from these simulations were stored on the disk, and a subroutine, *Read Data*, is used to retrieve these data. For each segment of the sample area, we import its Z-magnetic field at its different scanning heights and store them in an array on the same column but different row, as in *Figure [5.16]*. The following is the subroutine we used to achieve this result.

```
Dzz := | k ← 0
       | n ← -1
       | for i ∈ 0..nBy - 1
       |   for j ∈ 0..nBx - 1
       |     k ← j + i·(nBx)
       |     m ← 0
       |     D[m,k] ← b1z[i,j]
       |     D[m+1,k] ← b3z[i,j]
       |     D[m+2,k] ← b5z[i,j]
       |     D[m+3,k] ← b7z[i,j]
       |     D[m+4,k] ← b9z[i,j]
       | D
```

[C 5.15]

Dzz =

	0	1	2	3	4
0	2.866·10⁻⁵	3.008·10⁻⁵	3.342·10⁻⁵	3.622·10⁻⁵	3.937·10⁻⁵
1	2.738·10⁻⁵	2.942·10⁻⁵	3.168·10⁻⁵	3.417·10⁻⁵	3.695·10⁻⁵
2	2.63·10⁻⁵	2.702·10⁻⁵	2.889·10⁻⁵	3.093·10⁻⁵	3.314·10⁻⁵
3	2.262·10⁻⁵	2.396·10⁻⁵	2.539·10⁻⁵	2.689·10⁻⁵	2.845·10⁻⁵
4	1.959·10⁻⁵	2.053·10⁻⁵	2.149·10⁻⁵	2.246·10⁻⁵	[illegible]

T

Figure [5.16] Displays of the rearrange data from BFieldZ.

The following subroutine is for polynomial curve fitting operation of the data which is similar to BFieldY / ∂y. The only difference on this subroutine is the step size of the Z-derivative. For Y-derivative the step size is set to 1μm because each sample area segment is defined as 1μm square. For Z-derivative the step size is set to 2μm because it is the closest possible multiple of 7.7μm with the initial height as 1.7μm. *C 5.14* is the subroutine we used to achieve this. As a result, we have created an array with 5 rows and 4900 columns and each row contains data from different scanning heights, from 1.7μm to 9.7μm as what is shown in *Figure [5.17]*. Our interest is on row number 3, which *HighZ* is 7.7μm.

dCFz(Dzz, 1.7, 2) =

	4891	4892	4893	4894	4895	4896	4897	4898	4899
0	-0.025	-0.023	-0.021	-0.019	-0.017	-0.016	-0.015	-0.013	-0.012
1	-0.052	-0.048	-0.042	-0.04	-0.037	-0.034	-0.031	-0.029	-0.026
2	-0.075	-0.069	-0.064	-0.059	-0.054	-0.049	-0.046	-0.042	-0.039
3	-0.092	-0.085	-0.079	-0.073	-0.067	-0.062	-0.057	-0.053	-0.049
4	-0.103	-0.096	-0.089	-0.083	-0.077	-0.071	-0.066	-0.061	[illegible]

Figure [5.17] Displays of the Z derivative of Z-magnetic field. Row 0 is from HighZ 1.7μm and row 4 is from HighZ 9.7μm

```
dCFz(df, zi, zn) := | for m ∈ 0 .. (nD - 1)
                    |   y_m ← zi + m·zn
                    | for i ∈ 0 .. nDAxisZ - 1
                    |   | x ← submatrix(df/tesla, 0, nD - 1, i, i)
                    |   | z ← regress(y, x, Poly)
                    |   | k ← 0
                    |   | for n ∈ 0 .. (nD - 1)
                    |   |   | g ← zi + n·zn
                    |   |   | dCF_{k,i} ← (d/dg) interp(z, x, y, g)
                    |   |   | k ← k + 1
                    | dCF/μ
```

[C 5.16]

Finally, the reconstruction of the array is much simpler, since all desire data is laying on the same row. The subroutine of this function *C 5.15* is shown as follows.

```
Rgroupz(df, z) := | k ← 0
                  | for j ∈ 0 .. nBy - 1
                  |   for i ∈ 0 .. nBx - 1
                  |     | B_{j,i} ← df_{z,k}
                  |     | k ← k + 1
                  | B·kg/(m·s^2·A)
```

[C 5.17]

Figure [5.18] displays the original Z-magnetic field. *Figure [5.19]* displays the Z-derivative of Z-magnetic field. Figure [5.20] shows the horizontal cross section at y=35

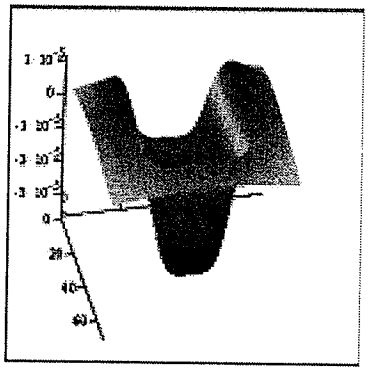

Figure [5.18] Displays of the Z-magnetic field.

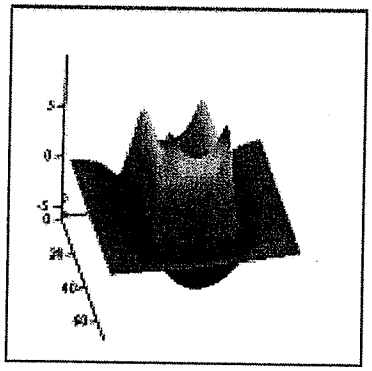

Figure [5.19] Displays of the Z-derivative of Figure [5.18]

of the z-magnetic field for each different scanning height, 1.7μm, 3.7μm, 5.7μm, 7.7μm and 9.7μm.

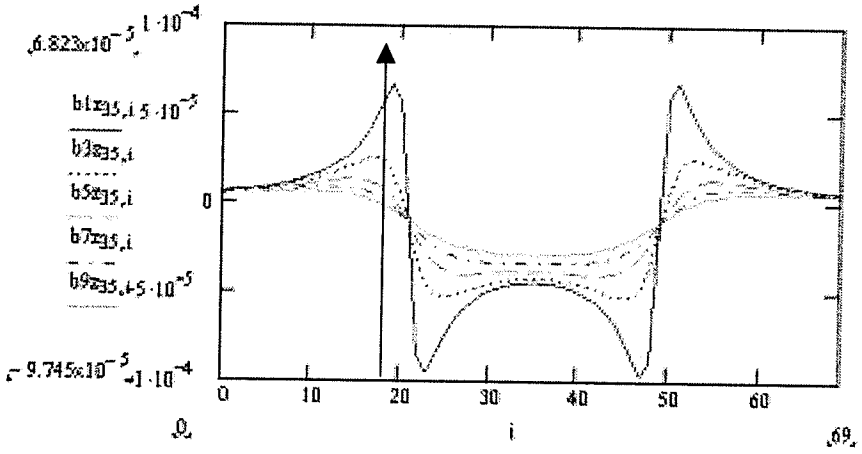

Figure [5.20] Shows the cross section of z-magnetic field for different scanning height. The arrow shows the direction that the Z derivative take place.

5.1.7 MathCAD Modeling -Magnetic Interaction Force, Fy and F_z

At the beginning of this section, we have defined Fy as follows:

$$F_y = \overrightarrow{M}\cos(15^0)\frac{\partial \vec{B}_z}{\partial y} + \overrightarrow{M}\sin(15^0)\frac{\partial \vec{B}_y}{\partial y} \quad \text{[E 4.3]}$$

The first item of the equation can be obtained by taking the magnetic moment of the tip in Z direction (*MomentZ*) [C5.7] and multiplying by the Z magnetic field in derivative of Y *Rgroupy(dCFy(Dyz,1))* [C 5.18] , it is a combination of functions *C 5.9, C 5.13* and *C 5.14.* The second item of the equation *E 4.3* can be obtained by multiplying the magnetic moment of the tip in Y direction (*MomentY*) [C 5.8] by the Y magnetic field in derivative of Y *Rgroupy(dCFy(Dyy,1))* [C 5.19] , it is a combination of functions *C 5.9, C 5.13* and *C 5.14. Figure [5.21]* below displays a plot for F_y which is the sum of Figure *[5.22]* as the first component of the F_y and *Figure [5.23]* as the second component of the F_y. The unit for the plots is in Tesla.

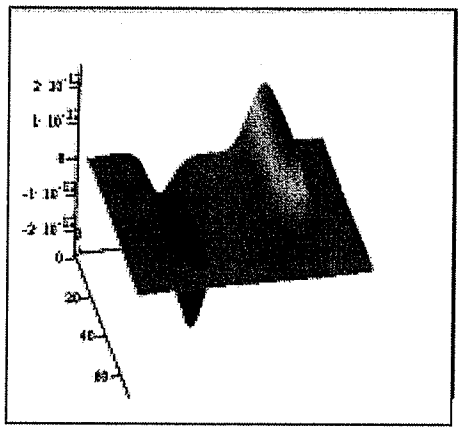

Figure [5.21] Displays of the plot of equation E4.3, which is a Y-magnetic interaction force. It is sum of Figure [5.22] and Figure [5.23]

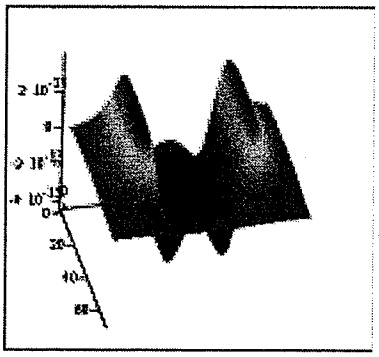

Figure [5.22] Displays of the plot of the first items in E4.3

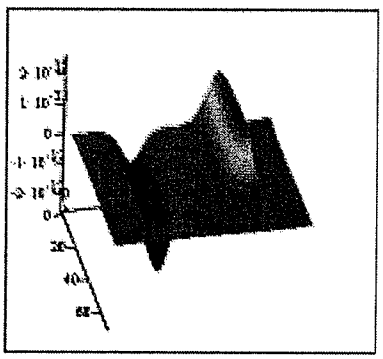

Figure [5.23] Displays of the plot of the second items in E4.3

F_z is also defined as follow and *Figure [5.24]* is the result plot.

$$F_z = \overrightarrow{M}\cos(15^0)\frac{\partial \vec{B}_z}{\partial z} + \overrightarrow{M}\sin(15^0)\frac{\partial \vec{B}_y}{\partial z} \text{ [E 4.4].}$$

To obtain the first component of the F_z in equation *E4.4*, we multiplying the magnetic moment of the tip in Z direction (*MomentZ*) [C5.7] by the Z magnetic field in derivative of Z, *Rgroupz(dCFz(Dzz,0.4),8)* [C 5.20] , it is a combination of functions *C 5.15, C 5.16* and *C 5.17*. The second item of the equation *E 4.4* can be obtained by multiplying the magnetic moment of the tip in Y direction (*MomentY*) [C 5.8] by the Y magnetic field in derivative of Z *Rgroupz(dCFz(Dzy,0.4),8)* [C 5.21] , it is a combination of functions *C 5.15, C 5.16* and *C 5.17*. The unit for the following plots is in Tesla.

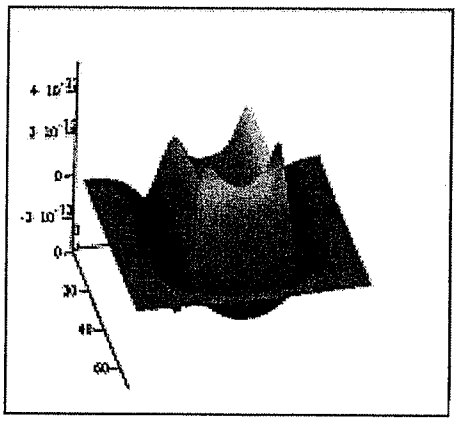

Figure [5.24] Displays of the plot of equation E4.4, which is a Z-magnetic interaction force. It is sum of Figure [5.25] and Figure [5.26]

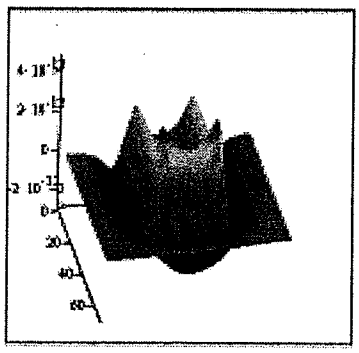

Figure [5.25] Displays of the plot of the first items in E4.4

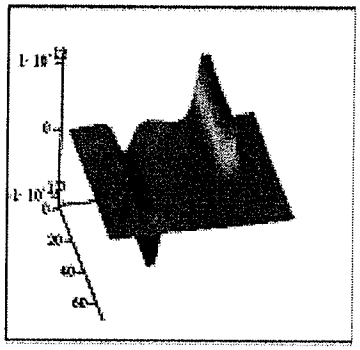

Figure [5.26] Displays of the plot of the second items in E4.4

For total magnetic interaction force, it is defined as follow:

$$\overrightarrow{F} = \cos(15^0)F_z + \sin(15^0)F_y; \text{[E 4.2]},$$

Figure [5.27] below shows the simulated result image of F by subroutine *C 5.22.*

$$F := Fz \cdot \cos(Tilt) + Fy \cdot \sin(Tilt) \cdot \text{[C 5.22]}$$

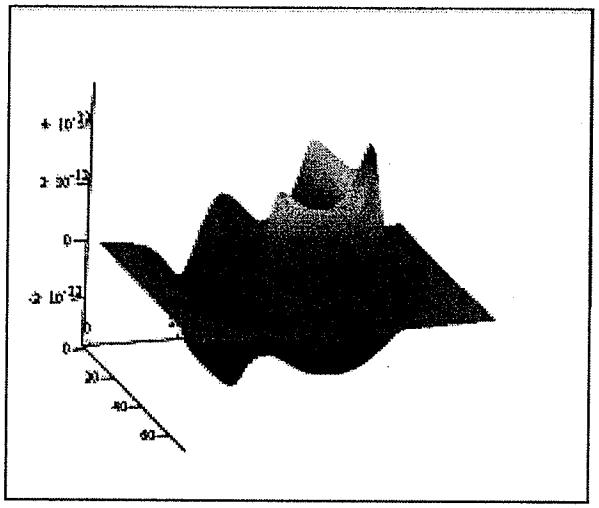

Figure [5.27] Display of the total interaction force between the tip and the surface. It is the sum of Figure [5.21] and Figure [5.24].

5.2 Scanning Effect

As what has been discussed in section 2.2.11 and 3.3.1, the result obtained by the MFM is no longer the direct interaction force between the tip and surface but is the Relative-Interaction-Force between the two due to the effect of our scanning technology. To model this using MathCAD, we need to know the initial location of the tip before the scanning starts. As what is written in section 4.1.1, X and Y offset of the scanning is set

to 30μm. After having done some correlation analysis on the MFM image result and the MathCAD simulation result, the closest approximation of the tip initial location is X=10 and Y=0. The magnetic force of this point is then becoming the reference zero for the total force. The *C 5.23* subroutine is used to obtain *Figure [5.28]*, which shows the Relative-Interaction-Force between the tip and surface and *Figure [5.29]* displays the comparison between the interaction force and the Relative-Interactive-Force at cross section y=35. As we can observe form the *Figure [5.29]*, there is no major difference between the two plot, since the magnetic filed at the initial tip location, where X=10 and Y=0 is very close to zero.

```
df := | for i ∈ 0 .. nBx - 1
      |   for j ∈ 0 .. nBy - 1
      |     | G[i,j] ← F[i,j-1] - F[i,j-2]  if j = nBy - 1
      |     | G[i,j] ← F[i,j+1] - F[0,10]   otherwise
      | G
```

[C 5.23]

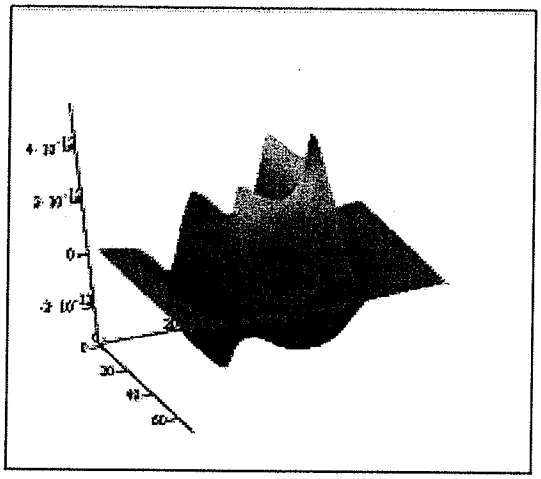

Figure [5.28] Display of the total Relative-Interaction-Force.

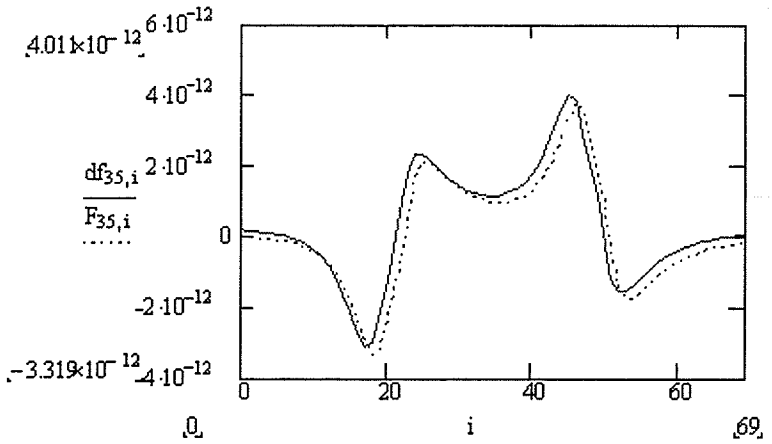

Figure [5.29] Display of the comparison between the total interaction force (in dotted blue) and the relative interaction force (in red).

5.3 Simulation Result and MFM Result Comparison

In this section, a comparison between MFM result and MathCAD simulated result is presented. Some suggestions and explanations are also presented on these differences. *Figure [5.30]* below displays the image result and some important parameters of MFM and MathCAD obtained in $4V_{pp}$ test scenario in two parallel columns side by side.

After we compared the two images result, we observed two major discrepancies existed. Firstly, the shape of the two surface plots does not fully coincide, especially the area at the right hand side of the image and the area in between the two parallel transmission lines. These two areas are shown in the blue circle area on *Figure [5.31]*. Secondly, the magnitude of the interaction force between the magnetic moment on the tip and the magnetic field on the surface of MFM result is about 7 times lower then the simulation.

Magnetic Force Microscopy		MathCAD Simulation	
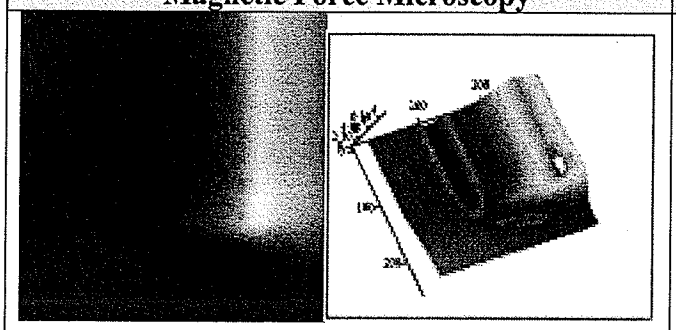		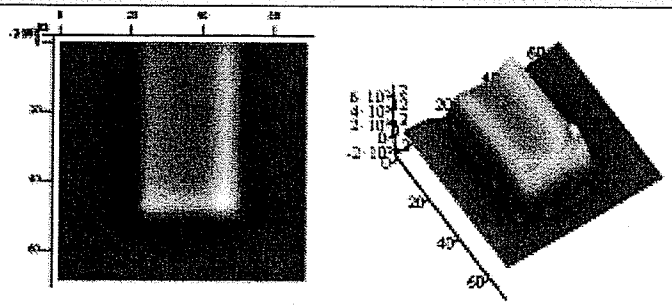	
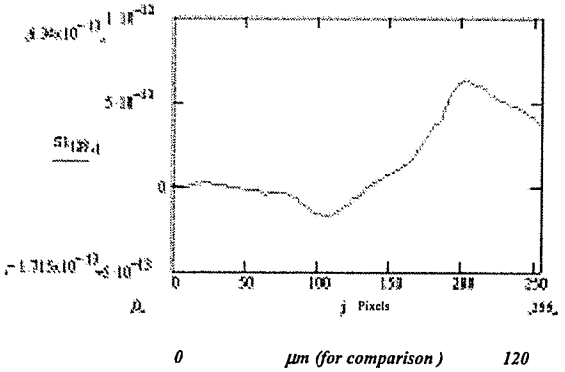		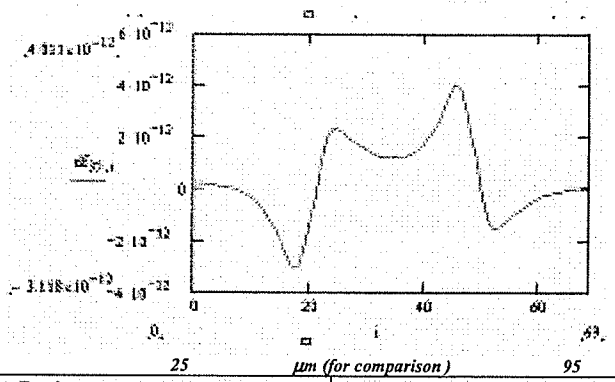	
0 μm (for comparison) 120		25 μm (for comparison) 95	
Peak-to-peak Deflection Force *(pN)*	**SNR ΔZ_{th}=0.03nm ΔZ=0.75nm**	**Peak-to-peak Deflection Force *(pN)***	**SNR ΔZ_{th}=0.03nm ΔZ=5.45nm**
0.79 @ k_{eff}=0.026N/m.	25	**8.65**	182
0.96 @ k_{eff}=0.032N/m.			
1.16 @ k_{eff}=0.038N/m.			

Figure [5.30] Display of the comparison of result image and parameters between MFM and MathCAD simulation result.

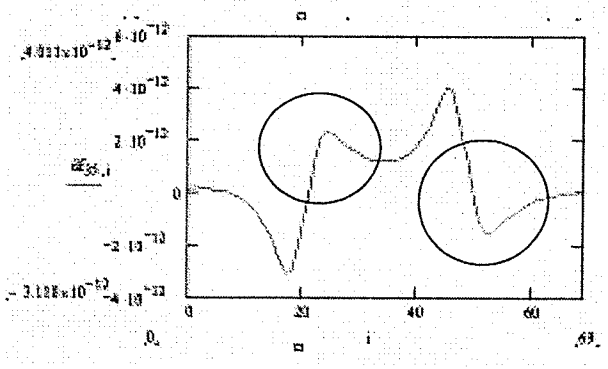

Figure [5.31] Highlight the two differences from waveform comparison.

The main suspect reason for having these differences on the image is the distribution of the magnetic moment on the backside of the tip. For simplicity reason, we model the magnetic moment on the tip as a single moment, but on reality the magnetic moment on the tip is combination of multiple magnetic moment in multiple direction. *Figure [5.32]* display the differences between the modeling we chose and the reality.

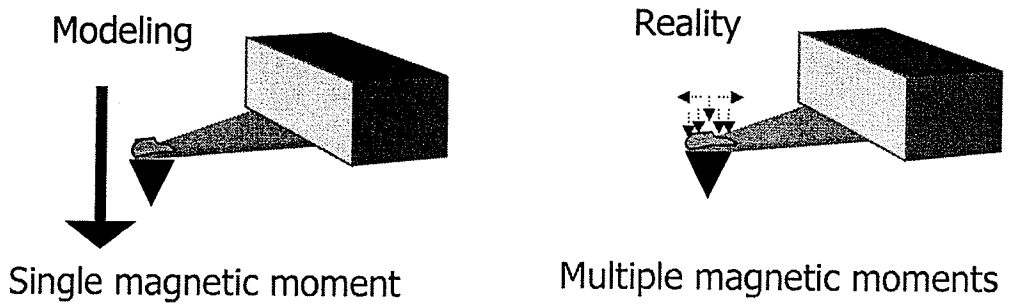

Figure [5.32] Display the different between the modeling (single magnetic moment) we chose and the reality (multiple magnetic moment).

To verify this argument, we simulated the force as the interaction between a distribution of multiple magnetic moments in single direction and the magnetic fields on the surface. From *Figure [5.33]*, we estimated the multiple magnetic moment area as a 10μm x 10μm square.

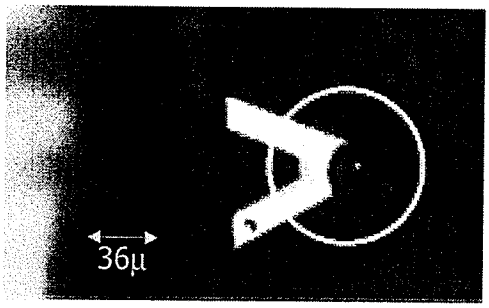

Figure [5.33] Display size of the γ–Fe_2O_3 deposition on the backside of the tip.

We scanned the square over the image with increment of 1μm. We take the average interaction force within the square and assigned it to the center of the square, as shown in *Figure [5.34]*.

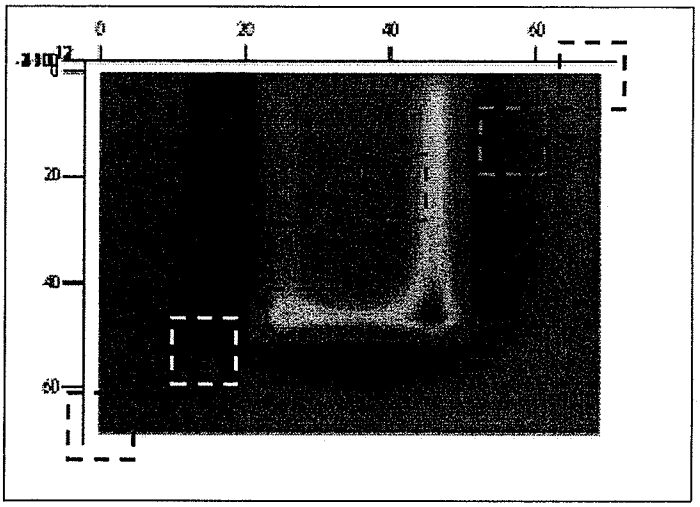

Figure [5.34] Display how we model the interaction force between multiple magnetic moment and magnetic field.

The results from the simulation with 6μm x 6μm-square, 10μm x 10μm-square, 20μm x 20μm-square with the comparison of the MFM result are displayed in *Figure [5.35]*. From the comparison, we concluded that the simulation with 10μm x 10μm-square yielded image result that is very closed to MFM result image.

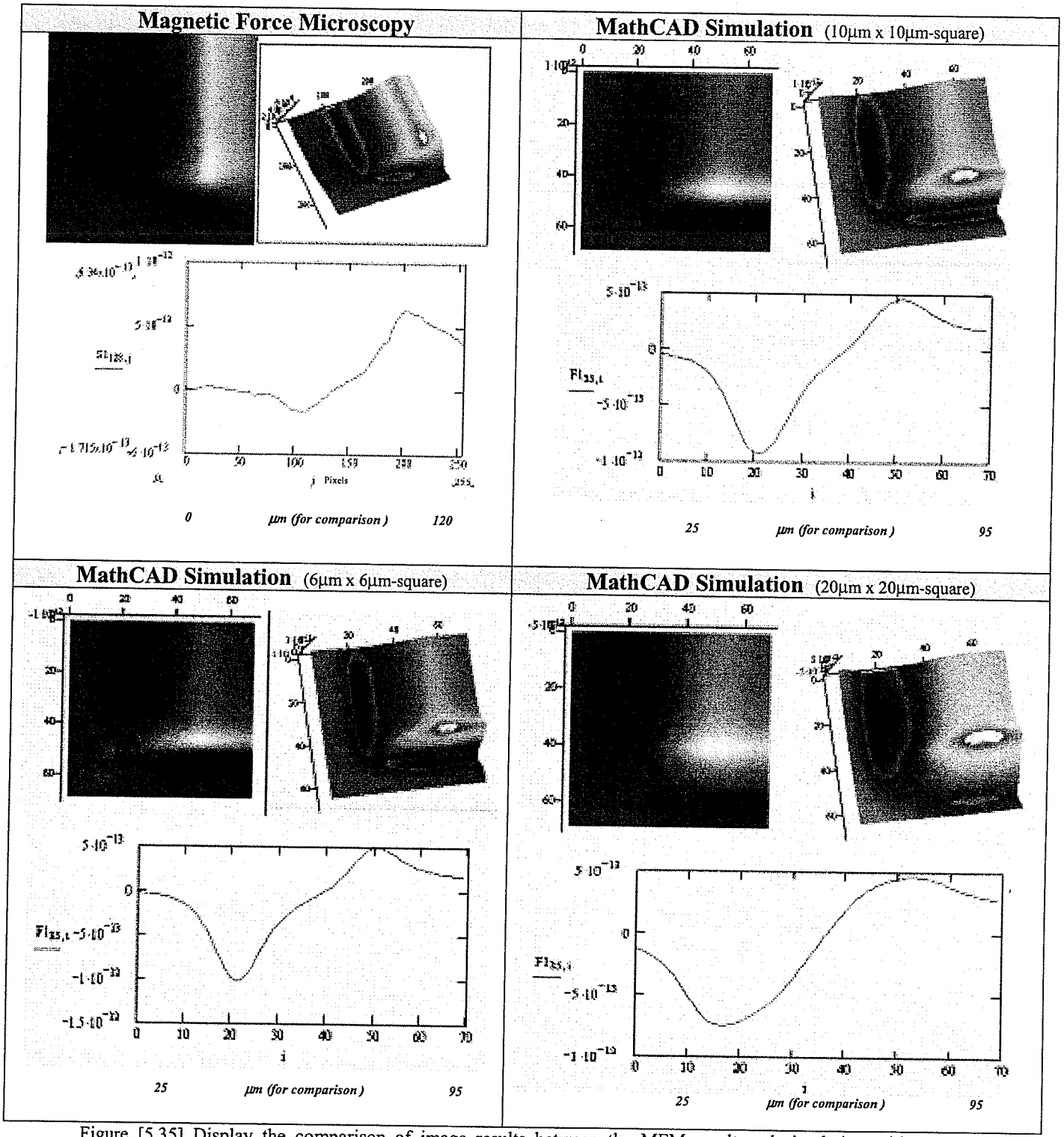

Figure [5.35] Display the comparison of image results between the MFM result and simulation with different square sizes.

Secondly, we also suspect the tilted angle of the tip which is mainly caused by human error when we manually assembled the tip on the cantilever. We cut the cantilever out from the carrier manually and attached the cantilever on a piece of PCB by glue. Unlike the tilted angle of the sample that can be detected and measured by the cross section profile plot of the MFM image, the tilted angle of the tip is very difficult to define and study. The unevenness of the PCB surface, glue thickness and misalignment of the cantilever and the PCB can create a very complicated 3-dimentional tilted angle. *Figure [5.36]* displays the possibility of the tip-tilted angle.

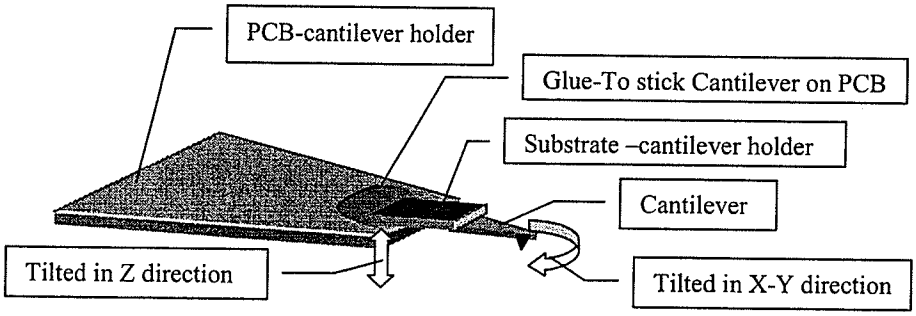

Figure [5.36] Display of the possibility of the tip tilted angle.

On the other hand, it was also not an easy job to deposit the γ–Fe_2O_3 powder evenly on the backside of the tip. From the picture in *Figure [5.33]*, which was taken on the tip, the possibility of having the powder not concentrated at the middle of the cantilever is high. This might also create a 3-dimentional tilted angle of the magnetic moment on the tip.

In order to validate this argument, we used MathCAD to simulate the tilted tip scenario. After many trials with different tilted angles in x, y and z, we find the closest possibility is to assume the Z-magnetic moment on the tip titled ~2 degree in the Y direction. As we compare the *Figure [5.39]* and *Figure [5.40]*, we can conclude that our assumption is quite close to reality. *Figure [5.37]* below displays the magnitude of the Z-magnetic moment over the scanning surface and *Figure [5.38]* displays the surface plot of the Relative-Interaction-Force result from *Figure [5.35]*(10μm x 10μm-square). *Figure [5.39]* displays the cross section profile plot of the *Figure [5.38]*. *Figure [5.40]* displays the cross section profile plot of the MFM result.

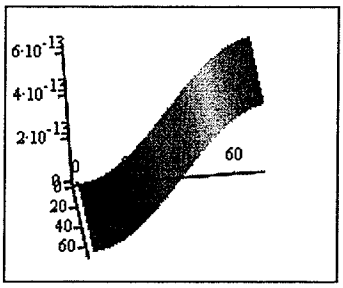

Figure [5.37] Displays of the Z-magnetic moment of a tilted tip.

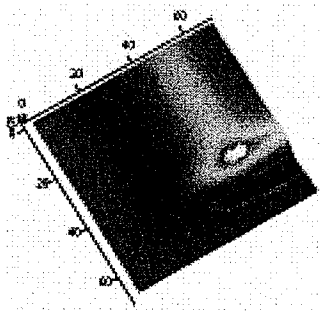

Figure [5.38] Displays of the surface plot of the Relative- Interaction-Force.

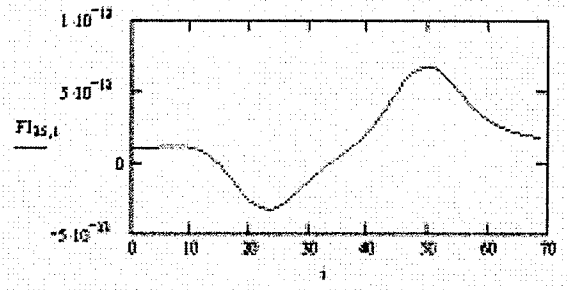

Figure [5.39] Displays of the cross section profile plot of the interaction force.

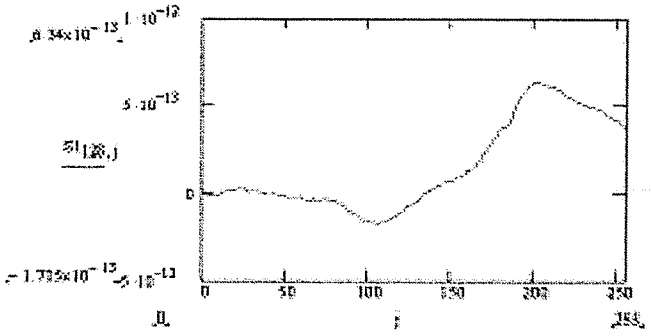

Figure [5.40] Displays of the cross section profile plot of the MFM $4mA_{pp}$ test scenario.

From the comparison, we also observed that the magnitude of interaction force extracted by MFM is quite low. One of the others causes that result in this weak reception of the reflected laser beam by the bi-cell photodiode might be the tip we use in this experiment. As we mentioned before, we deposited γ–Fe_2O_3 substance with an adhesive agent on the backside of the tip in order to have the tip sensitive to the magnetic interaction. The backside of a plain cantilever as manufactured is always flat and coated with a thin gold film so that we can have good light reflection on it.

Due to the deposition of the magnetic substance, the surface is no longer flat; unevenness and bump are created on the backside of the tip. Therefore the reflection efficiency of the laser beam on the cantilever decrease dramatically; only partial of the reflecting laser beam is directed to the bi-cell photodiode, while most of it are diverted to other directions, as what is shown in *Figure [5.41]*.

The best sum of the reflected laser beam received by photodiode in term of voltage that we can obtained for this experiment is recorded as around 30~40mV, which is about twice lower than the normal setup.

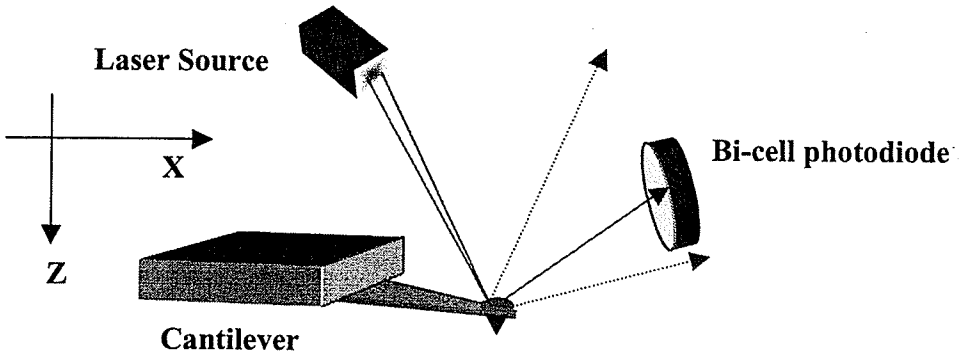

Figure [5.41] Illustration of how the deposition effected the laser reflection on the photodiode.

Chapter 6

Conclusion and Future Challenges

6.1 Conclusion

The ability to extracted current profile over a loop transmission line on a silicon substrate was demonstrated by implementing Magnetic Force Microscopy on the sample circuit. The interaction force between the magnetic dipole on the tip and the magnetic field induced by the current flow on the transmission line is enhanced by AC signal stimulation and is captured by laser beam bound system, with theoretical analysis and interpretations, current attributes on the transmission line can be obtained.

This is intended to provide useful information for failure analysis on IDDQ failed devices. Five different peck-to-peck current level signals are being used as test scenarios. A simulation program is written to verify the topographic and magnetic interaction force results obtained from the MFM scanning and to study the weaknesses of the MFM physical setup as well as the possibilities of future improvements.

The current sensitivity of the MFM instruments was theoretically derived and then compared with the MFM results we obtained. By experiment, current sensitivity was found to be $86\mu A_{rms}$ where SNR=3.5. To reach SNR=1, current sensitivity was found to be $20\mu A_{rms}$. This value is close to $17.3\mu A_{rms}$, which was derived theoretically.

6.2 Future Challenges

Few major reasons that bring discrepancies between the MFM result and the MathCAD simulated result are the tilted angle of the sample and the tip, weak reception of reflected laser beam on the bi-cell photodiode from the cantilever. Using a step control

motor to load the sample circuit will yield a relatively flat sample surface for scanning. Using high magnetic moment silicon probe which is available on the existing market will bring good laser beam reflection from the cantilever due to the flat gold coated surface on the backside, this can improve the current sensitivity of the system. Using magnetic probe fabricated by manufacturer will also provide us more accurate and confident information on the magnetic moment of the tip.

To have more accurate current sensitivity and SNR of the system, more test scenarios are needed to cover the possibilities. To prove our MFM system is useful for multilevel metal-interconnection IC design, designing a sample circuit with at least two levels of metal-interconnection, performing MFM with different current amplitude applied to different metal-interconnection is needed. With this experiment, we can demonstrate the capability of our MFM system to locate the current flow and to differentiate magnetic field induced by different metal layer.

In MathCAD simulation program, due to our current limited resources, we cannot have the sample area perfectly match between the simulation model and the practical. PC with higher performance capability will allow us to have simulation result faster and closer to reality.

Transmission line modeling using MathCAD software was simplified for faster computation yield. With more parameters of the transmission line taken into account while performing modeling, more precise information we can extract from MFM in term of magnetic field distribution.

Constant Definition

$Idir := -1$ **Current Direction**

$Mdir := 1$ **Magnetic Moment Direction**

$I := \frac{4 \cdot \frac{0.707}{2}}{1.02 \cdot 10^{3}} A \cdot Idir$ **Input current(with 4 Vp-p RMS, 1.02K Resistance, Current direction)**

$\mu o := 4 \cdot \pi \cdot 10^{-7} \frac{N}{A^2}$ **Permeability of free space**

$\mu := 10^{-6}$

$moment := 5 \cdot 10^{-13} \cdot A \cdot m^2 \cdot Mdir$ **Magnetic Moment of the Tip (with Moment direction)**

$TiltX := 0.06 \cdot deg$

$TiltY := 0.08237 \cdot deg$ **Tilted angle of the sample**

$Tilt := 15deg + TiltY$ **Tilted Angle of the Cantilever + Tilted angle of sample in Y direction**

$HZx := 0$ **Highest coordinate along X when sample tilts is taken into account.**

$HZy := 69$ **Highest coordinate along Y when sample titls is taken into account.**

Sample Circuit Geometry Definition

(with respect to scanning direction Y)
(Y zero is defined at the middle of the geometry)
(X and Z are defined in positive axis)

$unit := 1 \cdot \mu \cdot m$ **Base Unit Dimension**

Boundary

$Boundx := 70 \cdot \mu \cdot m$ $Boundy := 70 \cdot \mu \cdot m$ **X, Y boundary of the sample**

$nBx := \frac{Boundx}{unit}$ $nBy := \frac{Boundy}{unit}$ **Number of basic for each column and row**

$IniX := 0 \cdot \mu \cdot m$ $IniY := \frac{Boundy}{2} \cdot -1$ **Initial Coordinate for X and Y.**

$HighZ := 5.7 \cdot \mu \cdot m$

$nBz := 0$ **Distance between the sample and the tip. (From 1.7μm to 9.7μm)**

$IniZ := HighZ$ **Initial Coordinate for Z**

Number of Samples Taken in Derivation (For Curve Fitting)

$nD := 5$

Number of Derivation Along The Axis (For Curve Fitting)

$nDAxisX := \frac{nBx}{nD} \cdot nBy$

$nDAxisY := \frac{nBy}{nD} \cdot nBx$

$nDAxisZ := nBy \cdot nBx$

Enter degree of polynomial to fit: (For Curve Fitting)

$Poly := 4$

Subroutine for defining Coordinate to each Sampling unit on the sample surface.

Define Coordinate for Area

```
SumSegA := | x ← 1  if nBx = 0
           | x ← nBx  otherwise
           | y ← 1  if nBy = 0
           | y ← nBy  otherwise
           | z ← 1  if nBz = 0
           | z ← nBz  otherwise
           | return A ← x·y·z
```

Calculate the total number of sampling unit in X, Y and Z dimension.

```
CorA(x,y,z,inix,iniy,iniz,unit) := | c ← 0
                                   | for k ∈ 0..z
                                   |   for j ∈ 0..y − 1
                                   |     for i ∈ 0..x − 1
                                   |       A_{c,0} ← inix + (i·unit)
                                   |       A_{c,1} ← iniy + (j·unit)
                                   |       A_{c,2} ← [[iniz + (k·unit)] + tan(TiltX)·i·unit] + tan(TiltY)·j·unit  if HZx = 0 ∧ HZy = 0
                                   |       A_{c,2} ← [iniz + (k·unit) − tan(TiltX)·i·unit] + tan(TiltY)·j·unit  if HZx = nBx − 1 ∧ HZy = 0
                                   |       A_{c,2} ← [iniz + (k·unit) + tan(TiltX)·i·unit] − tan(TiltY)·j·unit  if HZx = 0 ∧ HZy = nBy − 1
                                   |       A_{c,2} ← [iniz + (k·unit) − tan(TiltX)·i·unit] − tan(TiltY)·j·unit  if HZx = nBx − 1 ∧ HZy = nBy − 1
                                   |       c ← c + 1
                                   | A
```

Assign coordinate to each sampling unit on the sample surface

Define Coordinate for Area

```
Area := CorA(nBx,nBy,nBz,IniX,IniY,IniZ,unit)
```

Executing the coordinate assigning subroutine

Subroutine for defining Coordinate to each Sampling unit on the Transmission Line

Defining TL steps

$$\text{Step}(Xini, Xend, Yini, Yend, Zini, Zend, unit) := \begin{| } Lx \leftarrow Xend - Xini \\ Ly \leftarrow Yend - Yini \\ Lz \leftarrow Zend - Zini \\ L \leftarrow \sqrt{(Lx)^2 + (Ly)^2 + (Lz)^2} \\ step \leftarrow \frac{L}{unit} \\ \text{return } step \end{|}$$

Define the number of steps needed for each TLine section in term of basic unit

Defining TL steps

The TLine is divided into three straight line section

Section 1

$T1Xini := 0 \cdot \mu \cdot m$ **Initial X coordinate in section 1**

$T1Yini := -14 \cdot \mu \cdot m$ **Initial Y coordinate in section 1**

$T1Zini := 0 \cdot \mu \cdot m$ **Initial Z coordinate in section 1**

$T1Xend := 50 \cdot \mu \cdot m$ **End X coordinate in section 1**

$T1Yend := -14 \cdot \mu \cdot m$ **End Y coordinate in section 1**

$T1Zend := 0 \cdot \mu \cdot m$ **End Z coordinate in section 1**

$$nT1X := \frac{|T1Xend - T1Xini|}{unit}$$ **Number of steps in X direction section 1 in term of basic unit**

$$nT1Y := \frac{|T1Yend - T1Yini|}{unit}$$ **Number of steps in Y direction section 1 in term of basic unit**

$$nT1Z := \frac{|T1Zend - T1Zini|}{unit}$$ **Number of steps in Z direction section 1 in term of basic unit**

$T1steps := \text{Step}(T1Xini, T1Xend, T1Yini, T1Yend, T1Zini, T1Zend, unit)$ **Executing the Steps calculation subroutine**

Section 2

$T2Xini := 50 \cdot \mu \cdot m$

$T2Yini := -14 \cdot \mu \cdot m$

$T2Zini := 0 \cdot \mu \cdot m$

$T2Xend := 50 \cdot \mu \cdot m$

$T2Yend := 14 \cdot \mu \cdot m$

$T2Zend := 0 \cdot \mu \cdot m$

$$nT2X := \frac{(|T2Xend - T2Xini|)}{unit}$$

$$nT2Y := \frac{|T2Yend - T2Yini|}{unit}$$

$$nT2Z := \frac{(|T2Zend - T2Zini|)}{unit}$$

$T2steps := Step(T2Xini, T2Xend, T2Yini, T2Yend, T2Zini, T2Zend, unit)$

Section 3

$T3Xini := 50 \cdot \mu \cdot m$

$T3Yini := 14 \cdot \mu \cdot m$

$T3Zini := 0 \cdot \mu \cdot m$

$T3Xend := 0 \cdot \mu \cdot m$

$T3Yend := 14 \cdot \mu \cdot m$

$T3Zend := 0 \cdot \mu \cdot m$

$$nT3X := \frac{(|T3Xend - T3Xini|)}{unit}$$

$$nT3Y := \frac{(|T3Yend - T3Yini|)}{unit}$$

$$nT3Z := \frac{(|T3Zend - T3Zini|)}{unit}$$

$T3steps := Step(T3Xini, T3Xend, T3Yini, T3Yend, T3Zini, T3Zend, unit)$

Define the Coordinate of the Transmission Line

Define Coordinate for TLine

$SumSegTL = nT1X + nT1Y + nT1Z + nT2X + nT2Y + nT2Z + nT3X + nT3Y + nT3Z$ **Number Of Total sampling units for Transmission Line**

$SumSegTL = 128$

$CorTL(Xini, Xend, Yini, Yend, Zini, Zend, Tsteps, unit) :=$

for $i \in 1 .. (Tsteps)$

$TL_{i-1,0} \leftarrow Xini + i \cdot unit - \frac{unit}{2}$ if $Xend - Xini \neq 0$

$TL_{i-1,0} \leftarrow Xini - (i \cdot unit) + \frac{unit}{2}$ if $Xend - Xini < 0$

$TL_{i-1,0} \leftarrow Xini$ otherwise

$TL_{i-1,1} \leftarrow Yini + (i \cdot unit) - \frac{unit}{2}$ if $Yend - Yini > 0$

$TL_{i-1,1} \leftarrow Yini - (i \cdot unit) + \frac{unit}{2}$ if $Yend - Yini < 0$

$TL_{i-1,1} \leftarrow Yini$ otherwise

$TL_{i-1,2} \leftarrow Zini + (i \cdot unit) - \frac{unit}{2}$ if $Zend - Zini > 0$

$TL_{i-1,2} \leftarrow Zini - (i \cdot unit) + \frac{unit}{2}$ if $Zend - Zini < 0$

$TL_{i-1,2} \leftarrow Zini$ otherwise

TL

Assign coordinate to each sampling unit on TLine
Point is taken at the center of the segment

Define Coordinate for TLine

$T1 := CorTL(T1Xini, T1Xend, T1Yini, T1Yend, T1Zini, T1Zend, T1steps, unit)$

$T2 := CorTL(T2Xini, T2Xend, T2Yini, T2Yend, T2Zini, T2Zend, T2steps, unit)$

$T3 := CorTL(T3Xini, T3Xend, T3Yini, T3Yend, T3Zini, T3Zend, T3steps, unit)$

Executing the coordinate assigning subroutine

$T := stack(T1, T2, T3)$

Combine the coordinate for each TLine section into an array

Subroutine for defining Current Unit Vector for each Sampling unit on the Transmission Line

Define Current Unit Vector(X, Y, Z) of each sampling unit of the Transmission Line

Defining Unit Vector of TLine

$$\text{Unit\_V\_TL}(\text{CorTL}, \text{SumSeg}) :=$$

for $i \in 0 .. \text{SumSeg} - 1$

$j \leftarrow 1 \text{ if } i = 0$

$j \leftarrow i \text{ otherwise}$

$$UV_{i,0} \leftarrow 0 \text{ if } \text{CorTL}_{i,0} - \text{CorTL}_{j-1,0} = 0$$

$$UV_{i,0} \leftarrow \frac{\left(\text{CorTL}_{i,0} - \text{CorTL}_{j-1,0}\right)}{\sqrt{\left(\text{CorTL}_{i,0} - \text{CorTL}_{j-1,0}\right)^2 + \left(\text{CorTL}_{i,1} - \text{CorTL}_{j-1,1}\right)^2 + \left(\text{CorTL}_{i,2} - \text{CorTL}_{j-1,2}\right)^2}} \text{ otherwise}$$

Unit Vector in X

$$UV_{i,1} \leftarrow 0 \text{ if } \text{CorTL}_{i,1} - \text{CorTL}_{j-1,1} = 0$$

$$UV_{i,1} \leftarrow \frac{\text{CorTL}_{i,1} - \text{CorTL}_{j-1,1}}{\sqrt{\left(\text{CorTL}_{i,0} - \text{CorTL}_{j-1,0}\right)^2 + \left(\text{CorTL}_{i,1} - \text{CorTL}_{j-1,1}\right)^2 + \left(\text{CorTL}_{i,2} - \text{CorTL}_{j-1,2}\right)^2}} \text{ otherwise}$$

Unit Vector in Y

$$UV_{i,2} \leftarrow 0 \text{ if } \text{CorTL}_{i,2} - \text{CorTL}_{j-1,2} = 0$$

$$UV_{i,2} \leftarrow \frac{\text{CorTL}_{i,2} - \text{CorTL}_{j-1,2}}{\sqrt{\left(\text{CorTL}_{i,0} - \text{CorTL}_{j-1,0}\right)^2 + \left(\text{CorTL}_{i,1} - \text{CorTL}_{j-1,1}\right)^2 + \left(\text{CorTL}_{i,2} - \text{CorTL}_{j-1,2}\right)^2}} \text{ otherwise}$$

Unit Vector in Z

UV

Defining Unit Vector of TLine

$$TUV := \text{Unit\_V\_TL}(T, \text{SumSegTL})$$

Executing the Unit Vector subroutine

Subroutine for defining Unit Vector from each sampling unit on the transmission Line to each sampling unit on the sample surface.

Define Unit Vector Between the Transmission Line and the Area

Defining UV from line to field

$$\text{Unit\_V\_TL\_Fp}(\text{CorTL}, \text{CorArea}) :=$$

for $i \in 0 .. \text{SumSegA} - 1$

for $j \in 0 .. \text{SumSegTL} - 1$

$UV_{j,0} \leftarrow 0 \text{ if } \text{CorArea}_{i,0} - \text{CorTL}_{j,0} = 0$

Unit Vector in X

$$UV_{j,0} \leftarrow \frac{\text{CorArea}_{i,0} - \text{CorTL}_{j,0}}{\sqrt{\left(\text{CorArea}_{i,0} - \text{CorTL}_{j,0}\right)^2 + \left(\text{CorArea}_{i,1} - \text{CorTL}_{j,1}\right)^2 + \left(\text{CorArea}_{i,2} - \text{CorTL}_{j,2}\right)^2}} \text{ otherwise}$$

$UV_{j,1} \leftarrow 0 \text{ if } \text{CorArea}_{i,1} - \text{CorTL}_{j,1} = 0$

Unit Vector in Y

$$UV_{j,1} \leftarrow \frac{\text{CorArea}_{i,1} - \text{CorTL}_{j,1}}{\sqrt{\left(\text{CorArea}_{i,0} - \text{CorTL}_{j,0}\right)^2 + \left(\text{CorArea}_{i,1} - \text{CorTL}_{j,1}\right)^2 + \left(\text{CorArea}_{i,2} - \text{CorTL}_{j,2}\right)^2}} \text{ otherwise}$$

$UV_{j,2} \leftarrow 0 \text{ if } \text{CorArea}_{i,2} - \text{CorTL}_{j,2} = 0$

Unit Vector in Z

$$UV_{j,2} \leftarrow \frac{\text{CorArea}_{i,2} - \text{CorTL}_{j,2}}{\sqrt{\left(\text{CorArea}_{i,0} - \text{CorTL}_{j,0}\right)^2 + \left(\text{CorArea}_{i,1} - \text{CorTL}_{j,1}\right)^2 + \left(\text{CorArea}_{i,2} - \text{CorTL}_{j,2}\right)^2}} \text{ otherwise}$$

$UV_{j,3} \leftarrow 0 \text{ if } \left(\text{CorArea}_{i,0} - \text{CorTL}_{j,0}\right)^2 + \left(\text{CorArea}_{i,1} - \text{CorTL}_{j,1}\right)^2 + \left(\text{CorArea}_{i,2} - \text{CorTL}_{j,2}\right)^2 = 0$

$$UV_{j,3} \leftarrow \frac{\left\lceil \left(\text{CorArea}_{i,0} - \text{CorTL}_{j,0}\right)^2 + \left(\text{CorArea}_{i,1} - \text{CorTL}_{j,1}\right)^2 + \left(\text{CorArea}_{i,2} - \text{CorTL}_{j,2}\right)^2 \right\rceil}{m^2} \text{ otherwise}$$

$\text{Table}_i \leftarrow UV$

Calculate the distance between the two reference points.

Table

Defining UV from line to field

$$AUV := \text{Unit\_V\_TL\_Fp}(T, \text{Area})$$

Executing the Unit Vector subroutine

Subroutine for Cross Product Operation on Unit Vector

CrossProduct of UV

$$
\begin{aligned}
&\text{CPofUV} := \left|\begin{array}{l}
\text{for } i \in 0 .. \text{SumSegA} - 1 \\
\quad \text{for } j \in 0 .. \text{SumSegTL} - 1 \\
\quad\quad \left|\begin{array}{l}
CP_{j,0} \leftarrow TUV_{j,1} \cdot (AUV_i)_{j,2} - TUV_{j,2} \cdot (AUV_i)_{j,1} \\
CP_{j,1} \leftarrow \left[TUV_{j,0} \cdot (AUV_i)_{j,2} - TUV_{j,2} \cdot (AUV_i)_{j,0}\right] \cdot (-1) \\
CP_{j,2} \leftarrow TUV_{j,0} \cdot (AUV_i)_{j,1} - TUV_{j,1} \cdot (AUV_i)_{j,0} \\
\text{Table}_i \leftarrow CP
\end{array}\right. \\
\text{Table}
\end{array}\right. \\
&\qquad\qquad \text{Result in x direction from cross product} \\
&\qquad\qquad \text{Result in y direction from cross product} \\
&\qquad\qquad \text{Result in z direction from cross product}
\end{aligned}
$$

CrossProduct of UV

Subroutine for computing Magnetic Field distribution over the sample surface corresponding to TLine

BField

$$\text{BField} := \left| \begin{array}{l} \text{for } i \in 0 .. \text{SumSegA} - 1 \\ \quad B_{i,0} \leftarrow \sum_{j=0}^{\text{SumSegTL}-1} \frac{\mu o \cdot I}{4 \cdot \pi \cdot (\text{AUV}_i)_{j,3} \cdot m^2} \cdot (\text{CPofUV}_i)_{j,0} \cdot \mu \cdot m \qquad \text{Result in x direction from Biot-Savart Law} \\ \quad B_{i,1} \leftarrow \sum_{j=0}^{\text{SumSegTL}-1} \frac{\mu o \cdot I}{4 \cdot \pi \cdot (\text{AUV}_i)_{j,3} \cdot m^2} \cdot (\text{CPofUV}_i)_{j,1} \cdot \mu \cdot m \qquad \text{Result in y direction from Biot-Savart Law} \\ \quad B_{i,2} \leftarrow \sum_{j=0}^{\text{SumSegTL}-1} \frac{\mu o \cdot I}{4 \cdot \pi \cdot (\text{AUV}_i)_{j,3} \cdot m^2} \cdot (\text{CPofUV}_i)_{j,2} \cdot \mu \cdot m \qquad \text{Result in z direction from Biot-Savart Law} \\ B \end{array} \right.$$

$$\text{BFieldX} := \left| \begin{array}{l} k \leftarrow 0 \\ \text{for } i \in 0 .. \text{nBy} - 1 \\ \quad \text{for } j \in 0 .. \text{nBx} - 1 \\ \quad\quad B_{j,i} \leftarrow \text{BField}_{k,0} \qquad \text{Convert the result in x direction into a plot able table format} \\ \quad\quad k \leftarrow k + 1 \\ B \end{array} \right.$$

$$\text{BFieldY} := \left| \begin{array}{l} k \leftarrow 0 \\ \text{for } i \in 0 .. \text{nBy} - 1 \\ \quad \text{for } j \in 0 .. \text{nBx} - 1 \\ \quad\quad B_{j,i} \leftarrow \text{BField}_{k,1} \qquad \text{Convert the result in y direction into a plot able table format} \\ \quad\quad k \leftarrow k + 1 \\ B \end{array} \right.$$

$$\text{BFieldZ} := \left| \begin{array}{l} k \leftarrow 0 \\ \text{for } i \in 0 .. \text{nBy} - 1 \\ \quad \text{for } j \in 0 .. \text{nBx} - 1 \\ \quad\quad B_{j,i} \leftarrow \text{BField}_{k,2} \\ \quad\quad k \leftarrow k + 1 \\ B \end{array} \right.$$

BField

Subroutine for computing Magnetic Moment on the Probe

Magnetic M of Tip

```
Moment := | for i ∈ 0 .. SumSegA − 1
          |   M_{i,0} ← moment·sin(TiltX)
          |   M_{i,1} ← moment·sin(Tilt)
          |   M_{i,2} ← moment·cos(Tilt)
          | M
```

Magnetic Moment of the probe in x direction, taking into account the x tilted angle of the sample.

Magnetic Moment of the probe in y direction, taking into account the y tilted angle of the sample and the tip.

Magnetic Moment of the probe in z direction, taking into account the y tilted angle of the sample and the tip.

```
MomentX := | k ← 0
           | for i ∈ 0 .. nBy − 1
           |   for j ∈ 0 .. nBx − 1
           |     M_{j,i} ← Moment_{k,0}
           |     k ← k + 1
           | M
```

Convert the result in x direction into a plot able table format

```
MomentY := | k ← 0
           | for i ∈ 0 .. nBy − 1
           |   for j ∈ 0 .. nBx − 1
           |     M_{i,j} ← Moment_{k,1}
           |     k ← k + 1
           | M
```

Convert the result in y direction into a plot able table format

```
MomentZ := | k ← 0
           | for i ∈ 0 .. nBy − 1
           |   for j ∈ 0 .. nBx − 1
           |     M_{i,j} ← Moment_{k,2}
           |     k ← k + 1
           | M
```

Convert the result in z direction into a plot able table format

Magnetic M of Tip

Subroutine for importing Data from Simulation in Different Scanning Height

Read Data

b1_7x := C:\..\1_7x.xls

b1_7y := C:\..\1_7y.xls

b1_7z := C:\..\1_7z.xls

b3_7x := C:\..\3_7x.xls

b3_7y := C:\..\3_7y.xls

b3_7z := C:\..\3_7z.xls

b5_7x := C:\..\5_7x.xls

b5_7y := C:\..\5_7y.xls

b5_7z := C:\..\5_7z.xls

b7_7x := C:\..\7_7x.xls

b7_7y := C:\..\7_7y.xls

b7_7z := C:\..\7_7z.xls

b9_7x := C:\..\9_7x.xls

b9_7y := C:\..\9_7y.xls

b9_7z := C:\..\9_7z.xls

Importing Data from different scanning height (1.7μm to 9.7μm)

b1x := b1_7x·tesla

b1y := b1_7y·tesla

b1z := b1_7z·tesla

b3x := b3_7x·tesla

b3y := b3_7y·tesla

b3z := b3_7z·tesla

b5x := b5_7x·tesla

b5y := b5_7y·tesla

b5z := b5_7z·tesla

b7x := b7_7x·tesla

b7y := b7_7y·tesla

b7z := b7_7z·tesla

b9x := b9_7x·tesla

b9y := b9_7y·tesla

b9z := b9_7z·tesla

Assigning Unit (Tesla) to the imported Data

Read Data

Subroutine for preparing Curve Fitting Data in Gradient Operation

Gradient Preparation

```
Dxx := | n ← -1
       | for i ∈ 0 .. nBy - 1
       |   for j ∈ 0 .. nBx - 1
       |     | n ← n + 1  if mod(j, nD) = 0
       |     | D_{mod(j,nD),n} ← b7x_{j,i}
       | D
```

Divide Magnetic Field(X) into a table with nD(define at the beginning) row along X direction

```
Dxz := | n ← -1
       | for i ∈ 0 .. nBy - 1
       |   for j ∈ 0 .. nBx - 1
       |     | n ← n + 1  if mod(j, nD) = 0
       |     | D_{mod(j,nD),n} ← b7z_{j,i}
       | D
```

Divide Magnetic Field(Z) into a table with nD(define at the beginning) row along X direction

```
Dxy := | n ← -1
       | for i ∈ 0 .. nBy - 1
       |   for j ∈ 0 .. nBx - 1
       |     | n ← n + 1  if mod(j, nD) = 0
       |     | D_{mod(j,nD),n} ← b7y_{j,i}
       | D
```

Divide Magnetic Field(Y) into a table with nD(define at the beginning) row along X direction

```
Dyy := | n ← −1
       | for i ∈ 0 .. nBx − 1
       |   for j ∈ 0 .. nBy − 1
       |     | n ← n + 1  if mod(j,nD) = 0
       |     | D_{mod(j,nD),n} ← b7y_{i,j}
       | D
```

```
Dyz := | n ← −1
       | for i ∈ 0 .. nBx − 1
       |   for j ∈ 0 .. nBy − 1
       |     | n ← n + 1  if mod(j,nD) = 0
       |     | D_{mod(j,nD),n} ← b7z_{i,j}
       | D
```

```
Dyx := | n ← −1
       | for i ∈ 0 .. nBx − 1
       |   for j ∈ 0 .. nBy − 1
       |     | n ← n + 1  if mod(j,nD) = 0
       |     | D_{mod(j,nD),n} ← b7x_{i,j}
       | D
```

Divide Magnetic Field(X,Y,Z) into a table with nD(define at the beginning) row along Y direction

```
Dzz := | k ← 0
       | n ← −1
       | for i ∈ 0 .. nBy − 1
       |   for j ∈ 0 .. nBx − 1
       |     | k ← j + i·(nBx)
       |     | m ← 0
       |     | D_{m,k} ← b1z_{i,j}
       |     | D_{m+1,k} ← b3z_{i,j}
       |     | D_{m+2,k} ← b5z_{i,j}
       |     | D_{m+3,k} ← b7z_{i,j}
       |     | D_{m+4,k} ← b9z_{i,j}
       | D
```

```
Dzy := | k ← 0
       | n ← −1
       | for i ∈ 0 .. nBy − 1
       |   for j ∈ 0 .. nBx − 1
       |     | k ← j + i·(nBx)
       |     | m ← 0
       |     | D_{m,k} ← b1y_{i,j}
       |     | D_{m+1,k} ← b3y_{i,j}
       |     | D_{m+2,k} ← b5y_{i,j}
       |     | D_{m+3,k} ← b7y_{i,j}
       |     | D_{m+4,k} ← b9y_{i,j}
       | D
```

```
Dzx := | k ← 0
       | n ← −1
       | for i ∈ 0 .. nBy − 1
       |   for j ∈ 0 .. nBx − 1
       |     | k ← j + i·(nBx)
       |     | m ← 0
       |     | D_{m,k} ← b1x_{i,j}
       |     | D_{m+1,k} ← b3x_{i,j}
       |     | D_{m+2,k} ← b5x_{i,j}
       |     | D_{m+3,k} ← b7x_{i,j}
       |     | D_{m+4,k} ← b9x_{i,j}
       | D
```

Divide Magnetic Field(X,Y,Z) into a table with nD(define at the beginning) row along Z direction (1.7μm to 9.7μm)

Subroutine for Gradient Operation (δX, δY, δZ)

Gradient (Derivative)

```
dCFx(df, xn) := | for m ∈ 0 .. nD − 1                                   Derivative operation in X direction
                |   y_m ← m
                | for i ∈ 0 .. nDAxisX − 1
                |   x ← submatrix(df / tesla, 0, nD − 1, i, i)          Extract data points from the table column by column
                |   z ← regress(y, x, Poly)                             Fit the curve with a Polynomial equation.
                |   k ← 0
                |   for n ∈ 0, xn .. nD − 1
                |     dCF_{k,i} ← (d/dn) interp(z, x, y, n)             Performing derivative operation on the equation within the range
                |     k ← k + 1
                | dCF / μ
```

```
Rgroupx(df) := | A ← 0
               | B ← 0
               | for i ∈ 0, nBx/nD .. nDAxisX − nBx/nD                  Convert the data into a plot able format
               |   for j ∈ 0 .. nBx/nD − 1
               |     if j = 0
               |       A ← 0
               |       A ← submatrix(df, 0, nD − 1, j + i, j + i)
               |     A ← stack(A, submatrix(df, 0, nD − 1, j + i, j + i))  otherwise
               |   B ← A  if i = 0
               |   B ← augment(B, A)  otherwise
               | B · kg / (m s^2 A)
```

$$\text{dCFy}(df, yn) := \left| \begin{array}{l} \text{for } m \in 0 .. nD - 1 \\ \quad y_m \leftarrow m \\ \text{for } i \in 0 .. nDAxisY - 1 \\ \quad \left| \begin{array}{l} x \leftarrow \text{submatrix}\left(\frac{df}{tesla}, 0, nD - 1, i, i\right) \\ z \leftarrow \text{regress}(y, x, Poly) \\ k \leftarrow 0 \\ \text{for } n \in 0, yn .. nD - 1 \\ \quad \left| \begin{array}{l} dCF_{k,i} \leftarrow \frac{d}{dn}\text{interp}(z, x, y, n) \\ k \leftarrow k + 1 \end{array} \right. \end{array} \right. \\ \frac{dCF}{\mu} \end{array} \right.$$

$$\text{Rgroupy}(df) := \left| \begin{array}{l} A \leftarrow 0 \\ B \leftarrow 0 \\ \text{for } i \in 0, \frac{nBy}{nD} .. nDAxisY - \frac{nBy}{nD} \\ \quad \left| \begin{array}{l} \text{for } j \in 0 .. \frac{nBy}{nD} - 1 \\ \quad \left| \begin{array}{l} \text{if } j = 0 \\ \quad \left| \begin{array}{l} A \leftarrow 0 \\ A \leftarrow \text{submatrix}(df, 0, nD - 1, j + i, j + i) \end{array} \right. \\ A \leftarrow \text{stack}(A, \text{submatrix}(df, 0, nD - 1, j + i, j + i)) \text{ otherwise} \end{array} \right. \\ B \leftarrow A \text{ if } i = 0 \\ B \leftarrow \text{augment}(B, A) \text{ otherwise} \end{array} \right. \\ B \cdot \frac{kg}{ms^2 A} \end{array} \right.$$

$$\text{dCFz}(df, zi, zn) := \left| \begin{array}{l} \text{for } m \in 0 .. (nD - 1) \\ \quad y_m \leftarrow zi + m \cdot zn \\ \text{for } i \in 0 .. nDAxisZ - 1 \\ \quad \left| \begin{array}{l} x \leftarrow \text{submatrix}\left(\frac{df}{tesla}, 0, nD - 1, i, i\right) \\ z \leftarrow \text{regress}(y, x, Poly) \\ k \leftarrow 0 \\ \text{for } n \in 0 .. (nD - 1) \\ \quad \left| \begin{array}{l} g \leftarrow zi + n \cdot zn \\ dCF_{k,i} \leftarrow \frac{d}{dg}\text{interp}(z, x, y, g) \\ k \leftarrow k + 1 \end{array} \right. \end{array} \right. \\ \frac{dCF}{\mu} \end{array} \right.$$

$$\text{Rgroupz}(df, z) := \left| \begin{array}{l} k \leftarrow 0 \\ \text{for } j \in 0 .. nBy - 1 \\ \quad \text{for } i \in 0 .. nBx - 1 \\ \quad \quad \left| \begin{array}{l} B_{j,i} \leftarrow df_{z,k} \\ k \leftarrow k + 1 \end{array} \right. \\ B \cdot \frac{kg}{m \cdot s^2 \cdot A} \end{array} \right.$$

Gradient (Derivative)

Subroutine for computing the Interaction Force

Gradient (Combination)

$Rzz := Rgroupz(dCFz(Dzz, 1.7, 2), 2)$

$Rzy := Rgroupz(dCFz(Dzy, 1.7, 2), 2)$

$Rzx := Rgroupz(dCFz(Dzx, 1.7, 2), 2)$

Executing the Gradient Operation Subroutine. (with 1.7μm as the low limit for the derivative range, 2μm is the increment, 2 is the second row of range.

$Fz1 := \overrightarrow{(Rzz \cdot MomentZ)}$

$Fz2 := \overrightarrow{(Rzy \cdot MomentY)}$

$Fz3 := \overrightarrow{(Rzx \cdot MomentX)}$

Multiplying the Result from Gradient Operation with Magnetic Moment of the Tip, and yield Interaction Force

$Fz := Fz1 + Fz2 + Fz3$

Summation of all interaction force between tip and sample in Z direction.

$Ryx := Rgroupy(dCFy(Dyx, 1))$

$Ryy := Rgroupy(dCFy(Dyy, 1))$

$Ryz := Rgroupy(dCFy(Dyz, 1))$

$Fx1 := \overrightarrow{(Rxx \cdot MomentX)}$

$Fx2 := \overrightarrow{(Rxz \cdot MomentZ)}$

$Fx3 := \overrightarrow{(Rxy \cdot MomentY)}$

$Fx := Fx1 + Fx2 + Fx3$

$Rxy := Rgroupx(dCFx(Dxy, 1))$

$Rxx := Rgroupx(dCFx(Dxx, 1))$

$Rxz := Rgroupx(dCFx(Dxz, 1))$

$Fy1 := \overrightarrow{(Ryy \cdot MomentY)}$

$Fy2 := \overrightarrow{(Ryz \cdot MomentZ)}$

$Fy3 := \overrightarrow{(Ryx \cdot MomentX)}$

$Fy := Fy1^T + Fy2^T + Fy3^T$

$F := Fz \cdot \cos(Tilt) + Fy \cdot \sin(Tilt)$

Summation of all interaction force between tip and sample in Y, Z direction. (X was insignificant)

Gradient (Combination)

To Generate Figures 5.4 Shown in Chapter 5

$$\text{PlotTL}(\text{Xini},\text{Xend},\text{Yini},\text{Yend},\text{Zini},\text{Zend},\text{Tsteps},\text{unit}) := \left|\begin{array}{l} \text{for } i \in 0..(\text{Tsteps}-1) \\ \quad \left|\begin{array}{l} \text{TL}_{i,0} \leftarrow \text{Xini} + (i\cdot\text{unit}) \text{ if } \text{Xend} - \text{Xini} \neq 0 \\ \text{TL}_{i,0} \leftarrow \text{Xini} - (i\cdot\text{unit}) \text{ if } \text{Xend} - \text{Xini} < 0 \\ \text{TL}_{i,0} \leftarrow \text{Xini} \text{ otherwise} \\ \text{TL}_{i,1} \leftarrow \text{Yini} + (i\cdot\text{unit}) \text{ if } \text{Yend} - \text{Yini} \neq 0 \\ \text{TL}_{i,1} \leftarrow \text{Yini} - (i\cdot\text{unit}) \text{ if } \text{Yend} - \text{Yini} < 0 \\ \text{TL}_{i,1} \leftarrow \text{Yini} \text{ otherwise} \\ \text{TL}_{i,2} \leftarrow \text{Zini} + (i\cdot\text{unit}) \text{ if } \text{Zend} - \text{Zini} \neq 0 \\ \text{TL}_{i,2} \leftarrow \text{Zini} - (i\cdot\text{unit}) \text{ if } \text{Zend} - \text{Zini} < 0 \\ \text{TL}_{i,2} \leftarrow \text{Zini} \text{ otherwise} \end{array}\right. \\ \text{TL} \end{array}\right.$$

$$\text{PlotA}(x,y) := \left|\begin{array}{l} \text{for } j \in 0..x \\ \quad \text{for } i \in 0..y \\ \quad\quad P_{i,j} \leftarrow -20\cdot 10^{-14} \\ P \end{array}\right.$$

$$\text{PlotArea} := \text{PlotA}\left(\frac{\text{Boundy} - 1\cdot\mu\cdot\text{m}}{\mu\cdot\text{m}}, \frac{\text{Boundx} - 1\cdot\mu\cdot\text{m}}{\mu\cdot\text{m}}\right)$$

PT1 := PlotTL(T1Xini, T1Xend, T1Yini, T1Yend, T1Zini, T1Zend, T1steps, unit)

PT2 := PlotTL(T2Xini, T2Xend, T2Yini, T2Yend, T2Zini, T2Zend, T2steps, unit)

PT3 := PlotTL(T3Xini, T3Xend, T3Yini, T3Yend, T3Zini, T3Zend, T3steps, unit)

PT := stack(PT1, PT2, PT3)

$\text{PThick} := 1\cdot 10^{-12}$ $\qquad$ LThick := 6

$$\text{PlotT}(\text{TL},\text{A}) := \left|\begin{array}{l} \text{for } i \in 0..\text{SumSegTL}-1 \\ \quad \left|\begin{array}{l} \text{if } i \le \text{T1steps} - 2 \\ \quad \left|\begin{array}{l} x \leftarrow \text{TL}_{i,0} \\ y \leftarrow \dfrac{\text{Boundy}}{2\mu\cdot\text{m}} - \text{TL}_{i,1} \\ \text{for } n \in 0..\text{LThick} \\ \quad A_{x.v\frac{\text{LThick}}{}+n} \leftarrow \text{PThick} \end{array}\right. \end{array}\right. \end{array}\right.$$

2

if $i = T1steps - 1$

$x \leftarrow TL_{i,0}$

$y \leftarrow \frac{Boundy}{2\mu \cdot m} - TL_{i,1}$

for $n \in 0..LThick$

$A_{x,y-\frac{LThick}{2}+n} \leftarrow PThick$

$A_{x+1,y-\frac{LThick}{2}+n} \leftarrow PThick$

$A_{x+2,y-\frac{LThick}{2}+n} \leftarrow PThick$

$A_{x+3,y-\frac{LThick}{2}+n} \leftarrow PThick$

$A_{x+4,y-\frac{LThick}{2}+n} \leftarrow PThick$

if $T1steps - 1 < i \leq T1steps + T2steps - 1$

$x \leftarrow TL_{i,0}$

$y \leftarrow \frac{Boundy}{2\mu \cdot m} - TL_{i,1}$

for $n \in 0..LThick$

$A_{\left(x-\frac{LThick}{2}\right)+n,y} \leftarrow PThick$

if $T1steps + T2steps < i \leq T1steps + T2steps + T3steps$

$x \leftarrow TL_{i,0}$

$y \leftarrow \frac{Boundy}{2\mu \cdot m} - TL_{i,1}$

for $n \in 0..LThick$

$A_{x,y+\frac{LThick}{2}-n} \leftarrow PThick$

```
if i = T1steps + T2steps
    x ← TL[i, 0]
    y ← Boundy/(2μ·m) − TL[i, 1]
    for n ∈ 0 .. LThick
        A[x + LThick/2 + n, y]   ← PThick
        A[x + LThick/2 + n, y−1] ← PThick
        A[x + LThick/2 + n, y−2] ← PThick
        A[x + LThick/2 + n, y−3] ← PThick
A
```

$$P := \text{PlotT}\left(\frac{PT}{\mu \cdot m}, \text{PlotArea}\right)$$

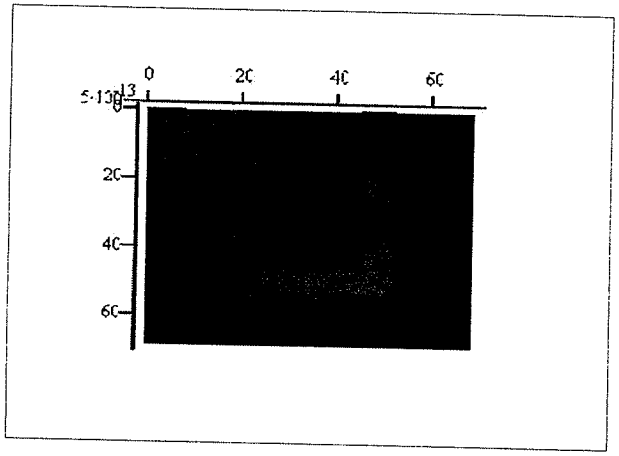

P

Open a "Surface Plot" Windows,
Type "P" at the cursor,
Set "rotation" angle to 0°, "tilt" angle to 90°,
Set "Fill Options" to fill surface, "Color Options" to colormap, and "Line Options" to No lines.

To Generate Figures 5.8 Shown in Chapter 5

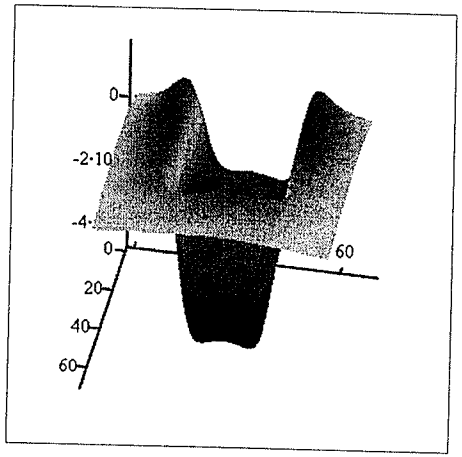

BFieldZ

Open a "Surface Plot" Windows,
Type "BFieldZ" at the cursor,
Set "Fill Options" to fill surface, "Color Options" to colormap, and "Line Options" to No lines.

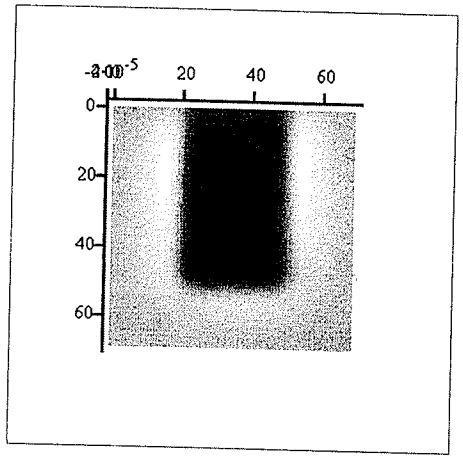

BFieldZ

Open a "Surface Plot" Windows,
Type "BFieldZ" at the cursor,
Set "rotation" angle to 0°, "tilt" angle to 90°,
Set "Fill Options" to fill surface, "Color Options" to colormap, and "Line Options" to No lines.
Set "Colormap" to Greyscale

To Generate Figures 5.9 Shown in Chapter 5

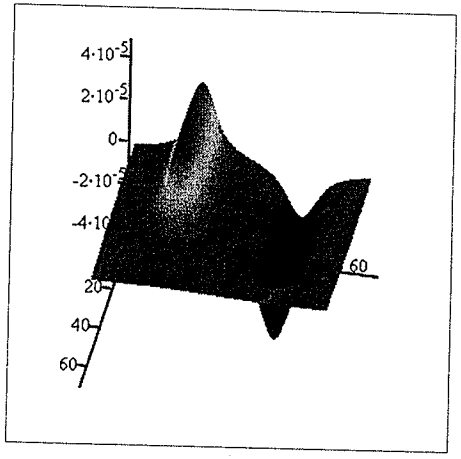

BFieldY

Open a "Surface Plot" Windows,
Type "BFieldY" at the cursor,
Set "Fill Options" to fill surface, "Color Options" to colormap, and "Line Options" to No lines.

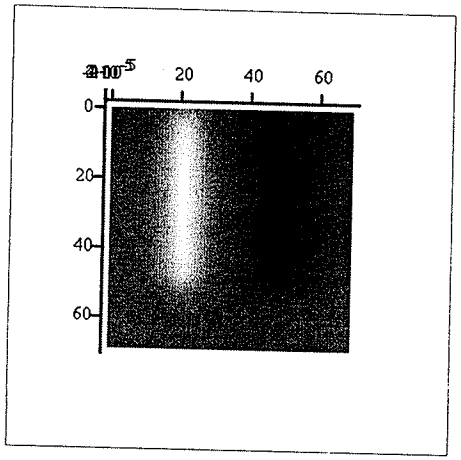

BFieldY

Open a "Surface Plot" Windows,
Type "BFieldY" at the cursor,
Set "rotation" angle to 0°, "tilt" angle to 90°,
Set "Fill Options" to fill surface, "Color Options" to colormap, and "Line Options" to No lines.
Set "Colormap" to Greyscale

To Generate Figures 5.10 Shown in Chapter 5

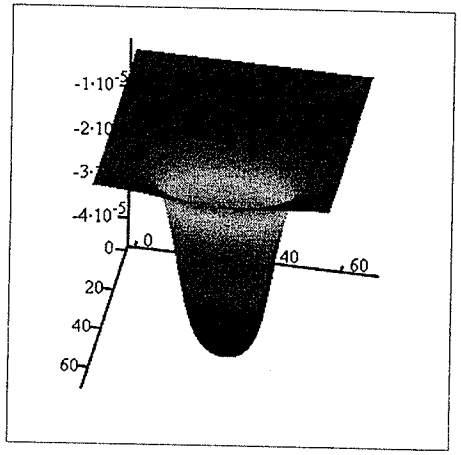

BFieldX

Open a "Surface Plot" Windows,
Type "BFieldX" at the cursor,
Set "Fill Options" to fill surface, "Color Options" to colormap, and "Line Options" to No lines.

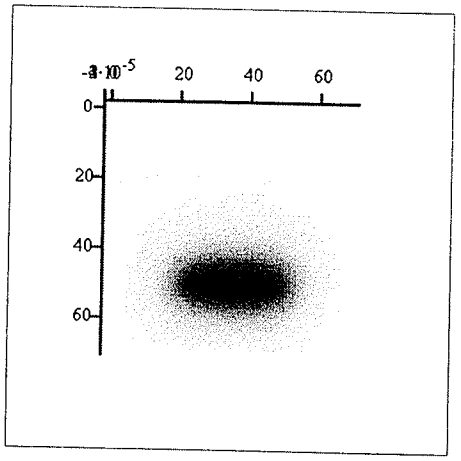

BFieldX

Open a "Surface Plot" Windows,
Type "BFieldX" at the cursor,
Set "rotation" angle to 0°, "tilt" angle to 90°,
Set "Fill Options" to fill surface, "Color Options" to colormap, and "Line Options" to No lines.
Set "Colormap" to Greyscale

To Generate Figures 5.11 Shown in Chapter 5

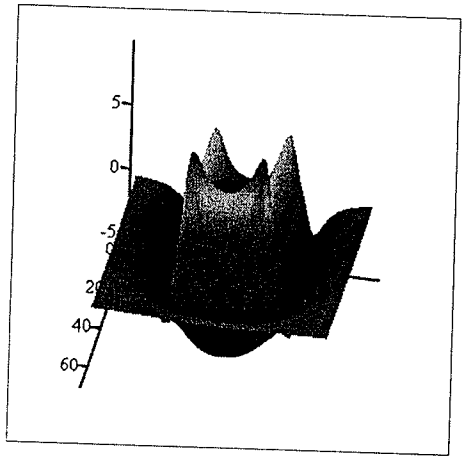

Rzz

Open a "Surface Plot" Windows,
Type "Rzz" at the cursor,
Set "Fill Options" to fill surface, "Color Options" to colormap, and "Line Options" to No lines.

To Generate Figures 5.12 Shown in Chapter 5

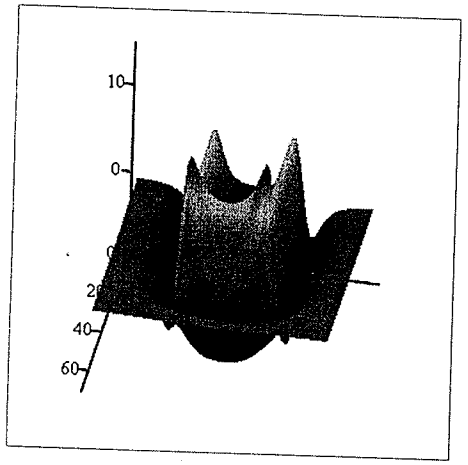

$$\frac{b5z - b3z}{2u}$$

Open a "Surface Plot" Windows,
Type "(b5z-b3z)/2μ" at the cursor, (Divide the different between Bfield at scan height 5μm and 3μm by 2μm)
Set "Fill Options" to fill surface, "Color Options" to colormap, and "Line Options" to No lines.

To Generate Figures 5.14 Shown in Chapter 5

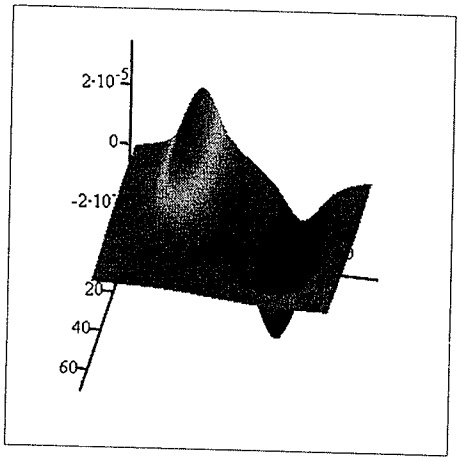

b7y

Open a "Surface Plot" Windows,
Type "b7y" at the cursor, (Y Bfield at scan height 7.7μm)
Set "Fill Options" to fill surface, "Color Options" to colormap, and "Line Options" to No lines.

To Generate Figures 5.15 Shown in Chapter 5

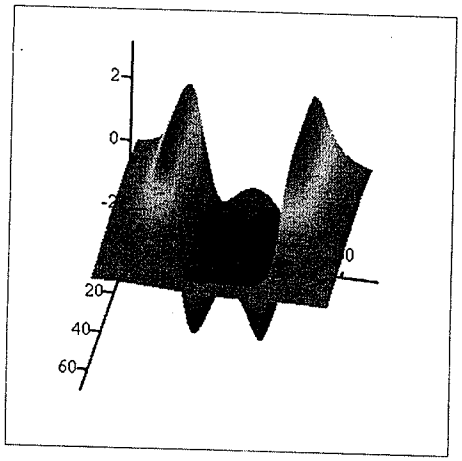

Ryy^T

Open a "Surface Plot" Windows,
Type "Ryy T" at the cursor, (Y Magnetic Field in Gradient Y, with "Matrix Tranpose")
Set "Fill Options" to fill surface, "Color Options" to colormap, and "Line Options" to No lines.

To Generate Figures 5.18 Shown in Chapter 5

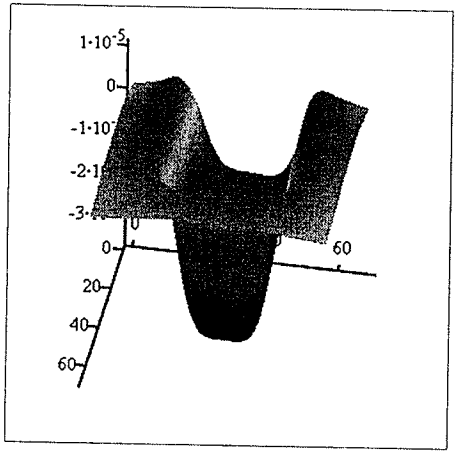

Open a "Surface Plot" Windows,
Type "b7z" at the cursor, (Z Bfield at scan height 7.7μm)
Set "Fill Options" to fill surface, "Color Options" to colormap, and "Line Options" to No lines.

b7z

To Generate Figures 5.19 Shown in Chapter 5

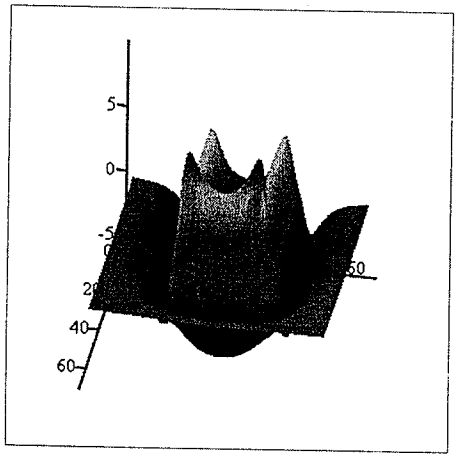

Open a "Surface Plot" Windows,
Type "Rzz" at the cursor, (Z Magnetic Field in Gradient Z)
Set "Fill Options" to fill surface, "Color Options" to colormap, and "Line Options" to No lines.

Rzz

To Generate Figures 5.20 Shown in Chapter 5

$i := 0 .. 70$ **Assign "i" as counter from 0 to 70.**

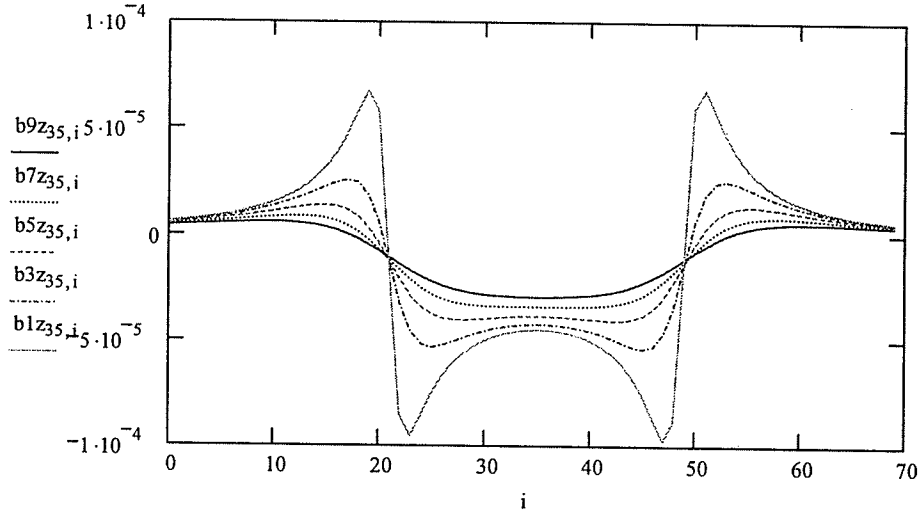

Open a "X-Y Plot" Windows,
Type "b9z" and subscrip "35,i"at the cursor, (we look at the Z magnetic field distribution at 35mm which is the centre of the sample)
Type the others.

To Generate Figures 5.21 Shown in Chapter 5

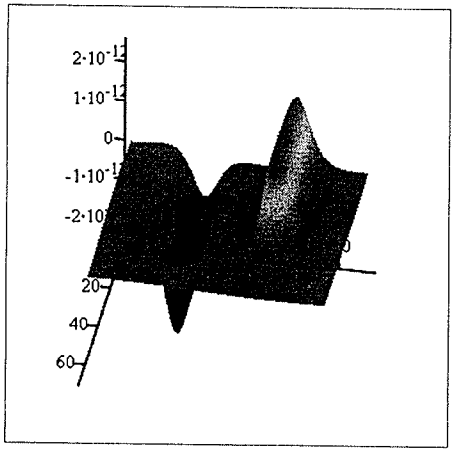

Open a "Surface Plot" Windows,
Type "Fy" at the cursor, (Y Magnetic interaction Force)
Set "Fill Options" to fill surface, "Color Options" to colormap, and "Line Options" to No lines.

Fy

To Generate Figures 5.22 Shown in Chapter 5

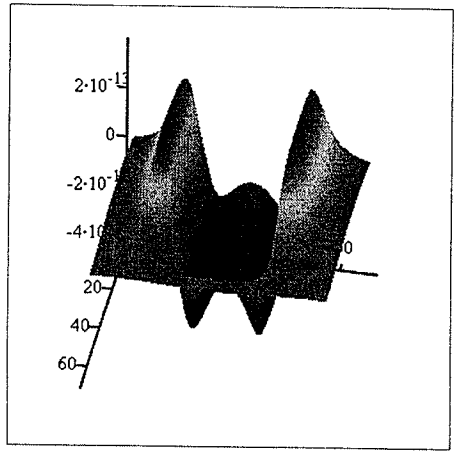

Open a "Surface Plot" Windows,
Type "Fy1 T" at the cursor, (Y Magnetic interaction Force, with "Matrix Tranpose")
Set "Fill Options" to fill surface, "Color Options" to colormap, and "Line Options" to No lines.

$Fy1^{T}$

To Generate Figures 5.23 Shown in Chapter 5

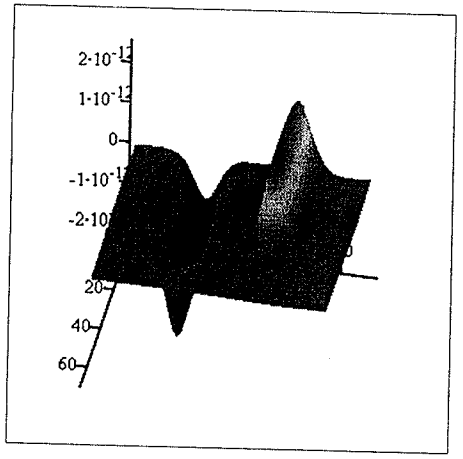

Open a "Surface Plot" Windows,
Type "Fy2 T" at the cursor, (Y Magnetic interaction Force, with "Matrix Tranpose")
Set "Fill Options" to fill surface, "Color Options" to colormap, and "Line Options" to No lines.

$Fy2^T$

To Generate Figures 5.24 Shown in Chapter 5

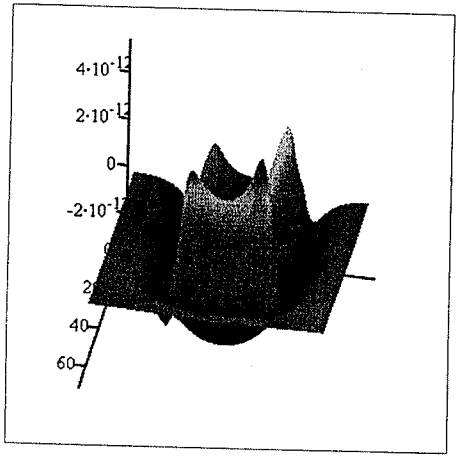

Open a "Surface Plot" Windows,
Type "Fz" at the cursor,
Set "Fill Options" to fill surface, "Color Options" to colormap, and "Line Options" to No lines.

Fz

To Generate Figures 5.25 Shown in Chapter 5

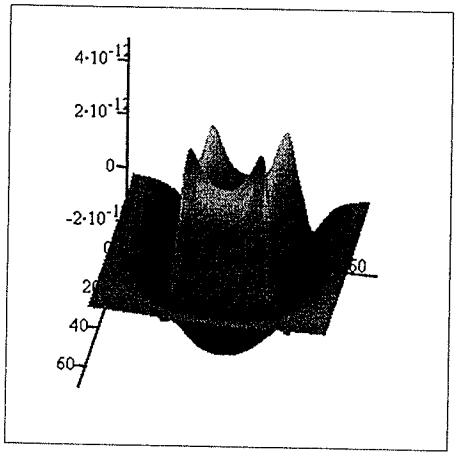

Fz1

Open a "Surface Plot" Windows,
Type "Fz1" at the cursor,
Set "Fill Options" to fill surface, "Color Options" to colormap, and "Line Options" to No lines.

To Generate Figures 5.26 Shown in Chapter 5

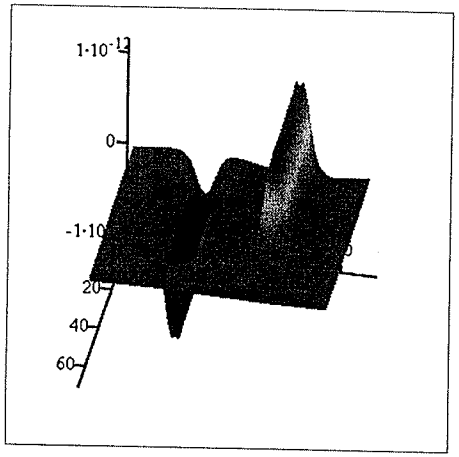

Fz2

Open a "Surface Plot" Windows,
Type "Fz2" at the cursor,
Set "Fill Options" to fill surface, "Color Options" to colormap, and "Line Options" to No lines.

To Generate Figures 5.27 Shown in Chapter 5

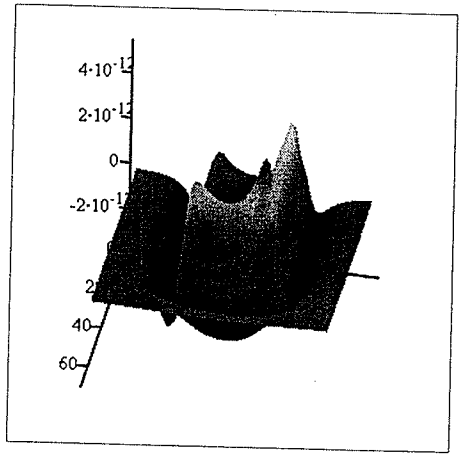

F

Open a "Surface Plot" Windows,
Type "F" at the cursor,
Set "Fill Options" to fill surface, "Color Options" to colormap, and "Line Options" to No lines.

To Generate Figures 5.28 Shown in Chapter 5

$$df := \left| \begin{array}{l} \text{for } i \in 0..nBx - 1 \\ \quad \text{for } j \in 0..nBy - 1 \\ \quad\quad \left| \begin{array}{l} G_{i,j} \leftarrow F_{i,j-1} - F_{i,j-2} \quad \text{if } j = nBy - 1 \\ G_{i,j} \leftarrow F_{i,j+1} - F_{0,10} \quad \text{otherwise} \end{array} \right. \\ G \end{array} \right.$$

Find the Relative Interaction Force with Initial Point at X=10, Y=0

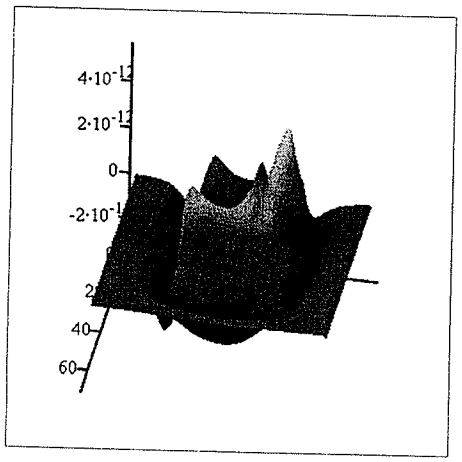

df

Open a "Surface Plot" Windows,
Type "df" at the cursor,
Set "Fill Options" to fill surface, "Color Options" to colormap, and "Line Options" to No lines.

To Generate Figures 5.29 Shown in Chapter 5

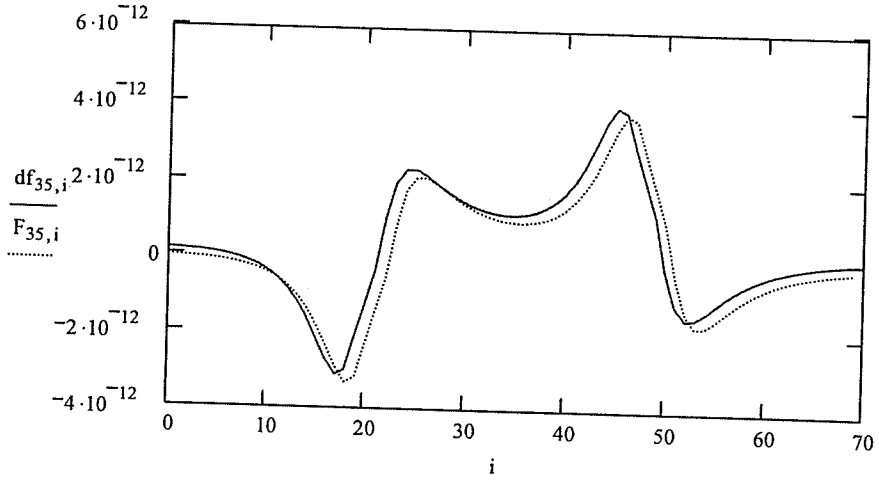

Open a "X-Y Plot" Windows,
Type "df" and subscrip "35,i"at the cursor, (we look at the Relative Interaction Force at 35μm which is the centre of the sample)
Type the others.

To Generate Figures 5.30 Shown in Chapter 5

m :=

C:\..\mm4.txt

Convert the EXP file from the MFM to txt file.
Import the MFM txt file, by "In sert Components", "File Read or Write".

$S1 := m \cdot 94.983 \cdot 10^{-18}$

Multiply the MFM result by a constant to adjust the amplitude limit range so that we can conpare the two result and assigned to S1

$j := 0..255$

Assign a new conter from 0 to 255, because the image is in 256X256 pixels

$G1 := df \cdot 2$

df is multiplied by 2 due to the effect of the beam bound system duiscribe in Chapter 3, ans assigned as G1

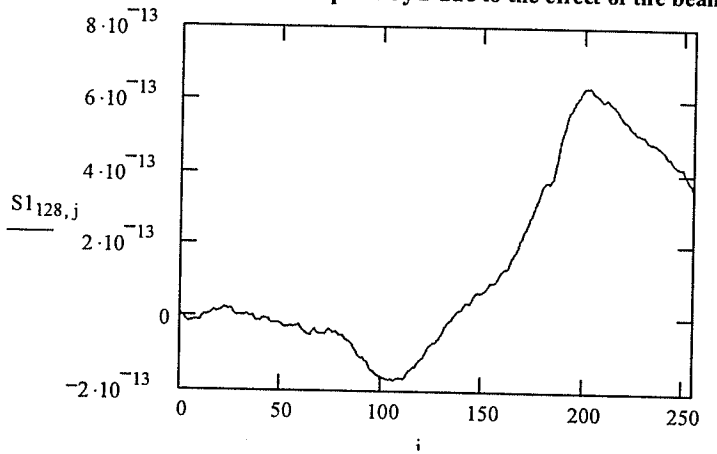

Open a "X-Y Plot" Windows,
Type "S1" and subscrip "128,j"at the cursor, (we look at the MFM result at 128μm which is the centre of the sample)

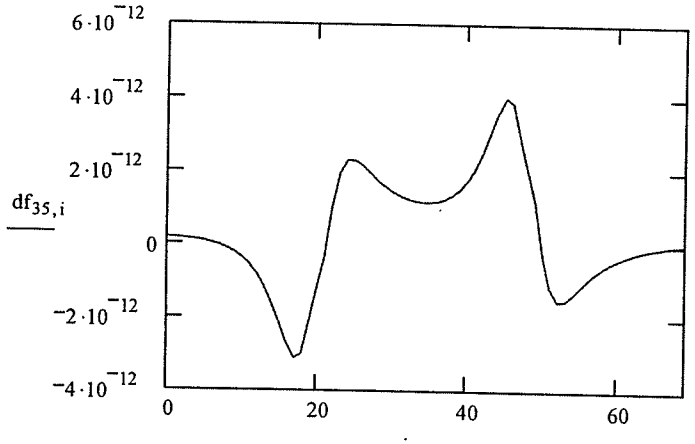

Open a "X-Y Plot" Windows,
Type df and subscrip "35,i"at the cursor, (we look at the Relative Interaction Force at 35μm which is the centre of the sample)
Type the others

i

To Generate Figures 5.35 Shown in Chapter 5

nBy := 70

size := 10

window(fw) :=
- for x ∈ 0 .. nBx − 1
  - W2 ← 0
  - count ← 0
  - for y ∈ 0 .. nBy − 1
    - xinit ← $x - \frac{size}{2}$
    - yinit ← $y - \frac{size}{2}$
    - for i ∈ 0 .. size − 1
      - W1 ← 0
      - for j ∈ 0 .. size − 1
        - t ← 0
        - if [nBx − 1 > (xinit + i) > 0] ∧ [nBy − 1 > (yinit + j) > 0]
          - t ← $fw_{(i+xinit),(j+yinit)}$
          - count ← count + 1
        - W1 ← W1 + t
      - W2 ← W2 + W1
    - $W_{x,y}$ ← $\frac{W2}{count}$
- W

F1 := window(F)

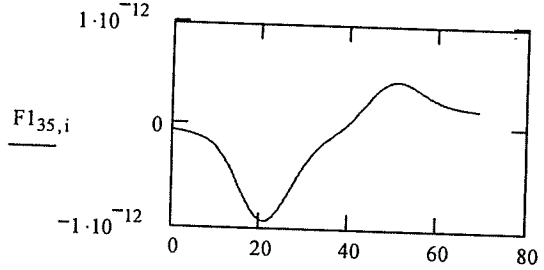

Open a "X-Y Plot" Windows,
Type F1 and subscrip "35,i"at the cursor, (we look at the Relative Interaction Force at 35μm which is the centre of the sample)
Type the others

i

To Generate Figures 5.37 Shown in Chapter 5

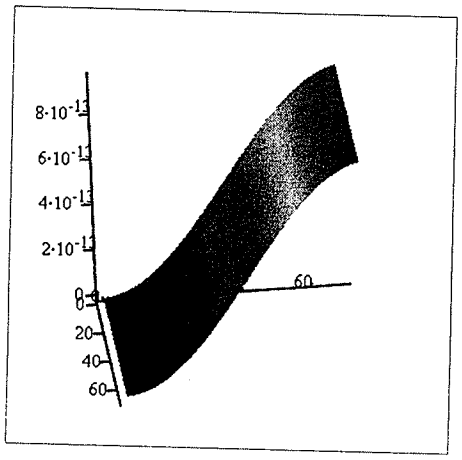

TMomentZ

$$\text{TMomentZ} := \left| \begin{array}{l} k \leftarrow 0 \\ \text{for } i \in 0..nBy - 1 \\ \quad \text{for } j \in 0..nBx - 1 \\ \quad\quad M_{i,j} \leftarrow Moment_{k,2} \cdot (1 - \cos(2.5deg \cdot j)) \\ \quad\quad k \leftarrow k + 1 \\ M \end{array} \right.$$

Assume Z magnetic moment on the tip tilted 2.5 degree in Y direction

Open a "Surface Plot" Windows,
Type "TMomentZ" at the cursor,
Set "Fill Options" to fill surface, "Color Options" to colormap, and "Line Options" to No lines.

To Generate Figures 5.38 Shown in Chapter 5

$\text{TFz1} := \overrightarrow{(Rzz \cdot TMomentZ)}$ $\quad \text{TFy2} := \overrightarrow{(Ryz \cdot TMomentZ)}$

$\text{TFz} := TFz1 + Fz2 + Fz3$ $\quad \text{TFy} := Fy1^T + TFy2^T + Fy3^T$

$\text{TF} := TFz \cdot \cos(Tilt) + TFy \cdot \sin(Tilt)$ $\quad TF2 := \text{window}(TF)$

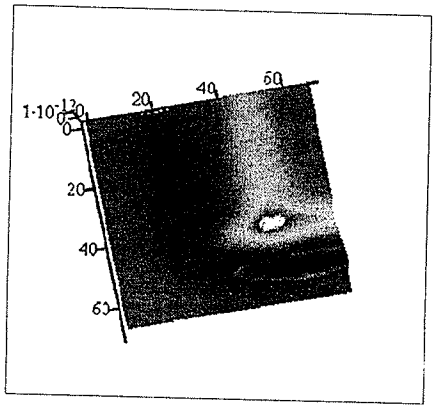

TF2

Open a "Surface Plot" Windows,
Type "TF2" at the cursor,
Set "Fill Options" to fill surface, "Color Options" to colormap, and "Line Options" to No lines.

To Generate Figures 5.39 Shown in Chapter 5

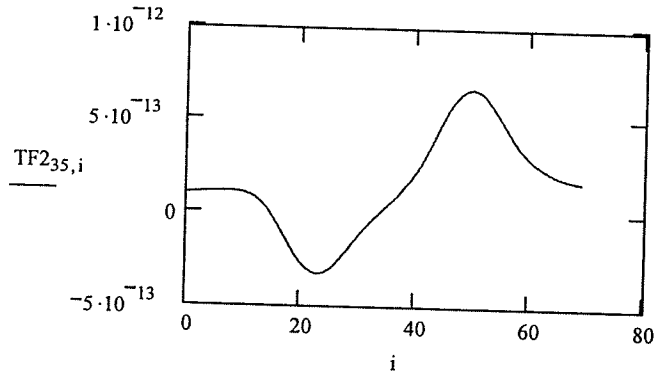

Open a "X-Y Plot" Windows,
Type "TF2" and subscrip "35,i"at the cursor, (we look at the Relative Interaction Force at 35μm which is the centre of the sample)

Appendix 2

University of Manitoba SPM Digital Control System Setup

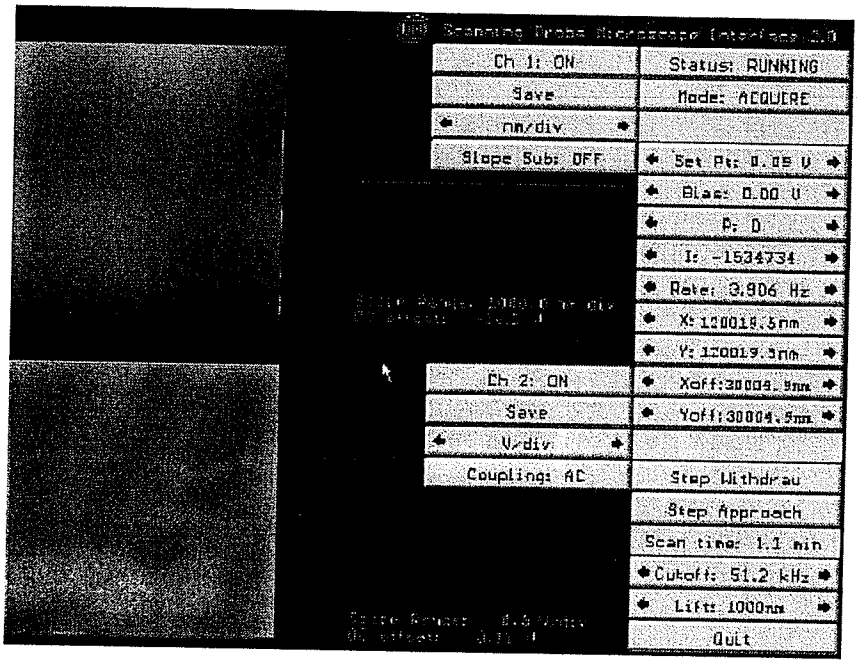

User interface layout in acquired mode of UM SPM Digital Control System.

Set point (Set Pt) is set to 0.09V, which is a representation of force between the tip and the sample in voltage. Gain (I) was set to –1534734, which is just a current gain proportional to the –18.18 to 18.18 real gain. X scan size (X) and Y scan size (Y) are both set to 120019.5nm. (Xoff) and (Yoff) are for offsetting the scan locations, which are set to 30004.9nm. (Lift) is to set the lifted distance between the tip and the surface of the sample when performing non-contact mode MFM, which is set to 1000nm. Scope for channel 1 is turned on and the range of the scope is set to 1000nm per division. Scope range for channel 2 is set to 0.5V per division.

In routing the signal, we feet the X, Y, and Z positional signal from Digital SPM Controller to the Piezo Positionner Controller through a 1/20 attenuator to control the nanopositionner remotely. The differential signal from bi-cell photodiode is taken into the Digital SPM Controller through channel *In6* as topographic signal of the sample surface from MFM contact mode. The output signal from lock-in amplifier is taken into the Digital SPM Controller through channel *In4* as relative magnetic force signal of the sample circuit from MFM non-contact mode.

References

1.1 International Technology Roadmap for Semiconductors,
http://public.itrs.net/

1.2 Sematech, Inc.,
The National Technology Roadmap for Semiconductor, 1997 Edition, Technological Section.

1.3 Q-Star Test,
IDDQ Efficiency, http://www.qstar.be/html/iddq_efficiency.html.

1.4 Neil H. E. Weste Kamran Eshraghian
Principles of CMOS VLSI Design
Addison Wesley, pg. 498

1.5 IBM,
A Methodology for Estimating Total Off-State Leakage Current (I_{ddq}) in CMOS Technology
MicroNews, First Quarter 2001, Vol. 7, No. 1

1.6 VLSI Test and Validation, University of Cincinnati,
IDDQ Testing
http://www.ececs.uc.edu/~ranga/courses/682/slides-spring-2001/iddq.pdf

2.1 University of Bristol Department of Physics Polymer Group,
Atomic Force Microscopy,
http://teddy.phy.bris.ac.uk/spm/techniques/afm.html

2.2 National University of Singapore
Scanning Probe Microscopy
http://courses.nus.edu.sg/course/phyweets/PC4250/Projects2002/Scanning%20Probe%20Microscopy.htm

2.3 Roland Wiesendanger,
Scanning Probe Microscopy and Spectroscopy Methods and Applications,
Cambridge University Press, pg. 207

2.4 G. Meyer and N.M. Amer,
Novel Optical Approach to Atomic Force Microscopy,
Applied Physics Letters, vol. 53, no. 24, pp. 2400-2402, 12 December 1988.

2.5 D. J. Thomson,
Experimental Methods for Electronics Materials,
Lecture Notes, University of Manitoba, 1996

2.6 Roland Wiesendanger,
Scanning Probe Microscopy and Spectroscopy Methods and Applications,
Cambridge University Press, pg. 237

2.7 Roland Wiesendanger,
Scanning Probe Microscopy and Spectroscopy Methods and Applications,
Cambridge University Press, pg. 246

2.8 Ann N. Campbell, Edward I. Cole Jr. Bruce A. Dodd and Richard E. Anderson,
Internal Current Probing of Integrated Circuits Using magnetic Force Microscopy
CH3194-B/93/0000-0168, CISTI, IRPS, IEEE 1993

2.9 William H. Hayt, Jr,
Engineering Electromagnetics, Third Edition,

McGraw-Hill, Inc., pg. 232

2.10 HyperPhysics (©C.R. Nave, 2003)
Biot-Savart Law
http://hyperphysics.phy-astr.gsu.edu/hbase/hframe.html

2.11 Raymond A. Serway,
Physics For Scientists and Engineers with Modern Physics Third Edition,
Saunders College Publishing, pg855

2.12 Walter Hauser,
Introduction To The principles of Electromagnetism,
Addison-Wesley Publishing Company, Pg 252

2.13 *Paul Lorrain, Dale Corson,*
Electromagnetic Fields and Waves Second Edition,
W. H. Freeman and Company, San Francisco. Pg 386

2.14 Roland Wiesendanger,
Scanning Probe Microscopy and Spectroscopy Methods and Applications,
Cambridge University Press, pg. 258, 256

3.1 D. Sarid,
Scanning Force Microscopy with Applications to Electric, Magnetic and Atomic Forces,
Oxford University Press, Inc., 200 Madison Avenue, N.Y., N.Y. 1991

3.2 Roland Wiesendanger,
Scanning Probe Microscopy and Spectroscopy Methods and Applications,
Cambridge University Press, pg. 217

3.3 **Scanning Probe Microscopy and Spectroscopy Methods and Applications,**
Cambridge University Press, pg. 243

3.4 Sunny Cheung,
Electrostatic Force Sampling of Digital Waveform Using Synchronous Time Domain Gating,
Master of Science Thesis, pg.17, 2000

3.5 Park Scientific Instruments, Mountain View, California, U.S.A.
https://store.veeco.com/webapp/wcs/stores/servlet/VeecoStoreDisplay?storeId=10101&langId=-1&catalogId=10051

3.6 Sunny Cheung,
Electrostatic Force Sampling of Digital Waveform Using Synchronous Time Domain Gating,
Master of Science Thesis, pg.19, 2000

3.7 Roland Wiesendanger,
Scanning Probe Microscopy and Spectroscopy Methods and Applications,
Cambridge University Press, pg. 245-246

3.8 U. Mueller, C. Boehm, J. Sprengepiel, C. Roths, E. Kubalek and A. Beyer,
Geometrical and Voltage Resolution of Electrical Sampling Scanning Force Microscopy,
IEEE MTT-S Digest, pp. 1005-1008, 1994

3.9 Roland Wiesendanger,
Scanning Probe Microscopy and Spectroscopy Methods and Applications,
Cambridge University Press, pg. 259

3.10 Robert C. Weast,
CRC Handbook of Chemistry and Physics 64th Edition,
CRC Press, Inc. Boca Raton, Florida. Pg E-107.

3.11 Robert C. Weast,
CRC Handbook of Chemistry and Physics 64th Edition,

CRC Press, Inc. Boca Raton, Florida. Pg B-101.

3.12 Raymond A. Serway,
Physics For Scientists and Engineers with Modern Physics Third Edition,
Saunders College Publishing, pg342

3.13 G. Meyer and N.M. Amer,
Novel Optical Approach to Atomic Force Microscopy,
Applied Physics Letters, vol. 53, no. 24, pp. 2400-2402, 12 December 1988.

3.14 A. D. Dimarogonas,
Vibration for Engineers,
Prentice-Hall, Inc., NJ, U.S.A. 1996

3.15 D. J. Thomson,
Experimental Methods for Electronics Materials,
Lecture Notes, University of Manitoba, 1996

3.16 Endel Uiga,
Optoelectronics,
Prentice-Hall Inc., 1995

3.17 Sunny Cheung,
Electrostatic Force Sampling of Digital Waveform Using Synchronous Time Domain Gating,
Master of Science Thesis, pg.23, 2000

3.18 L.W. Couch II,
Digital and Analog Communication Systems,
Fourth Edition, Macmillan Publishing Company, NY, NY, 1993

3.19 Terry Ritter,
Random Electrical Noise: A Literature Survey,
http://www.io.com/~ritter/RES/NOISE.HTM

3.20 C.A.J. Putman, B.G. De Grooth, N.F. Van Hulst and J. Greve,
A Detailed Analysis of the Optical Beam Deflection Technique for use in Atomic Force Microscopy,
Journal of Applied Physics, vol. 72, no. 1 pp. 6-12, July 1992.

3.22 Hewlett_Packard GmbH,
HP80000 Data Generator System Installation Guide,
Edition 1.2, Hewlett-Packard GmbH, Germany, 1993

3.23 Northern Telecom,
NT25 Electrical Specifications and Layout Design Rules Version 1S01.2 CMC,
Northern Telecom for CMC Release. Pg 13-15

3.24 David T. Shimizu,
University of Manitoba Digital Scanning Probe Microscope Controller,
Department of Electrical and Computer Engineering, August, 1998 Pg. 3

3.25 Melles Griot,
Specifications: Piezoelectric Controllers with Feedback.

3.26 Stanford Research Systems
SR510/SR530 Lock-In Amplifier Specifications
http://www.thinksrs.com/html/analoglock-inamplifierstechnot.html

3.27 Howard Stone, Dept. of Physics, Princeton University
Power and Quality Factor
http://pupgg.princeton.edu/~phys104/lguides/lg06_notes/node5.html

Wolfram Research, Inc.
***Q*, "quality factor"**
http://scienceworld.wolfram.com/physics/Q.html

3.28 Ann N. Campbell, Edward I. Cole Jr.. Bruce A. Dodd and Richard E. Andersan
Internal Current probing of Interated Circuits Using Magnetic Force Microscopy.
IEEE / IRPS 1993, CH3194-B/93/0000-0168

4.1 David T. Shimizu,
University of Manitoba Digital Scanning Probe Microscope Controller,
Department of Electrical and Computer Engineering, August, 1998 Pg. 25

4.2 Park Scientific Instruments, Mountain View, California, U.S.A.
https://store.veeco.com/webapp/wcs/stores/servlet/VeecoStoreDisplay?storeId=10101&langId=-1&catalogId=10051

4.3 Northern Telecom,
NT25 Electrical Specifications and Layout Design Rules Version 1S01.2 CMC,
Northern Telecom for CMC Release. Pg 13-15